2015

# Fiber-Reinforced Polymer (FRP) Composites in Retrofitting of Concrete Structures: Polyurethane Systems Versus Epoxy Systems

Elie El Zghayar
*University of Central Florida*

# FIBER-REINFORCED POLYMER (FRP) COMPOSITES IN RETROFITTING OF CONCRETE STRUCTURES: POLYURETHANE SYSTEMS VERSUS EPOXY SYSTEMS

by

ELIE EL ZGHAYAR
B.S.C.E University of Central Florida, 2007
M.S. University of Central Florida, 2010

A dissertation submitted in partial fulfilment of the requirements
for the degree of Doctor of Philosophy in Civil Engineering
in the Department of Civil, Environmental, and Construction Engineering
in the College of Engineering and Computer Science
at the University of Central Florida
Orlando, Florida

Fall Term
2015

Major Professor: Kevin Mackie

# ABSTRACT

Fiber reinforced polymer (FRP) composites have been of interest to the structural engineering society since the earliest days of FRP composites industry. The use of such systems has been implemented in both new construction and for repair and rehabilitation of existing structures. Since the 1980s, researchers have developed a significant body of knowledge to use FRP composites in infrastructure applications; however, most of this established knowledge was concentrated on the use of traditional epoxy (EP) systems (epoxy matrix FRPs and epoxy adhesives). FRP composites with polyurethane (PU) matrices and adhesives have recently attracted the attention of a few researchers due to their potential advantages in constructibility and mechanical properties. The deployment of these systems is currently limited by a lack of knowledge on mechanical and durability performance. The objective of this research is to quantify the mechanical behavior of PU composites utilized in externally-bonded repair of common flexural and flexural-axial reinforced concrete systems. In addition, the mechanical performance, strength, and failure modes are compared directly with an epoxy-based composite by subjecting reinforced concrete specimens utilizing each of the matrix types (EP and PU) to the same protocols. The study presented therefore allows an objective comparison (advantages and disadvantages) between the two composite system used for repair and rehabilitation of concrete infrastructure. An experimental research program was designed with different length scales. Small-scale experiments were utilized to characterize the component level properties of the materials and bond to concrete, which include the flexural behavior as well as the pure shear behavior. The results of these small scale experiments were used to calibrate analytical models of the interface behavior between FRP laminate and concrete, and paved the way for the next level of the research which studied the behavior of each composite system at larger scales. The large scale experiments included flexural retrofitting of reinforced concrete girders and retrofitting of circular columns using FRP laminates. The large-scale experimental specimens

were mechanically damaged prior to FRP repair and testing, making the testing more appropriate compared to common practice of repairing undamaged specimens.

I dedicate this dissertation to my mom and dad, Mora and Atallah Zghayyar for their unwavering support and love, without whom I could have never done this work. I also dedicate my five years of hard work on this research to my sister and brother Aline and Michel Zghayyar.

# ACKNOWLEDGMENTS

First and Foremost I would like to thank Dr. Kevin Mackie for his continuous support and guidance in every step of this project and my entire career at UCF. The gratitude I have to Dr. Mackie cannot be expressed in words.

I would also like to thank Dr. Manoj Chopra, Dr. Hae-Bum Yun, and and Dr. Ashraf El-Bahy for taking the time from their very busy schedules and serving on my committee, providing great feedback, and improving this manuscript.

I would like to express gratitude to Neptune Research Inc. (NRI) for funding and supporting this project, and the staff at NRI, specifically Christopher Lazzara, and Erblina Vokshi.

Last but definitely not least, I would extend my special thanks to the UCF Structures Lab personnel for their countless hours of support, help, and hard work: Juan Cruz, Jacob Solomon, Blake Lozinski, Daniel Kellner, Mathew Adamira, Kyle Paradis, Justin Bartusek, Brice Latham, and James Duryea.

# TABLE OF CONTENTS

# LIST OF FIGURES

# LIST OF TABLES

# CHAPTER 1: INTRODUCTION

## 1.1 Background

Fiber-reinforced polymer (FRP) composites have been used for decades in aerospace and manufacturing applications where low weight, high tensile strength, and corrosion resistance are desirable properties. FRP composite materials have also received considerable attention from researchers, structural engineers, and contractors for use in structural strengthening and repair applications around the world. High strength-to-weight ratios combined with superior environmental durability have made FRP composites a competitive alternative to the conventional strengthening methods using materials such as steel and concrete. In particular for many civil engineering repair applications, carbon fiber-reinforced polymers (CFRP) have proven to be extremely effective as externally-bonded reinforcement. Investigations on externally-bonded flexural strengthening started in the late 1980s. It was shown through numerous experimental and analytical studies that externally-bonded FRP composites can be applied to improve and/or repair structural performance criteria such as stiffness, load-carrying capacity, ductility, and even durability of various structural members including columns, beams, slabs, and walls. Flexural strengthening projects for bridge beams and slabs have been carried out in almost every state in the US [2].

Retrofitting applications can be classified into two types: (1) Strengthening: the structure's original design strength or ductility (typically displacement capacity) necessitates an increase due to new applied loads (or displacements) for which the structure was not originally designed. The increase may also be necessitated by the desire to make the structure compatible with existing building codes, particularly in the case of seismic retrofitting. (2) Repair: the FRP composite is used to retrofit an existing and deteriorating structure to bring its load-carrying capacity or ductility back to the loads or displacements for which it was designed. Repair is necessitated by several factors

such as: deterioration due to environmental effects, damage of the structure while in service, or due to construction or design errors. Fiber reinforced polymer (FRP) composites have become popular in such retrofitting applications.

There are several advantages offered by FRP retrofitting over conventional strengthening methods for existing reinforced concrete (RC) structures. The most attractive property of FRP materials to structural engineers is that they are lightweight, so increases in superimposed dead loads on structures due to this strengthening solution are negligible. Equally as important, FRP materials are relatively easy to install with minimal invasive modifications to the existing structures, therefore attracting architects and contractors to FRP solutions.

CFRP has proven to be extremely effective as externally-bonded reinforcement. Flexural strengthening projects for bridge beams and slabs have been carried out in almost every state in the US [2]. Investigations on externally-bonded flexural strengthening started in the late 1980s. FRP systems have been used extensively in seismic zones for confinement of concrete columns and walls. A number of FRP systems have been qualified for use for wrapping circular and rectangular bridge columns. The majority of structural deficiencies in existing concrete columns can be attributed to lack of transverse reinforcement. This is especially true for columns in seismically active regions, designed prior to the enactment of modern seismic codes. The FRP wrap method also protects the RC column from the flexural plastic hinge failure mode. Assuming continuous fibers are used, the wrap helps prevent concrete spalling and provides lateral support to the steel longitudinal reinforcement. The uniform confinement, provided by the composite wrap, enhances both the strength and ductility of the concrete.

FRP sheets and fabrics have been used in many other retrofitting applications as externally-bonded FRP. Some of the common application areas for concrete are: flexural and shear retrofitting and seismic repair of reinforced concrete beams, shear walls, slabs, tilt-ups, and submerged and un-

derwater piles. Masonry has also received considerable attention as a substrate suitable for FRP repair with applications most commonly as flexural and shear strengthening of masonry parapets and walls, and wall blast strengthening and protection. While metallic substrates are not typically as well matched to the strength and stiffness of FRP, numerous retrofitting studies have been performed with steel and aluminum substrates, including flexural and shear retrofitting of beams and pipes (particularly when they have degraded due to environmental conditions or contain cracks), flexural and shear retrofitting of columns, and repair of utility poles. Timber applications have also been investigated, including retrofitting of beams, trusses, and timber piles.

At this point in time, design guidance is only available for FRP retrofitting of reinforced concrete structures [3] and more recently for unreinforced masonry [4], particularly as applied to strengthening. Guidelines are also limited to FRP composites with epoxy matrices and epoxy adhesives [5, 6, 7].

## 1.2 Motivation

The use of FRP composites for retrofitting of concrete structures has evolved in the late 1980s in the US, Europe, and Japan at relatively the same time. Since then intensive research had been invested in the topic and researchers have provided the structural engineering field with a lot of knowledge for the use epoxy composite systems (epoxy matrices and epoxy adhesives) as the only alternative. Epoxy has several advantages (listed in previous section); however, epoxy also has several disadvantages. Polyurethane composites is a material that has been recently been introduced to this field and has several advantages over epoxy. Table 1.1 shows a comparison between epoxy and PU FRP composites and shows that PU can be a better option than epoxy, given that the PU FRP composite materials are suitable for the same retrofitting applications. Moreover, polyurethane is a unique material that offers the elasticity properties which allow the composite system to perform

Table 1.1: Epoxy Vs. PU FRP Composites

| **Epoxy FRP Composites** | **PU FRP Composites** |
|---|---|
| Epoxy systems is most commonly installed as wet lay ups. The main disadvantage of wet layups is quality control since the matrices and adhesives are prepared in the field and more importantly the impregnation of the fibers is dependent on the installer. | The PU composite materials are pre-impregnated by the manufacturer. The pre-impregnation ensures high saturation levels of the matrices in the fibers producing higher quality and controlled laminate. The pre-impregnated composite is delivered in sealed bags because curing is dependent on moisture which is a catalyst that can be isolated. |
| While curing, epoxy releases a large concentration of fumes that have been proven to be harmful to the human health if inhaled. These fumes also cause irritation to the skin and eyes. | The only byproduct during the cure of PU systems is $CO_2$. |
| Epoxy bond can be affected tremendously by the environment in which substrate is present. Most importantly, moisture plays a detrimental role in epoxy bonding to substrate. | Moisture is needed because $H_2O$ is the catalyst for curing of PU matrices. |

better than epoxy FRP composites for strengthening of structures in seismic regions and/or under high cyclic loads, and in certain environmental such as wet conditions.

## 1.3 Scope and Objectives

It is believed that there is a misunderstanding in the code where the only variable that is considered for FRP retrofit of structures is the strength of the polymer material and bond. The flexibility of the material plays an even more important role in such applications. Polyurethanes' flexibility gives the FRP material an important role in energy dissipation during cyclic loading and even provides better performance under static loads. This was proven in the first stage of experiments performed

in this research, which will be presented in later parts of this dissertation.

An experimental procedure to evaluate polyurethane (PU) FRP composites and highlight their advantages alongside the epoxy systems when used for retrofitting of existing structures is described below, in Chapter 3. In order to evaluate the mechanical properties for the PU systems at the component level, small scale experiments were performed. Based on the small scale experimental program, analytical models are developed to predict the behavior of the material in large scale retrofitting applications. This paved the way the way for the larger scale experiments to validate findings from the analytical models. The larger scale experiments include wrapped columns and reinforced girders.

At the end of the research, the PU FRP composites are evaluated, under the same testing conditions with the epoxy composites, as an alternative for external retrofitting of common reinforced concrete members. This research provides the structural engineering field with a much better understanding of material properties that are overlooked. This research is first of a kind and will have the potential to change the current design guides' visions of polyurethane FRP composites as an alternative for retrofitting.

# CHAPTER 2: LITERATURE REVIEW

## 2.1 Fiber Reinforced Polymer Composite Materials

FRP materials are composites consisting of high-strength fibers encapsulated in a polymeric resin to form a laminate. Fibers in FRP composite materials carry the load, while the resin protects the fibers and keeps them in alignment. In addition to encapsulating the fibers, the resin can act as an adhesive, in the case of epoxy wet layups, to bond the laminate to the concrete substrate. When polyurethane resins are used, usually the fibers are pre-impregnated by the manufacturer which allows the use of different types of adhesives to bond to the substrate. Commonly available fibers are manufactured of carbon, glass, and aramid. The fibers are typically provided in a woven sheet matrix, pre-cured laminates, or solid bars.

### *2.1.1 Reinforcing Fibers*

The fiber phase of an FRP composite materials is made up of thousands of individual micrometer-diameter filaments. The mechanical properties of the fibers are typically orders of magnitude greater than those of the polymer resins that they reinforce. Since these fibers are filamentary in nature, they must be impregnated with the matrix in order to realize their superior mechanical properties. There are several kinds of fibers but the most commonly used are carbon, glass, and aramid. In this research carbon fibers will be the main type to be used; however, during the component testing a carbon-glass hybrid type of fabric was also tested when evaluating the different types of fabric to be used in the larger scale experiments.

Table 2.1: Approximate Properties of Common Grades of Carbon Fibers

| **Grade of Carbon Fiber** | **Density lb/in$^3$** | **Tensile Modulus (Msi)** | **Tensile Strength (ksi)** | **Max Elongation (%)** |
|---|---|---|---|---|
| Standard | 0.061 | 36.3 | 537 | 1.2 |
| High Strength | 0.065 | 36.3 | 696 | 1.4 |
| High Modulus | 0.068 | 72.5 | 435 | 0.5 |
| Ultra High Modulus | 0.076 | 116.0 | 348 | 0.2 |

#### *2.1.1.1 Carbon Fibers*

Table 2.1 shows the mechanical properties of carbon fibers and their superiority over other types of commonly used fibers such as glass. Durability studies have shown that carbon fibers perform very well in hot and moist environments. They do not absorb moisture and they have a very low coefficient of thermal expansion in their longitudinal direction giving them excellent dimensional stability. They also have excellent fatigue life. Carbon fibers are electrically and thermally conductive, which means that care must be taken when used to reinforce metals such as steel. A galvanic cell can develop due to the electro-potential mismatch between the carbon fiber and the metal substrate that could potentially lead to degradation [8].

#### *2.1.1.2 Glass Fibers*

Table 2.2 lists some mechanical properties of glass fibers and shows that glass fibers are inferior to carbon fibers when it comes to strength properties. However, there are several advantages to glass fibers. They are considered excellent thermal and electrical insulators, hence their extensive use in buildings and the electric power industry as insulation materials and in reinforcing metallic structures such as steel. They are most inexpensive of high performance fibers. Glass fibers are

Table 2.2: Approximate Properties of Common Grades of Glass Fibers

| **Grade of Carbon Fiber** | **Density lb/in$^3$** | **Tensile Modulus (Msi)** | **Tensile Strength (ksi)** | **Max Elongation (%)** |
|---|---|---|---|---|
| E | 0.093 | 10.5 | 493 | 2.5 |
| A | 0.089 | 10.6 | 400 | 2.5 |
| C | 0.089 | 10.7 | 340 | 2.5 |
| S | 0.089 | 12.8 | 667 | 3.0 |

particularly sensitive to moisture, especially in the presence of salts and elevated alkalinity, and need to be well protected by the resin. Glass fibers are also susceptible to creep and rupture and lose strength under sustained stresses [2].

### *2.1.2 Polymer Resins*

These polymers include epoxy, polyurethane, unsaturated polyester, vinylester, phenolic and others. Unsaturated polyester resins are widely used to make pultruded FRP profiles for use in structural engineering and is used to make some FRP rebar. When greater corrosion resistance is required, vinylester resins are generally used in manufacturing FRP rebar. Phenolic resins have not been very widely used in FRP products due to the difficulty in reinforcing them [9].

#### *2.1.2.1 Epoxy*

Epoxy resins are the most commonly used resins although epoxy is considered costlier than other polymer matrices. The main reasons why epoxy is the most used polymer matrix material are:

- High strength

Table 2.3: Generic Properties of Epoxy Resins

| **Density g/cm$^3$** | **Tensile Strength (ksi)** | **Tensile Modulus (ksi)** | **Poisson's Ratio** | **Coeficient of Thermal Expansion ($10^6$ in/in/ °F)** | **Cure Shrinkage (%)** |
|---|---|---|---|---|---|
| 1.2-1.3 | 8-19 | 400-5950 | 0.2-0.33 | 28-44 | 1-5 |

- Low viscosity and low flow rates, which allow good wetting of fibers and prevent misalignment of fibers during processing
- A Poisson's ratio ranging between 0.2 and 0.33 which is similar to the values of steel and concrete
- Low shrink rates, which reduce the tendency of gaining large shear stresses of the bond between epoxy and its reinforcement
- Available in many grades to meet specific property and processing requirements

In addition to the several disadvantages mentioned in table 1.1, epoxies have the highest cost and a prolonged curing time. Table 2.3 shows the range of mechanical properties for the epoxy resins [10].

#### *2.1.2.2 Polyurethane*

Polyurethane is a broad class of primarily thermosetting polymers with widely varying properties when cured. A majority of applications of polyurethanes are in foams and plastic parts, and the constituent materials can be tweaked to achieve hardness values appropriate for different industries. Polyurethane is often inaccurately referred to as a collection of urethanes. However, polyurethane

does not contain ethyl carbamate (which is commonly called urethane). There is not a lot of published work on polyurethane as a matrix for FRP composites. The majority of the polyurethane studies have been made on thermosetting polyurethane composites fiber reinforced elastomeric polyurethanes which do no exhibit mechanical performance suitable for infrastructure applications. Polyurethanes can also be used as high performance adhesives, and have a number of advantages, among which include:

- Cost effective
- Adjustable cure time using a catalyst (water)
- Small molecular size allows the adhesive to permeate substrates (such as concrete)

Some of the disadvantages include:

- Limited thermal stability due to molecular constituents
- Issues with hydrolytic stability
- During curing continuous rolling is required to prevent voids due to $CO_2$

## 2.2 Polyurethane Matrix Composites

Setiadi et al. [11] concluded that a urethane matrix composite performed better, under the imposed conditions, than of a polyester matrix composite. The researchers studied damage scenarios induced onto FRP composites by static and cyclic loading. Two different types of polymeric matrices were considered for the study: a thermosetting polyurethane and a modified polyester employing a methyl ethyl ketone peroxide (MEKP) initiator. Test specimens per ASTM D 628-01 were reinforced with 5 layers of random oriented E-glass mat. The static loading tests showed that the

urethane matrix composite had significantly higher ultimate strength, strain, and energy absorption at failure than the polyester composite. However the urethane composite had lower tensile stiffness. Fatigue testing was conducted at 0.3 Hz at a stress range of 0 to 50% of the ultimate stress of each of the two specimen types. Results from fatigue testing lead the authors to believe that both matrix types show an increase in strains with cycle number. However, it was observed that the strain increases in the urethane composite were smaller than those observed in the polyester composite. Furthermore, a decrease in elastic modulus was observed for both specimen types but was less significant in the urethane composite. The urethane matrix composite also exhibited a lower amount of matrix cracking at 1000 cycles. Moreover, cracks in the urethane matrix were observed to originate from micro-voids caused by $CO_2$ during cure.

Saenz et al. [12] completed a field project that focused on the repair of severely damaged underwater bridge piles using the same polyurethane composite system. After two years of service, direct tension bond pull-off tests revealed that the polyurethane system tended to exhibit inter-layer failure. Such a failure indicates good bond to concrete but poor layer-to-layer adhesion. Furthermore, the ease in which the system could be used was noted. Mechanical testing to determine the ultimate load-bearing capacity of strengthened piles was not completed.

Haber et al. [13] published the results on PU composite system performance and durability. The PU system showed considerable consistency ductility, load bearing capacity, failure modes, and post conditioning bond integrity. According to Haber, the governing mode of flexural failure was de-bonding in the adhesive layer. Micro analysis on PU composite samples showed micro voids forming during curing due to $CO_2$ release tend to propagate and connect under applied loads, however these observations did not affect the mechanical behavior of the material.

## 2.3 Polyurethane and Epoxy Adhesives

Polyurethane adhesives were developed in early 1960s. They are very versatile and adjustable to meet design requirements. This is due to the chemistry of polyurethanes which is discussed in details in the literature [14]. The key determining factors which influence the properties of polyurethanes is that they are mainly built up via difunctional and trifunctional OH-terminated molecues which react with di- or triisocyanates. This chain length and stiffness of the chain determine the mechanical properties of the final polymer [14]. The structural stiffness of the cured polyurethane is adjusted by adjusting the concentration of the trifunctional molecules which determines the cross-link density [15]. In structural applications, a trifunctional groups must exist to guarantee a covalent 3-dimensional network; otherwise the polymer would have thermoplastic properties [15]. Polyurethanes become the adhesive of choice in many applications where the stiffness and brittleness of epoxies may become detrimental in its application because of this inherent flexibility of the polyurethane chain.

The reaction between a hardener and an epoxy resin or the reaction between the epoxy resins with themselves create the properties of epoxy adhesives. Epoxy resins are a large class of polymers and prepolymers containing glycidyl or oxirane groups [14]. The majority of epoxy resins are derived from petroleum and are themselves the result of a reactive process involving epoxide units. Due to the chemistry of the epoxy adhesive, the end product stiffness can be controlled; however, the higher level of flexibility provided by the PU adhesives cannot be achieved in epoxies.

## 2.4 Current Design Methodology

The American Concrete Institute (ACI) Committee 440 produced design guidelines [3] for FRP strengthening of reinforced concrete structures. Some of its key requirements include:

1. Strengthening Limit - Prior to strengthening a concrete structure with FRP, the unstrengthened structure must have a reasonable level of existing load capacity in the event that the proposed FRP retrofit is damaged by fire, vandalized, or negated by other causes. The current strengthening limit requires that the existing structure have sufficient capacity to resist service loads. ACI 440.2 [3] is based on the load and strength reduction factors of ACI 318 [16]. If the structure does not satisfy these criteria, then FRP strengthening is probably not a viable option. It is the responsibility of the engineer of record to verify adherence to this criteria prior to specifying FRP as a repair solution.

2. Environmental Exposure - Environmental conditions should be verified to determine whether the FRP application could be damaged by exposure to detrimental factors such as ultraviolet light, salt water, chemicals, high temperatures, high humidity, or freeze/thaw. ACI 440.2 [3] provides FRP strength reduction factors depending on the application exposure conditions - interior, exterior, or aggressive environmental exposures. A UV-resistant top coating can be applied in an exterior application to extend the service life of the retrofit.

3. Failure Modes - Several failure modes should be considered in the design calculation for the FRP retrofit solution, since the failure of the applied FRP material may not control the design capacity. Examples include concrete crushing prior to steel yielding, steel yielding followed by rupture of the FRP, steel yielding followed by concrete crushing, cover de-lamination, and FRP de-bonding.

4. Strength Reduction for Multiple Plies - Multiple-ply FRP applications have a greater stiffness and are subject to a strength reduction since they are more prone to peeling/ de-lamination or FRP de-bonding. Increasing the number of plies does not necessarily equate to a better performing strengthening option. The maximum ply limit is typically 4 to 5 plies, due to the diminishing strength gain from additional plies.

5. Debonding is still not a desirable failure mode due to the complex behavior and ”unpredictability”. ACI 440 also stipulates that an unacceptable failure mode is within the adhesive layer. Although explicitly frowned upon in the ACI440.2R, cohesive failure of substrate material is considered an acceptable mode of debonding failure. Stresses in FRP materials are limited in design guidelines to prevent the failure triggered in the bond line [3]. These guidelines lead to stress limitations preventing high strength FRP to be fully utilized in externally bonded FRP systems in flexural retrofitting applications.

6. ACI 440.2R specifies that for bond critical applications (flexural and shear retrofitting for example), the tension adhesion strength shall exceed 200 psi and the failure shall be exhibited within the concrete substrate. Figure 2.1 shows a schematic diagram of the test method. The test method requires a dolly to be bonded to the surface of the FRP concrete system. A tensile force, perpendicular to the surface, is applied to the dolly until it is detached (that is, until failure occurs). Typically, the surface of the FRP at around the dolly is scored or cut into the concrete substrate. The size of the cut depends on the size of the dolly and ranges between 0.25 in and 0.50 in. Scoring the surface is done to ensure that the load is applied uniformly over the surface area of the dolly. The resulting stress is solely tensile. Because of the heterogeneous nature of concrete, 2 in diameter test dollies should be used. The maximum tensile stress or bond strength is calculated based on the applied load and the area of the dolly face.

While ACI 440.2 [3] primarily addresses FRP applications to buildings, the technology can be (and is) applied to other structures such as bridges and dams. The ACI guidelines continue to evolve with changes in materials, research, and new laboratory test findings. As this research evolves, light will be shed on a lot of misconceptions in the standard for FRP applications for retrofitting of structures.

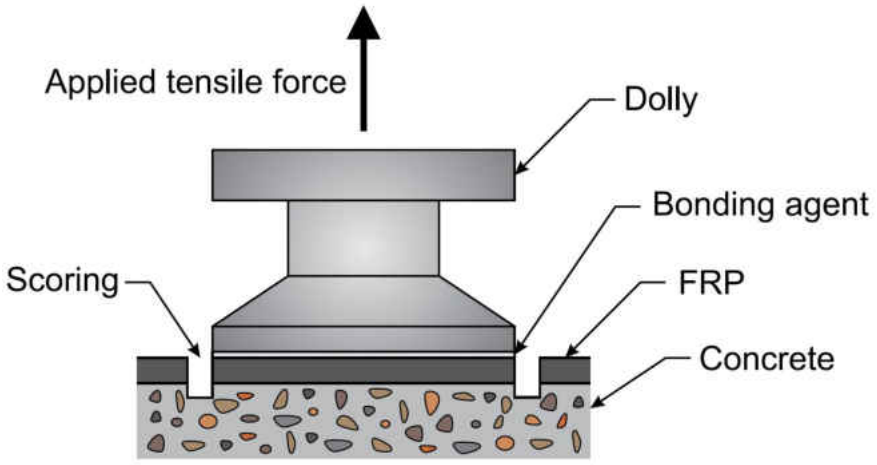


Figure 2.1: Schematic Diagram Showing Pulloff Test Application

## 2.5 Flexural Retrofitting

The most common retrofitting applications of CFRP are flexural strengthening of beams and girders. Flexural strengthening projects for bridge beams and slabs have been carried out in almost every state in the US [2]. Investigations on externally-bonded flexural strengthening started in the late 1980s [2]. It was found that applying externally-bonded FRP to the tension soffit of an RC beam could significantly increase the load bearing capacity of the member. Typically, flexural strengthening is achieved by bonding pre-formed FRP plates or field impregnated fiber sheets to the tension face of the member using a number of different adhesive systems, i.e., epoxy, polyester, vinylester, and polyurethane. Furthermore, different types of reinforcing fiber can be selected depending on the application environment, i.e., glass, aramid, carbon, and basalt.

Extensive research and engineering practices in the past decade proved the efficiency in strengthening RC members in flexure using externally bonded FRP reinforcement. The primary concern for this type of retrofitting is the local de-bonding in the FRP/concrete interfaces, which negatively

affects the structural integrity and long-term durability of strengthened members. Typically when local interface de-bonding initiates, the de-bonding propagates fast and leads to a sudden drop in loads and loss of ductility or brittle failure of the whole FRP/RC composite system. In general, stresses in FRP materials are limited in design guidelines to prevent the failure triggered in the bond line [3]. These guidelines lead to stress limitations preventing high strength FRP to be fully utilized in externally bonded FRP systems in flexural retrofitting applications.

Chajes et al. [17] experimentally investigated fourteen reinforced concrete beams with the same steel reinforcement in. The authors evaluated the strength behavior by retrofitting beams with aramid fabric (1 layer), E-glass fabric (3 layers) and carbon fiber fabric (2 layers) and their thickness of 0.041, 0.056 and 0.048 inches, respectively. They found that use of external composite fabric reinforcement increased the flexural capacity by 36 to 57% and 45 to 53% increase in flexural stiffness.

Brena et al., [18] carried out experiments on twenty rectangular beams. Two beams were control beams and eighteen beams were strengthened using CFRP. Four composite material systems used such as two of which were uni-directional carbon fibers, and the others were woven fabrics and pultruded plates. The CFRP composites were applied to the surface of the beams using four different layouts. In the first layout the composites were attached to the soffit of beams (tension side). In the second layout FRP straps were wrapped around the bottom of the cross section and extended vertically to within 3 inches of the compression face. The third layout had longitudinal composites applied on the sides of the beams rather than on the bottom surface. In the fourth layout the longitudinal composites were applied on the sides of the beams rather than on the bottom surface and transverse straps were applied also on the sides. The author concluded that the de-bonding can be prevented or delayed by adding transverse straps along the shear span. Also the authors concluded that the flexural capacity of reinforced concrete beams can be increased by attaching CFRP laminate than control beams.

Grace, et al. [19] investigated the effect of repeated loading on the flexural response of CFRP strengthened RC beams. Specimens were loaded in a 4-point bending configuration at 3.25 Hz for 2 million cycles, with load ranges at 15%, 25%, or 40% of the ultimate flexural capacity. The study concluded that fatigue did not affect the ultimate load carrying capacity of the strengthened beam. It was noted that for the 40% of ultimate load range that specimens for both CFRP plate and fabric experienced softening without increase in applied load.

Toutanji, et al. [20] investigated the cyclic behavior of reinforced concrete beams strengthened with CFRP sheets impregnated and bonded with an inorganic matrix. The fatigue load ranges were between between 50% and 80% of the ultimate static load capacity. It was concluded that crack initiation and propagation occurs during that first few hundred fatigue cycles. However, since the failure mode was rupture of steel rebar, the study concluded that member deflections and laminate strains are not significantly affected. It was also concluded that due to the higher ultimate strength of CFRP compared to that of steel that the application of CFRP can increase the fatigue load capacity of a strengthened RC member.

The PU- FRP-retrofitted beams under cyclic loading was investigated by Haber [13] The authors concluded that cyclic loading had little or no negative effects on strengthening of this system. Among the conclusions also was that PU retrofitted beams under fatigue loads are expected to crack more due to softer adhesive interface.

### *2.5.1 Flexural Bond*

Bonacci and Maalaj [21] compiled a database of laboratory beam specimens that were tested in flexure with bonded FRP laminates. The study concluded that 69% of laboratory specimens failed via laminate de-bonding. The failure mode most commonly associated with flexural retrofitting of concrete with externally bonded FRPs is laminate de-bonding. De-bonding is a complex mode of

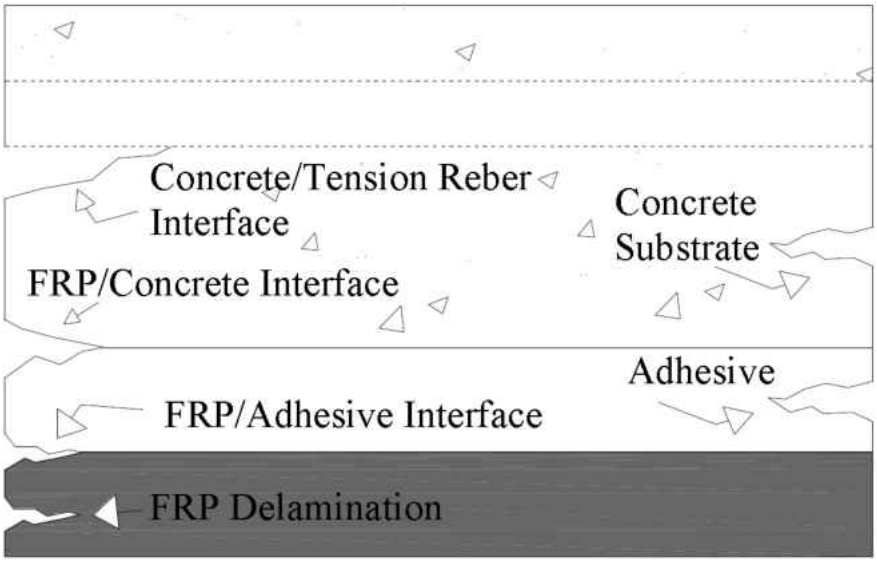


Figure 2.2: Typical Failure Modes Associated with Debonding of FRP from Concrete substrate

failure that depends on a number of variables such as concrete strength, FRP composite properties, and adhesive properties [22]. The debonding modes of failure are shown in figure 2.2[13].

### *2.5.2 Shear Characterization*

In external retrofitting of structures, the performance of the FRP-to-substrate bond is of crucial importance in providing an effective stress transfer. A number of failure modes in FRP-strengthened concrete members are directly caused by de-bonding of the FRP from the concrete. These are shown in figure 2.2 [13]. On the other hand the failure modes in de-bonding of FRP-to-steel would never be in the substrate layer. For the safe and economic design of externally-bonded FRP systems, a sound understanding of the behavior of FRP-to-concrete and FRP-to-steel bond needs to be defined and a reliable bond-slip model needs to be established.

In various de-bonding failure modes, the stress state of the interface is similar to that in a shear

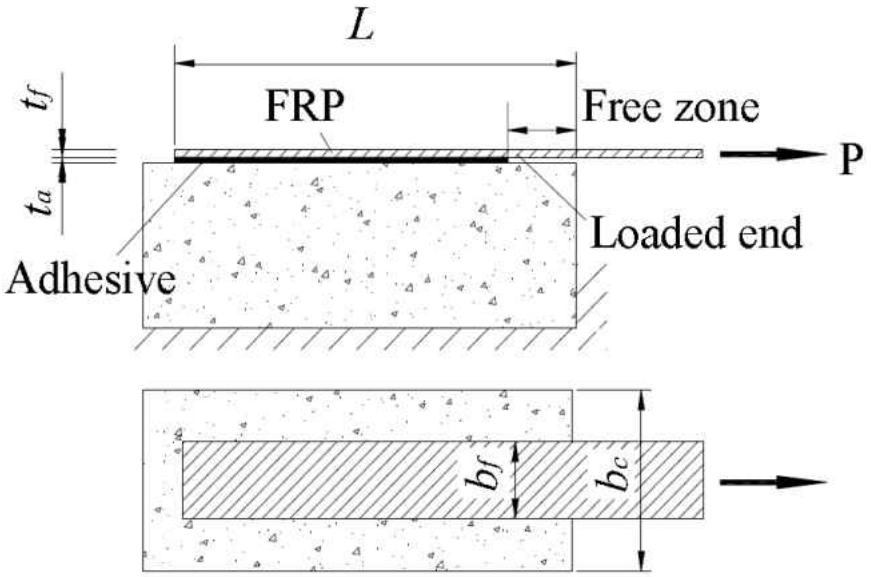


Figure 2.3: Lap Shear Schematic and Test Setup

test specimen in which a plate is bonded to a concrete prism and is subject to tension (figure 2.3). Existing studies only exist for epoxy FRP composites and most suggest that the main failure mode of FRP-to-concrete bonded joints in shear tests is concrete failure under shear, occurring generally at a few millimeters from the concrete-to-adhesive interface [23]. In addition, the plate-to-concrete member width ratio also has a significant effect.

A very important aspect of the behavior of these bonded joints is the transfer length. The transfer length is also known as the effective length. It is a property of the material that defines an effective bond length beyond which an extension of the bond length cannot increase the ultimate load. This transfer length provides the fundamental difference between an externally bonded plates and an internal reinforcing bar for which a sufficiently long anchorage length can always be found so that the full tensile strength of the reinforcement can be achieved.

#### *2.5.2.1 Bond-Slip Models*

Existing research has led to a numerous of bond stress-slip models based on the direct interpretation of results from shear tests [24, 25]. The general process of force transfer from the concrete to the FRP, through bond, is described in figure 2.4. Up to point A, the bond forces vary pretty much linearly from the point of zero force in the laminate to the point where the force in the laminate is a maximum [26]. With continued loading, points B and C are reached on the bond stress versus slip curve with the bond stresses being developed further as the initiation point moves along the specimen. Point D defines the limit of bond and integrating under the bond-stress curve along the effective length, $le$, gives the theoretical maximum force that can be applied to the specimen. Any attempt to increase the applied load beyond this point leads to a rapid shifting of the bond region along the specimen until the initiation point reaches the end of the laminate. In reality, a small increase in force may occur due to variances in the preparation of the glued region and some friction along the debonded length. Nevertheless failure occurs rapidly as the energy stored in the specimen is released and the test becomes unstable [27].

## 2.6 Column Retrofitting

FRP systems have been used extensively in seismic zones for confinement of concrete columns. FRP materials are increasingly being considered for use as wraps/jacket/casings, due to their high strength-to-weight and stiffness-to-weight ratios, corrosion and fatigue-resistance, and overall durability. Several types of FRP systems have been qualified by researchers and practicing engineers for retrofitting circular and rectangular bridge columns. Such systems include wet layups, procured systems, near surface mounted applications. The first two of-which would be investigated in this study. Considerable improvements in ductility factors of have been achieved through the use of FRP column wrapping without considerable stiffness amplifications, thereby maintaining

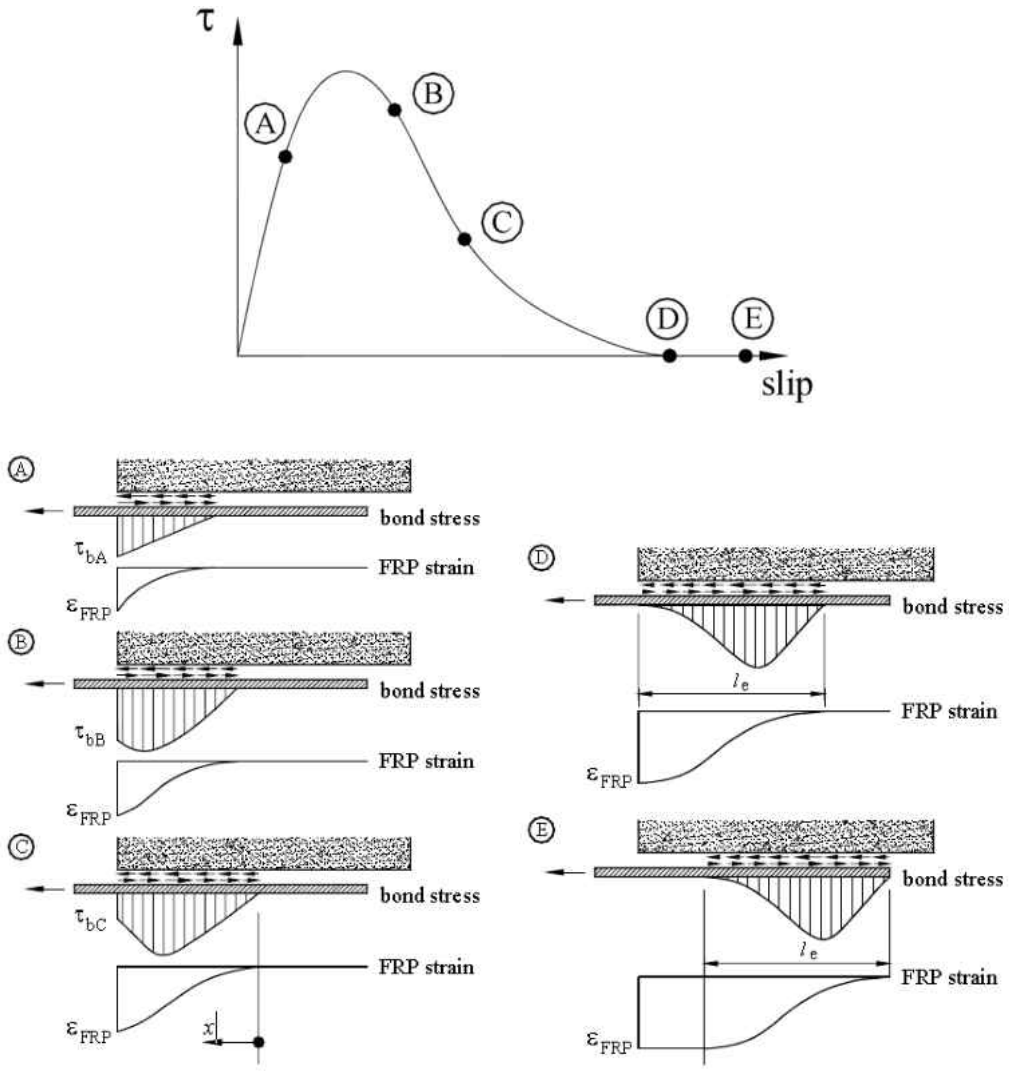


Figure 2.4: Development of Bond Stresses in Single Lap Shear Test

the structure's dynamic properties [28]. The retrofit techniques for reinforced concrete columns, commonly critical components due to lack of redundant vertical load-carrying mechanisms, are aimed at increasing the confinement for the concrete. This follows from the well-known fact that lateral confinement enhances the strength and, more importantly, ductility of reinforced concrete columns.

The majority of structural deficiencies in existing concrete columns can be attributed to lack of transverse reinforcement. This is especially true for columns in seismically active regions, designed prior to the enactment of modern seismic codes. Many older bridges were designed primarily for gravity loads with little or no consideration of lateral forces from seismic loading. Another detail commonly used in the pre-1971 columns is insufficient splicing length of the longitudinal bars at the base of the columns, which is a potential plastic hinge region [28, 29]. As a result of such deficiencies, older columns are more susceptible to premature shear failures, brittle crushing of unconfined concrete and/or reinforcement splice failure when the longitudinal splices are located near a potential plastic hinge region. FRP sheets provide an excellent opportunity to enhance column resistance in all three areas of weakness.

Picher at el. [30] conducted a series of tests on confined circular, square and rectangular concrete specimens. Axial loads were applied to concrete specimens wrapped with different orientation of carbon FRP wraps. It was clearly shown and concluded that the confinement of concrete with CFRP wraps increased the compressive strength and ductility of the tested specimen. The results showed increase in the axial strength of up to 41% and about 500% axial strain increase for cylinders confined with three layers of carbon sheets with fibers oriented in the hoop direction compared to unconfined specimens. The authors also showed that the axial stiffness decreases with the increase of fiber angle orientation; however, the ductility and modes of failure remain the same.

Lateral confinement increases the strength and ductility of concrete in the axial direction. The stress-strain curves of confined concrete show a remarkably enhanced energy dissipation characteristic for confined concrete. Such behavior is of great importance as it can prevent sudden and catastrophic failures structures under overload conditions. Figure 2.5 shows stress-strain curves for confined and unconfined concrete [31].

Many researchers [32, 33] study the effects of confining pressures due to FRP wrapping using the

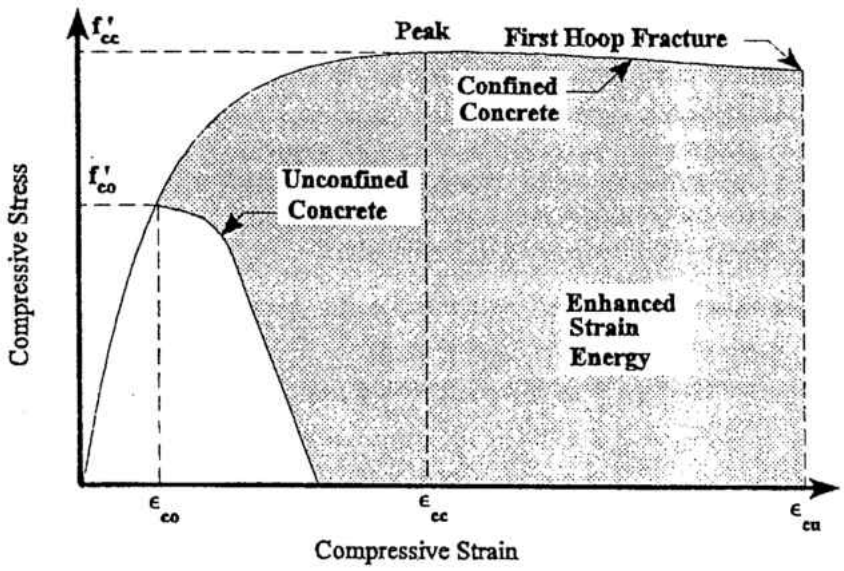


Figure 2.5: Stress-Strain Curves for confined and Unconfined Concrete

mechanics of thin walled cylinders. The confining pressure in a confined column can be determined to be

$$f_r = 2(f_t \cdot t \cdot n)/D \tag{2.1}$$

where $t$ is the thickness of the wrap per layer, $f_t$ is the circumferential stress of wrap, $n$ is the number of wrap layers, and $D$ is the diameter of the concrete cylindrical column.

The maximum confining pressure, $f_{ru}$ is determined by the ultimate tensile strength of the wrap $f_{tu}$ given by:

$$f_{ru} = 2(f_{tu} \cdot t \cdot n)/D = 2(E\epsilon_{tu} \cdot t \cdot n)/D \tag{2.2}$$

where $E$ is the modulus of elasticity of the wrap and $\epsilon_{tu}$ is the wrap ultimate strain. The relationship between confined compressive strength ($f'_{cc}$), unconfined compressive strength ($f'_c$), and the lateral

stress in core concrete produced by confining pressure ($f_r$) is:

$$f'_{cc} = f'_c + k \cdot f_r \tag{2.3}$$

The average value of the confinement effectiveness coefficient $k$ was found to be equal to 4.1 [34]. For circular column with spiral steel, the confining pressure $f_r$ is given by [35].

$$f_r = \frac{2A_{sp}f_y}{d_c s} \tag{2.4}$$

where $A_{sp}$ is the cross-sectional area of the spiral steel, $d_c$ is the outside diameter of the spiral, $s$ is the pitch of the spiral, and $f_y$ is spiral steel yield stress.

Substituting $f_{ru}$ from equation (2.2) into equation (2.3) yields the maximum compressive strength due to confinement with FRP wraps. More generally, for round and rectangular cross sections, the maximum confining pressure may be expressed as [36]:

$$f_{ru} = 0.5\kappa_s \rho_j E \epsilon_{tu} t \tag{2.5}$$

where $\rho_j = 4n/D$ for circular columns, $\rho_j = 2n(d+b)/db$ for rectangular columns, $n$ is the number of layers of wrap, $D$ is the overall diameter of circular column, $b$ is the overall width of rectangular column, and $d$ is the overall depth of rectangular column. $\kappa_s$ is a shape factor determined as the ratio of effectively confined concrete to the gross area of the section and is equal to 1 for circular columns.

Circular and rectangular specimens and full scale columns wrapped with glass and carbon FRPs were studied by Kestner at el. [32]. They found that axial strength and deformation improvements are proportional to jacket strength and stiffness. It was also found that due to the ineffectively

confined concrete region in the square cross sections, the jackets provided to square cross sections were not as effective as those provided to circular cross sections. A shape factor, $\kappa_s$, was used to account for the ineffectively confined regions of concrete within the rectangular and square cross sections.

One of the more recent studies was performed by Rutledge et al. [37] where two damaged RC bridge columns which had buckled longitudinal bars were repaired by relocating the plastic hinge using CFRP. In the study by, the circular columns were tested under a earthquake lateral loading. 6% axial load ratio was applied to represent the super structure mass. The first column was damaged with buckled longitudinal bars. The second column was also subjected to the same loading as the first column with additional cyclic loading to represent "aftershock" loads. The result of the damage phase was also buckled longitudinal bars in addition to concrete failure and spalling. The first column in the study [37] was repaired by having the formed plastic hinge retrofitted with longitudinal and transverse CFRP plates externally anchored to the footing using carbon fiber anchors. CFRP composites were also wrapped around the expected new plastic hinge region (transverse direction) to achieve higher curvature at the new plastic hinge location. This was done with the goal of restoring the displacement capacity at the top of the column. Test results revealed that the repaired column under the same constant axial load and cyclic lateral displacements showed an increase in lateral load capacity compared to that of the original column. However, the plastic hinge region did not form in the expected location. This was attributed to underestimation of the confinement provided by the spiral reinforcement. The repair of the second column was similar to that of the first one, with one difference: CFRP composites were not wrapped around the new expected plastic hinge. The test results of the repaired second column revealed that a similar increase in lateral load capacity compared to the column from the damage phase, and the plastic hinge was relocated to the expected location. The conclusion of the experimental work that the repair procedures were able to restore the initial stiffness and increase the lateral strength capacities.

Figure 2.6: Column Wrapping with FRP (Photo Courtesy of Neptune Research, Inc Website)

An example of a column being wrapping with FRP is shown in figure 2.6.

# CHAPTER 3: EXPERIMENTAL PROGRAM

## 3.1 Introduction

An experimental program was designed to evaluate the mechanical behavior of concrete and reinforced concrete members strengthened with both polyurethane and epoxy FRP composites. The component-level investigations involved small-scale experiments on composite plates (tension tests), single-lap shear tests of laminates bonded to concrete, and small-scale flexural beams (without internal steel reinforcement). The primary focus of the component-level investigations was to investigate the FRP bond to concrete. After the small scale experiments were performed, the larger-scale tests were performed on flexurally retrofitted reinforced concrete girders, and cyclic testing of columns confined with FRP jackets. Each of the component-level investigations is described in more detail in the subsections below. Based on the results, analytical models were generated and calibrated to understand the transfer of forces between the concrete and polyurethane or epoxy laminates. The comparison of analytical and experimental results is presented at the end of the paper, with the bond behavior determined from lap shear testing providing a good model of observed cracking in the flexural specimens. The analytical models enable future investigations on alternative geometries and flexural systems, as well as allowing predictive modeling for the larger-scale testing program.

The component-level tests were performed on all permutations of different fiber and matrix combinations. There were a total of three types of fibers and two types of matrices (polyurethane and epoxy) utilized in the study. In addition, for the polyurethane matrix composites, three different types of adhesives/primers were evaluated. All materials were provided by Neptune Research Inc. (NRI). The three types of fibers considered were a unidirectional carbon (denoted as Uni), a bidirectional carbon (denoted as 12k3k), and a bidirectional carbon/glass hybrid (denoted as VS). All

the fabrics had a weight of 18 oz/yd2 and a thickness of 0.02 in. The bidirectional carbon (12k3k) has 12k tows in the longitudinal (warp) direction and 3k tows in the transverse (weft) direction. The hybrid carbon/glass is a balanced weave with carbon in the longitudinal (warp) direction and glass in the transverse (weft) direction.

The pre-impregnated (pre-preg) polyurethane matrix was paired with each type of fiber as well as each primer/adhesive, for a total of 9 pairs. The same three types of fibers (bare fibers in this case) were also paired with one epoxy system (where the epoxy was used as both the impregnating matrix and the adhesive). The combinations are summarized in Table 2. The three polyurethane primers were labeled Ad1, Ad2, and Ad3 (detailed below).

- Ad1 is the same type of water-cured polyurethane used in the matrix of all the prepreg fibers in this paper.
- Ad2 and Ad3 are similar in chemical content (also polyurethane based), but with major differences in the consistency and viscosity of the adhesives prior to application and difference in cure time. Ad2 is more viscous than Ad3.

A total of three specimens per combination from table 3.2 were prepared and tested. The epoxy composite system was installed on the specimens using a wet layup procedure. The manufacturer provided the dry fibers and the same type of epoxy for the primer and matrix of composite. The concrete blocks were primed with epoxy. After the epoxy became slightly tacky (2 to 3 minutes after the primer application), the dry fiber was laid and more epoxy was placed on top and rolled with a FRP roller to ensure complete impregnation of the fibers in the matrix. In the case of PU specimens, each different primer was placed on the concrete blocks until they become slightly tacky, then the pre-impregnated FRP composite was placed on the top of the primer after being misted with water to catalyze the curing procedure. After laying the PU composites on the concrete

Table 3.1: Fabric Properties

| | **Uni)** | **12k-3k** | **ViperSkin** |
|---|---|---|---|
| Weave and Fiber Type | Unidirectional Carbon | Bidirectional Carbon | Bidirectional hybrid: Carbon in long direction and Glass in Transverse |
| Weight (oz/yd$^3$) | 18 | 18 | 18 |
| Thickness (in) | 0.02 | 0.02 | 0.02 |

Table 3.2: Combinations of Fibers, Matrices, and Primers for Steel and Concrete Specimens

| **Fiber** | **Primer** | **Matrix** |
|---|---|---|
| Pre-impregnated Uni | Ad1, Ad2, Ad3 | PU |
| Bare Uni | Epoxy | Epoxy |
| Pre-impregnated 12k-3k | Ad1, Ad2, Ad3 | PU |
| Bare 12k-3k | Epoxy | Epoxy |
| Pre-impregnated ViperSkin | Ad1, Ad2, Ad3 | PU |
| Bare ViperSkin | Epoxy | Epoxy |

blocks, the laminate was rolled for 15-30 minutes to ensure that there are no air bubbles (carbon dioxide) in the adhesive layer.

The larger scale concrete girders were poured on February 11, 2011. Concrete cylinders were taken and the slump was measured at 3 inches. The control girder was tested on March 28, 2013. Based on the results from the control beam, the damage loading protocol was generated. The damage phase for the 8 beams occurred between March 28, and March 30th of 2013. The girders were repaired after the damage phase and epoxy-injected between April 24 and April 25 of 2013. Concrete cylinders were tested between March 30th and April 30th. The average concrete strength was 6325 psi. The concrete design mix details can be found in Appendix B. Three FRP systems were used in retrofitting of the damaged girders: Titan 118, LV Titan 118 and Viper Skin 118.

Table 3.3: Reinforced Concrete Girders Testing Matrix

| **Specimen ID)** | **Damage Ductility Level** | **Repair System** |
|---|---|---|
| 0 (Control) | Complete Failure | None |
| 1 | 1 | Titan 118 (EP) |
| 2 | 1 | Viper Skin 118(PU) |
| 3 | 1 | Viper Skin 118(PU) |
| 4 | 1 | LV Titan 118 (EP) |
| 5 | 1 | LV Titan 118 (EP) |
| 6 | 1 | Titan 118 (EP) |
| 7 | 3 | Viper Skin 118 (PU) |
| 8 | 2 | Viper Skin 118 (PU) |

Titan 118 and LV Titan 118 are epoxy based systems. Viper-Skin 118 uses a pre-impregnated PU matrix FRP composite with the same PU materials used as a primer. All 3 systems use the same type of unidirectional carbon fiber. The testing matrix is shown in table 3.3.

The concrete columns were poured on January 07, 2013. Concrete cylinders were taken and the slump was measured at 8 inches. The control column was tested on November 13, 2014. Based on the results from the control column, the damage loading protocol was generated. The damage phase for the 6 columns occurred between December 7, 2014, and January 26, 2015. The columns were repaired after the damage phase and epoxy-injected between February of 2015. Concrete cylinders were tested February 5, 2013 and June 7, 2013. The average concrete strength was 7023 psi. Three FRP systems were used in retrofitting of the damaged girders: Titan 118 (epoxy), and Viper Skin 118 (PU) All systems use the same type of unidirectional carbon fiber. The testing matrix is shown in table 3.4. The concrete design mix details can be found in Appendix B.

Table 3.4: Reinforced Concrete Columns Testing Matrix

| **Specimen ID)** | **Damage Ductility Level** | **Repair System** |
|---|---|---|
| 1 | Complete Failure (Monotonic Lateral with Axial Load) | Viper Skin 118(PU) |
| 2 | 4 (Monotonic Lateral without Axial) | Viper Skin 118(PU) |
| 3 | 1 | Titan 118 (EP) |
| 4 | 2 | Titan 118 (EP) |
| 5 | 1 | Viper Skin 118(PU) |
| 6 | 2 | Viper Skin 118(PU) |

Table 3.5: Concrete Mix Details for Small Scale Beams

| | |
|---|---|
| **Cement Type** | Portland Type I/II |
| **Maximum Aggregate Size** | 1 in |
| **Specified 28 Day Strength** | 5000 psi |
| **Measured Slump** | 3.75 in |
| **Average Strength (June 1, 2011 Just After Test Completion)** | 6100 psi |

## 3.2 Small Scale Flexural Beams

Along with the lap shear specimens, all the small-scale concrete beams were poured on February 11, 2011 in the UCF structures laboratory. During casting, 90 (4 in x 8 in) concrete cylinders were poured according to ASTM C39. Details regarding the concrete mix used for small-scale beam specimens can be found in table 3.5. All specimens were allowed to cure undisturbed in forms for a minimum of 7 day prior to removal. During curing, forms were covered with plastic to ensure minimal escape of moisture.

Once removed from forms, beams were prepared for application of FRP. The substrate surface of

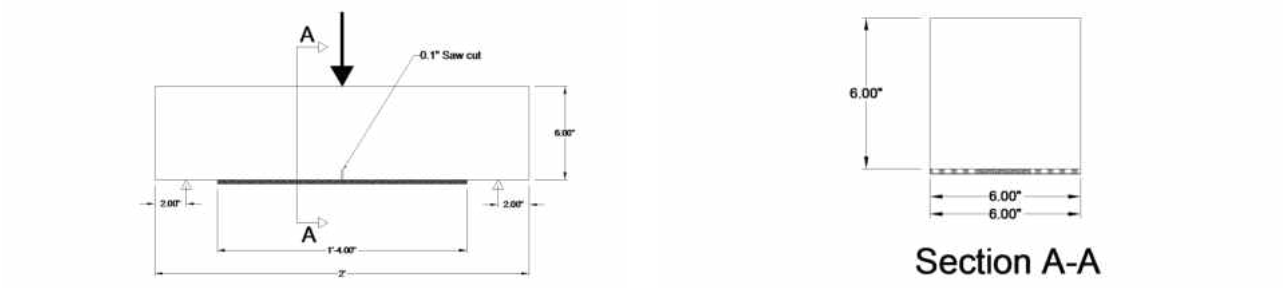


Figure 3.1: Small Scale Flexural Test Setup for Concrete Beams

each beam was treated with a grinder to remove the thin layer of cement and exposing the aggregate where the FRP would be laid. Also, a 0.1 in saw cut was introduced in the mid span to initiate the flexural crack at the specified location. A single layer of FRP was applied to each beam and a single 5 mm foil-backed strain gage was installed at mid span. The bond length was 16 in, 8 in on each side of the induced crack (saw cut).

The testing employed a three-point bending configuration. Displacement measurements were taken at the mid-span of specimens using one Duncan 9600 series LVDTs and at the two supports using an LVDT of the same type. The LVDT displacements are representative of the section displacements at the LVDT location. On the other hand the table displacements obtained from the UTM measure the relative displacement of the beam at the load location with respect to a global axis. The table displacements include any support or local displacements that affect the global displacement of the beam. This small-scale beam flexure test setup is shown in figure 3.1 and photographs taken during testing can be found in figure 3.2. A total of 40 beams were tested for each type of substrate. 3 control unreinforced beams and 3 beams for each combination of fibers and primers (27 PU FRP composite reinforced beams and 9 epoxy FRP composite reinforced beams).

Figure 3.2: Photos from Small Scale Flexure Test

## 3.3 Lap Shear

All the lap shear specimens were poured along with the small scale concrete beams and a brief description of the pour and concrete properties is found in table 3.5. The direct lap shear method shown in figure 2.3 was implemented in this experiment to get the bond properties, where the following were dimensions were used: $L$ = 6 in, bonded length $L_b$ = 4 in, $b_f$ = 2 in, and $b_c$ = 4 in.

The free 2 in free zone is an un-bonded length of FRP introduced at the loaded end in order to prevent a transverse shear failure of the concrete at the edge closest to the loaded end. Five 3 mm foil-backed resistive strain gages were installed along the length of the bonded region. A schematic of the lap shear experimental setup and details regarding the gage locations can be found in figure 3.3. A photo of the test setup is shown in figure 3.4. While the experiment is designed to impose a state of pure shear between the laminate and the concrete, the true behavior inadvertently includes some out of plane stresses, in addition to normal stresses within the concrete due to the boundary conditions of the concrete block.

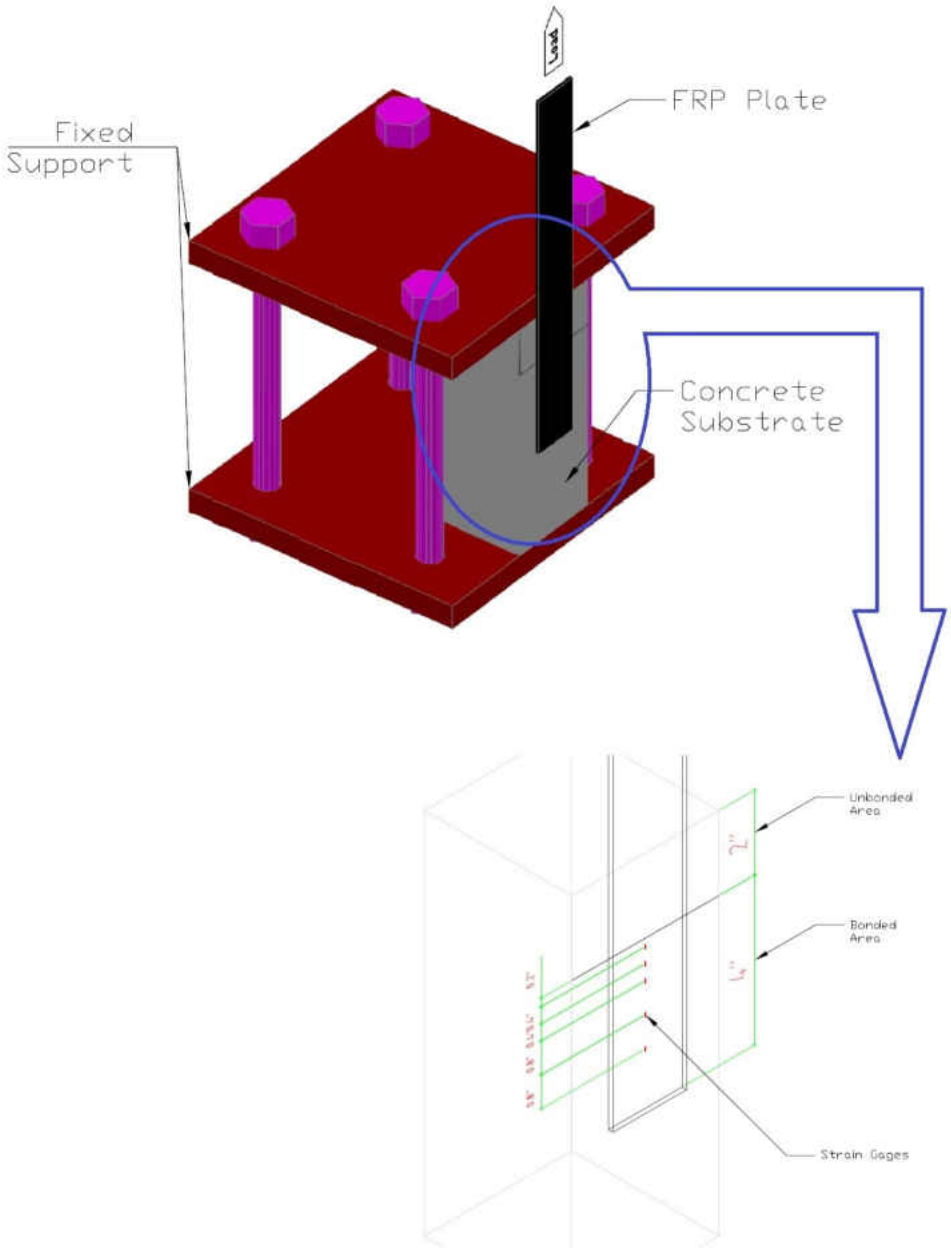


Figure 3.3: Lap Shear Instrumentation

Figure 3.4: Lap Shear Test Setup Photo

## 3.4 Large Scale Girders

Nine reinforced concrete girders were designed, built and tested at a full scale at the UCF structures lab. figure 3.5 shows half the span of the girders. The other half is symmetrical. 4 point bending tests were performed for a clear span of 102 inches. The 2 loads were applied mid-span with 12 inches separation. Linear variable differential transformers (LVDTs) were used to measure the mid-span and end displacements. A photo of the setup is shown in figure 3.6.

General use foil strain gages with 3 mm and 6 mm gage lengths were used to monitor the strains

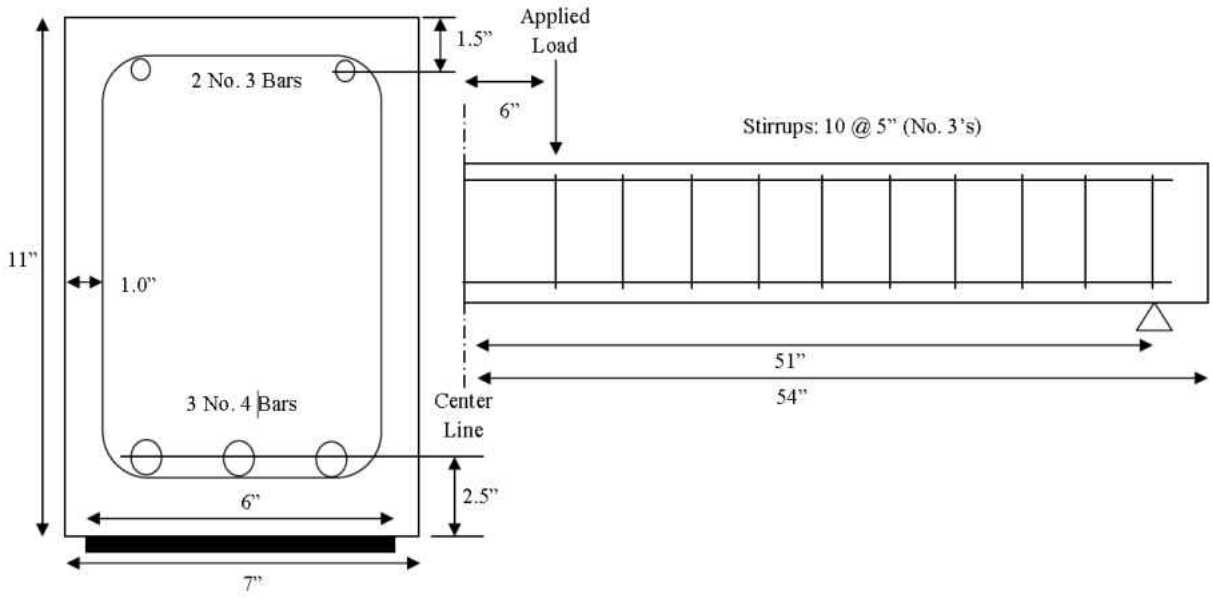


Figure 3.5: Large Scale Girder Test Setup for Retrofitting with FRP

in the rebar and concrete during the experiment. The strain gage instrumentation is shown in figure 3.7. Strain gages were installed at the concrete surface before the damage phase. During the damage phase some of the strain gages were lost and replaced with 5 mm general purpose foil strain gages. After the repair was done, 5 mm general purpose strain gages were installed on the FRP at the same locations shown in figure 3.7.

The reinforced concrete girders were designed per ACI 318-08 [16] to allow the reinforcing steel to yield at a combined load of 13 kips and the concrete crushing to occur at 14 kips. The design was based on an assumed concrete compressive strength of 5000 psi, grade 60 reinforcing steel ($F_y$ = 60 ksi) and without any FRP retrofitting, the reinforced concrete beams were designed to allow the reinforcing steel to yield at a combined load of 13 kips and the concrete crushing to occur at 14 kips. The ultimate design shear capacity of the girders exceeded 32 kips.

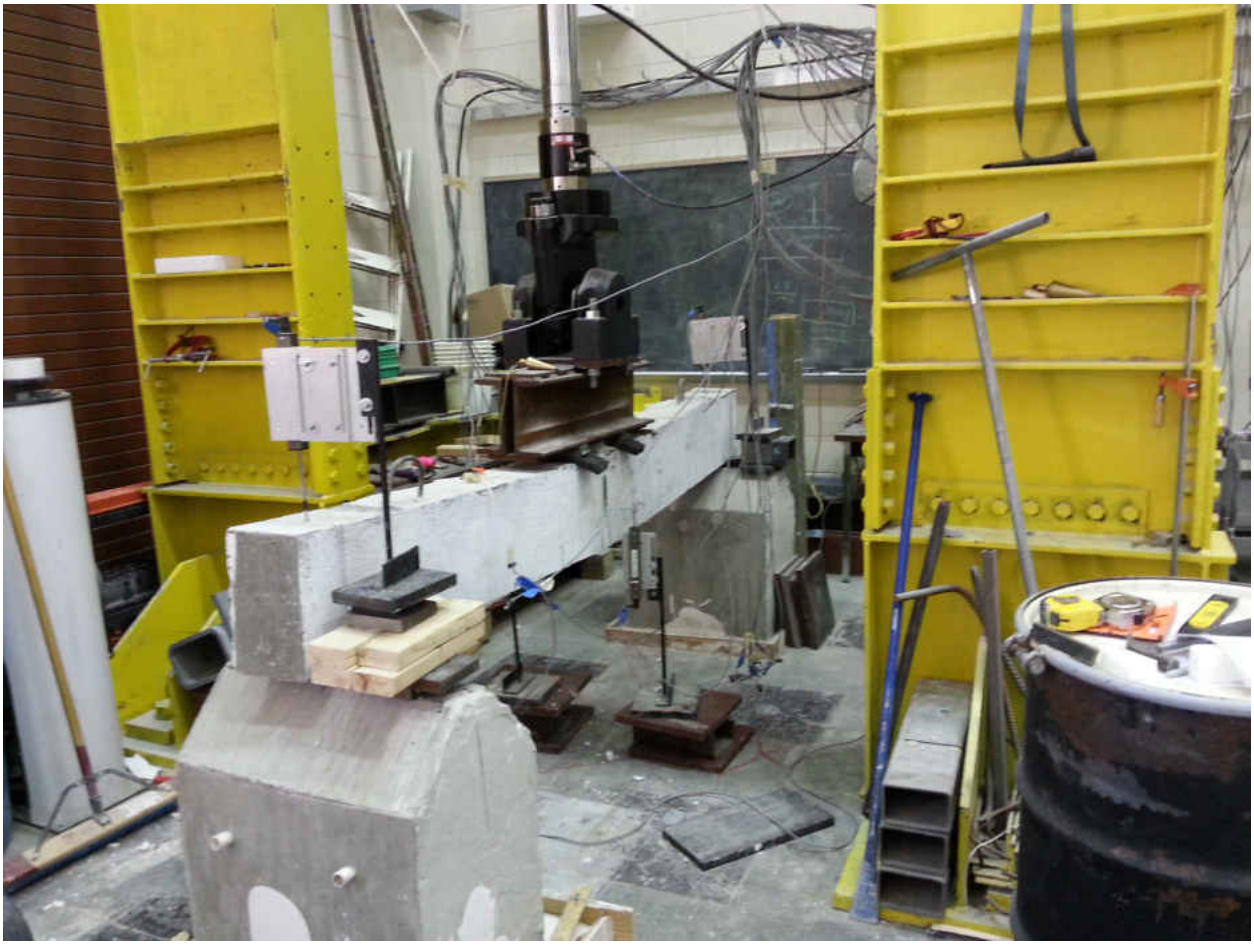

Figure 3.6: Large Scale Girder Test Setup for Retrofitting with FRP

## 3.5 Medium Scale Columns

The 6 circular columns were constructed using bridge design typical details of bridges in California in accordance with the Seismic Design Criteria [38]. The structural configuration is similar to columns tested at University of Nevada at Reno [39]. The scaling factor is 1/4, therefore the diameter was 12 in. and the height 54 in. yielding an aspect ratio was 4.5, which allows for flexural dominated behavior [39]. The columns were reinforced with 10 Number 4 deformed longitudinal

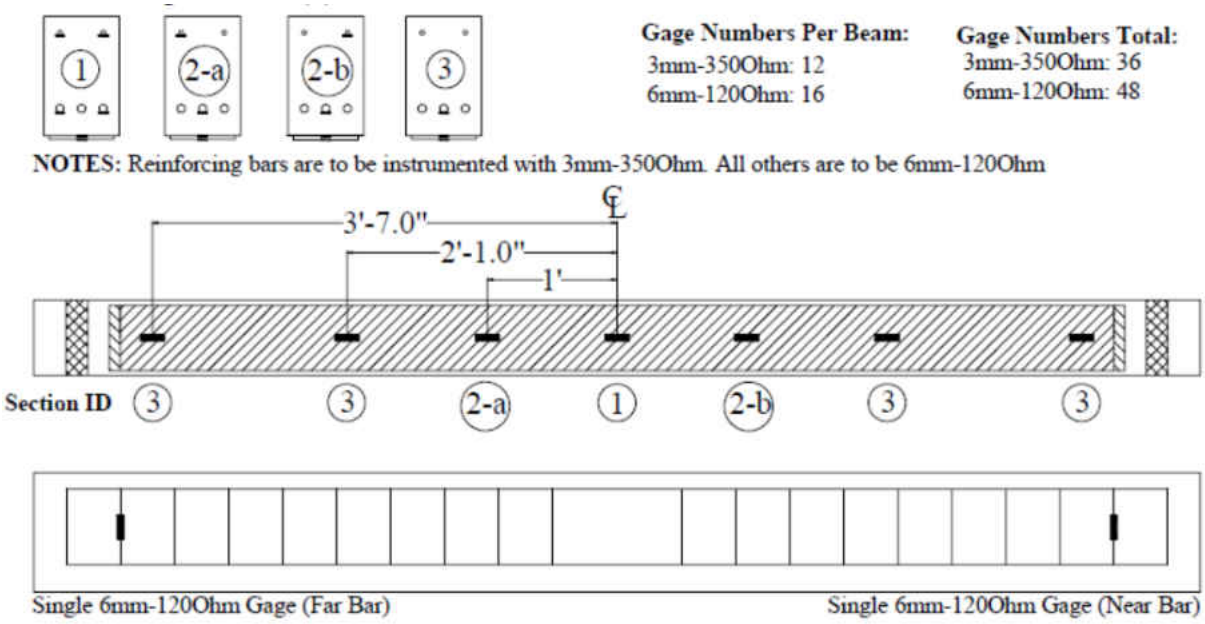


Figure 3.7: Large Retrofitting with FRP

bars, distributed uniformly around the perimeter and fully developed with 90 degree hooks in the footing. This resulted in a longitudinal reinforcement ratio of 2%. The confinement consisted of a continuous spiral made from steel wire reinforcing (W5.0) steel wire with a diameter of 0.25 in. and a pitch of 1.5 in. The clear cover was set to 0.75 in. and the resulting volumetric ratio of the spiral reinforcement was 0.92%. Because the confining effect of spiral steel was based on outward hoop stress and not the development bond stresses, using undeformed wire was acceptable. The column details are shown in figure 3.8, figure 3.9 figure 3.10. A photo of the column reinforcing prior to concrete placement and forming is shown in figure 3.11.

The column setup is shown in figure 3.12. The concrete footing was attached to a reaction block (Reaction Block 2) using four 1" diameter post-tensioned rods. One MTS Actuator was attached to the second reaction block using four 1" diameter post-tensioned rods. This actuator applied

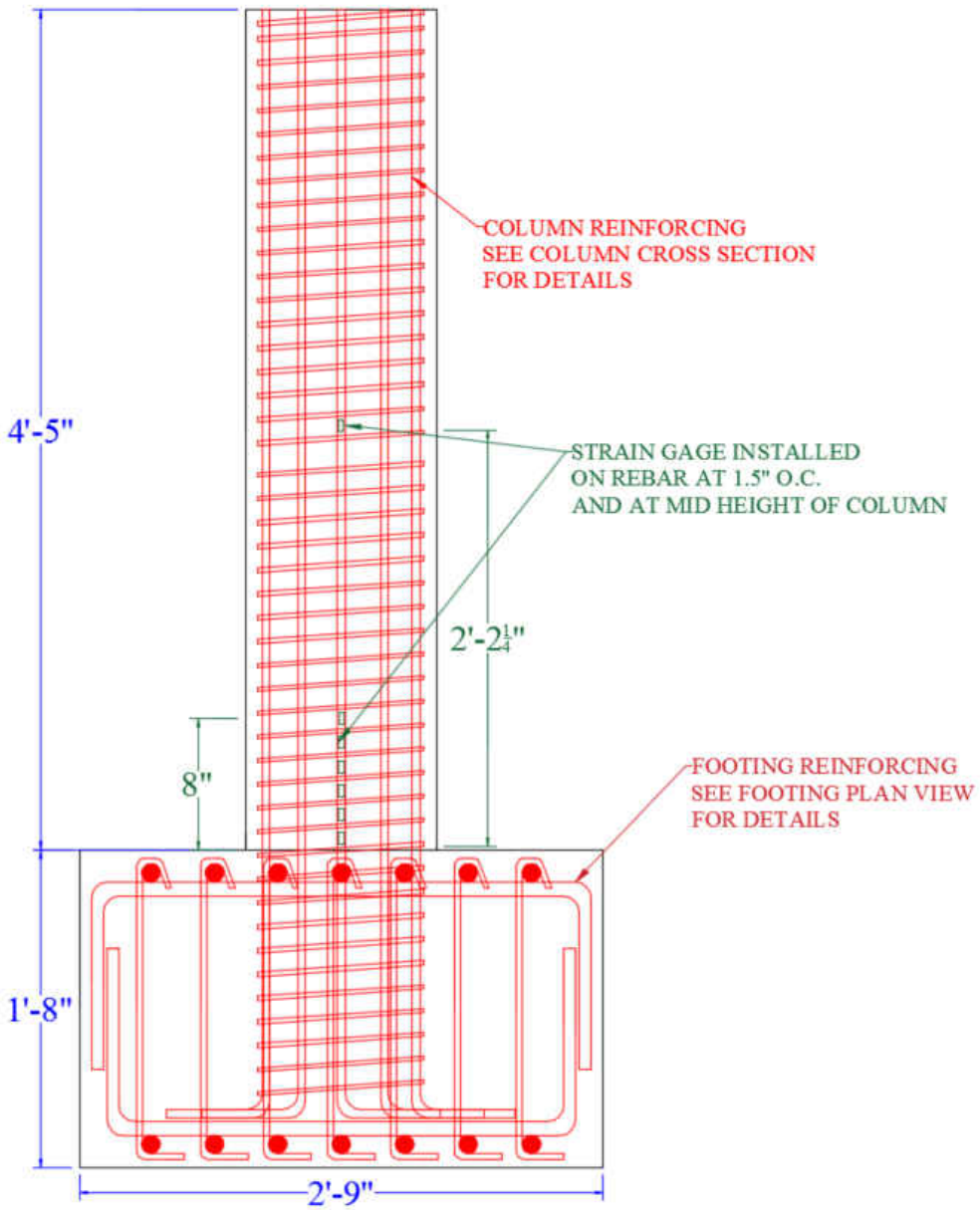


Figure 3.8: Column Specimen Reinforcement and Strain Gage instrumentation

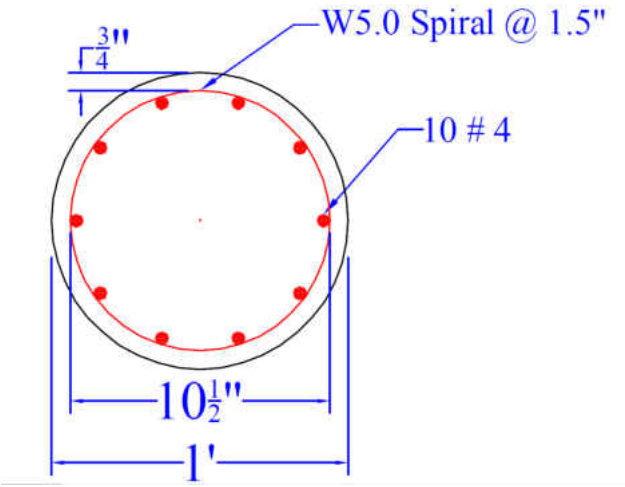


Figure 3.9: Column Specimen Cross Section

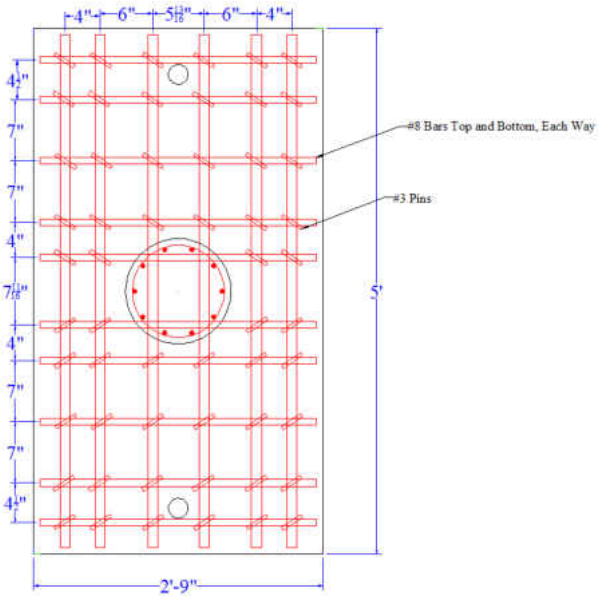


Figure 3.10: Column Specimen Footing Detail

Figure 3.11: Photo of Column Reinforcing

the axial load on the column to represent the superstructure mass which was defined as 40 kips, which is equivalent to an axial load of 6% of $A_g f'_c$. The second MTS Actuator was attached to the structural steel built-up reaction frame. This actuator was used to apply the lateral load on the columns. The steel reaction frame and concrete reaction blocks were attached to the laboratory's strong floor using 2.5" post-tensioned rods. The reaction blocks were grouted after the PT rods were tensioned.

General use foil strain gages with 3 mm and 6 mm gage lengths were used to monitor the strains in the longitudinal rebar during the different phases of the experiment. The strain-gage instrumen-

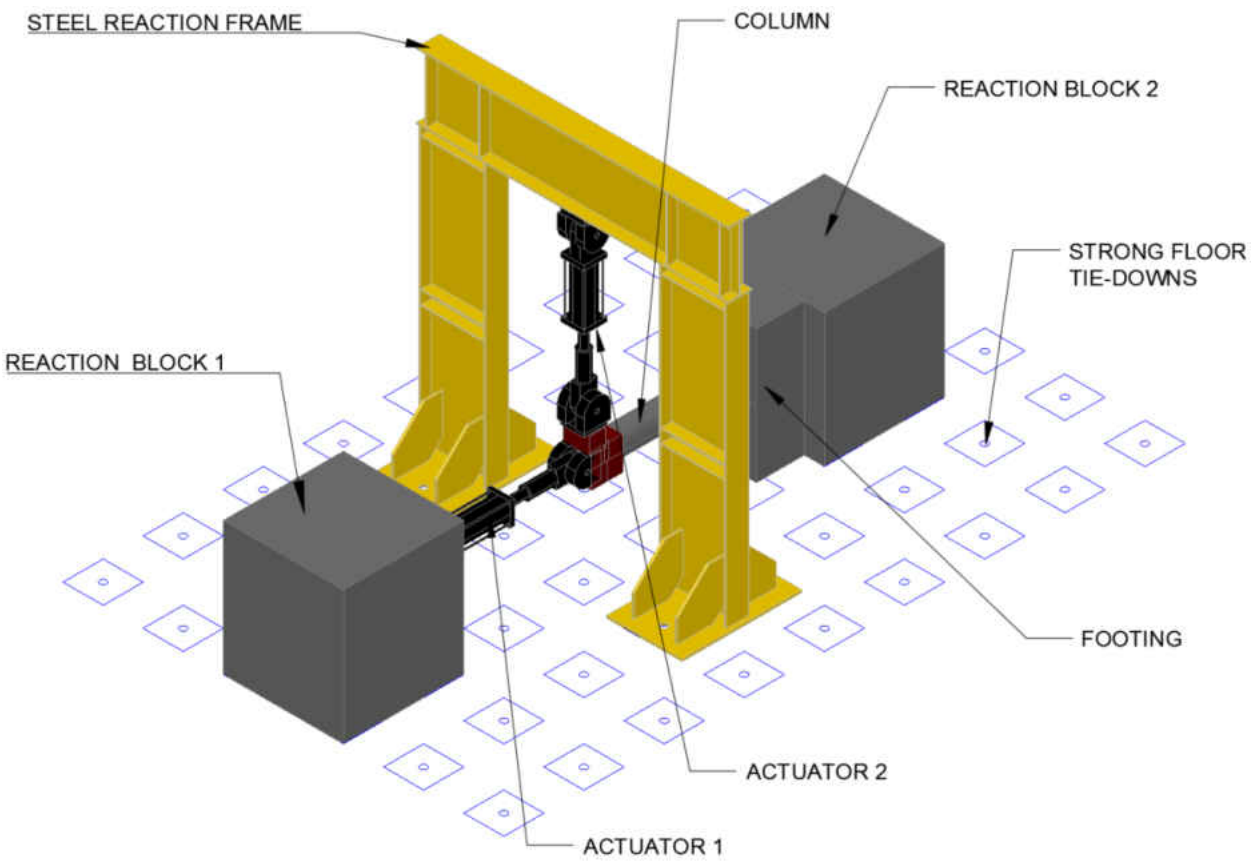


Figure 3.12: Column Setup at The UCF Structures Laboratory

tation is shown in figure 3.8. Many strain gages were lost while the columns were stored outside the Stormwater Lab at the UCF main campus even though protection was provided.

# CHAPTER 4: EXPERIMENTAL TESTING AND RESULTS

## 4.1 Lap Shear Experimental Results and Bond-Slip Models from Experimental Data

Experimental strains along the FRP plate have been post-processed to calculate shear stress and slip distributions along the bonded lengths. Denoting by $x_i$ the strain gauge position and $\epsilon$, the corresponding measured strain, the average value of shear stress between two subsequent strain gauges can be written as:

$$\bar{\tau}_{\frac{(i+1)}{2}} = \frac{E_p A_p(\epsilon_{i+1} - \epsilon_i)}{b_p(x_{i+1} - x_i)} \tag{4.1}$$

With $A_p$ being cross section of the composite. Moreover, assuming, for the sake of simplicity, perfect bonding (no slip) at the last strain gauge position and neglecting concrete strain with respect to FRP counterpart, integration of strain profile gives the following expression for the slip at $x$, with $x_i \leq x \leq x_{i+1}$ :

$$s(x) = s(x_i) + \int_0^x \epsilon(x)\, dx \; = s(x_i) + \frac{\epsilon_{i+1} - \epsilon_i}{x_{i+1} - x_i} \cdot \frac{x^2}{2} + \epsilon_i x \tag{4.2}$$

The above equation is used to compute the average slip between the two positions $x_i$, $x_{i+1}$, denoted by $s_{i+1}/2$. When computing shear stresses and slips, some irregular values in FRP strain profiles for high loadings have been removed. For the four bonded lengths, shear stress - slip data obtained from experimentally measured FRP-strains.

The bond slip models were obtained for all the systems. Figure 4.1 shows the bond slip models for the PU matrix Uni + Ad1 to concrete, and figure 4.2 shows the bond slip model for the Uni epoxy system to concrete. The slopes of the shear stress-slip are very close, while the peak shear stress is greater for the reference specimens. The peak shear stress depends not only on the maximum load,

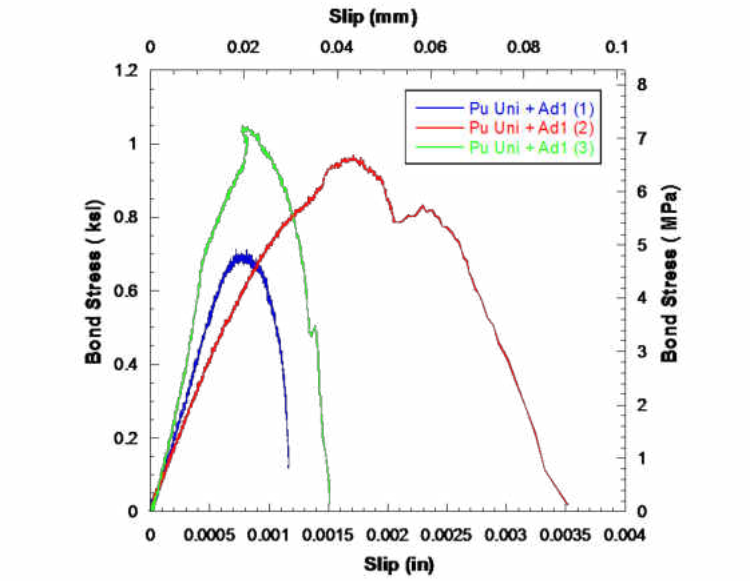


Figure 4.1: PU Matrix Uni + Ad1 Bond Slip Model

but also on the distribution of the stresses along the bond length.

The epoxy systems have consistently higher local bond strengths and higher stiffnesses (initial slope of the bond-slip curve) than the polyurethanes. Figure 4.1 illustrates the similar stiffness and strength values obtained between specimens, attributable to the consistent failure of all polyurethane systems in the adhesive layer. The epoxy Uni (1) specimen results in an unusual bond-slip curve because of the fluctuations observed in the strain data recorded in the top strain gage. The bond-slip curve obtained by post-processing the shear stress data between the second and third gages yields a curve similar to the other two; however, with a lower peak stress. The bond-slip curves were subsequently fit for inclusion in the analytical models, as described in the finite element section of the dissertation.

The average bond stresses at ultimate load (ultimate load divided by the total bonded area) for all

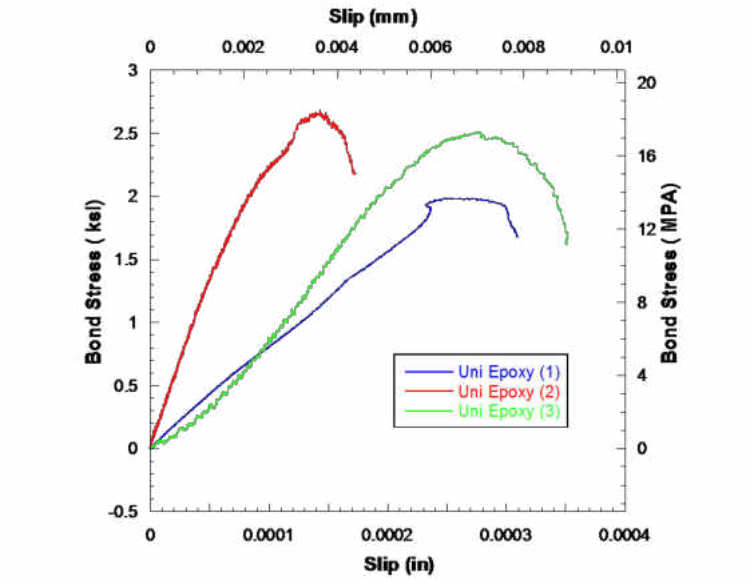


Figure 4.2: Epoxy Uni Bond Slip Model

of the concrete specimens are shown in figure 4.3, separated by composite system and specimen number. While the local bond strength from the bond-slip curves indicates the peak interfacial shear stress the adhesive can transfer at a material point, this plot is more representative of the transfer length and consistency of bond over the entire bonded area. For example, the epoxy local bond strength was approximately 2.5 times the polyurethane for the Uni fabric (figure 4.2), whereas the average bond stresses at ultimate load are approximately equal. The Ad2 primer was even more successful at bond promotion and resulted in typically a 50% increase in average bond stress over the epoxy counterparts, except for the hybrid fabric (VS).

As mentioned previously, the polyurethane specimens all failed in the adhesive layer, as shown in figure 4.4. These types of failures are consistent with other published work [26, 13]. Of the three polyurethane primers, only Ad3 yielded inconsistent results, exhibited both in the average bond

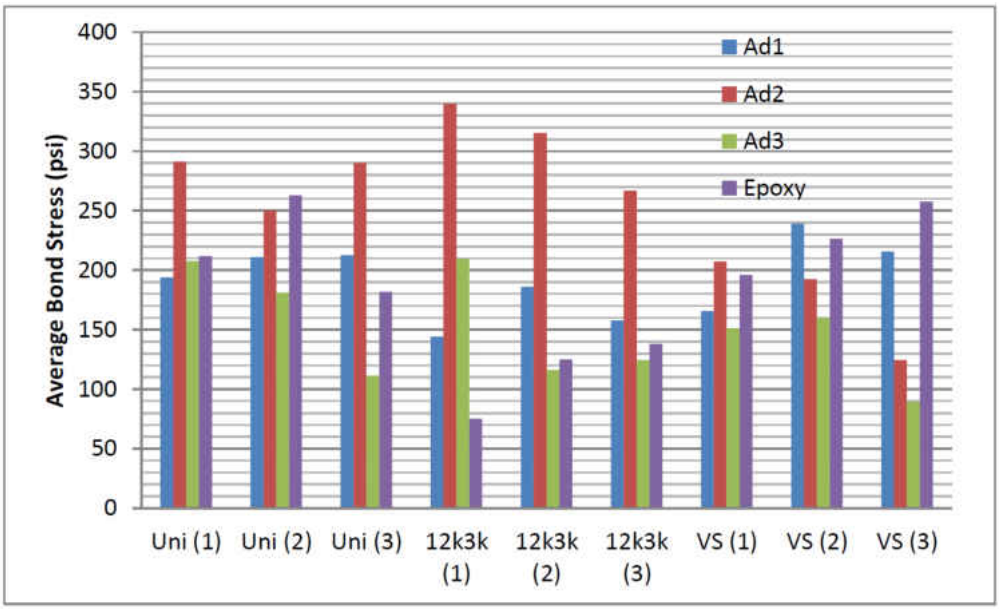


Figure 4.3: Average Shear Bond Stress at Ultimate Load from Lap Shear Experiments

stress, as well as the uniform failure in the adhesive layer. Interestingly, this may have been related to not only the increased mechanical properties of the primer, but also the ability of the primer to penetrate the top concrete substrate layer to promote bond. However, this caused occasional failure within the substrate, which is the failure mode typical of all the epoxy lap shear specimens, as seen in figure 4.5. The right image in figure 4.5 shows the substantial thickness of concrete substrate that remains on the laminate after failure that is typical of both the lap shear specimens as well as the flexural specimens discussed next. This failure in the top layer of substrate also implies the resulting bond-slip relationships are not indicative of purely the behavior of the adhesive, but also contain a component of the cohesive energy of the concrete itself.

Figure 4.4: Photo of a Typical PU FRP Composite Lap Shear Failure

## 4.2 Small Scale Flexural Beams Experimental Results

The results of the load versus displacement of polyurethane Uni + Ad1 and epoxy Uni FRP-reinforced beams are presented in figure 4.6 and figure 4.7, respectively, consistent with the systems presented from the lap shear testing. These two figures show the behavior of the strengthened beams for each composite system compared with the non FRP-reinforced control beams. The strengthened beam response followed a characteristic progression of initial concrete cracking (small drop in load) after the elastic region, post-cracking stiffness representative of the contribution of the bond between concrete and the laminate, and an ultimate load governed by debonding failure of the laminate. Due to the presence of the saw cut at the center of the beam and the three-

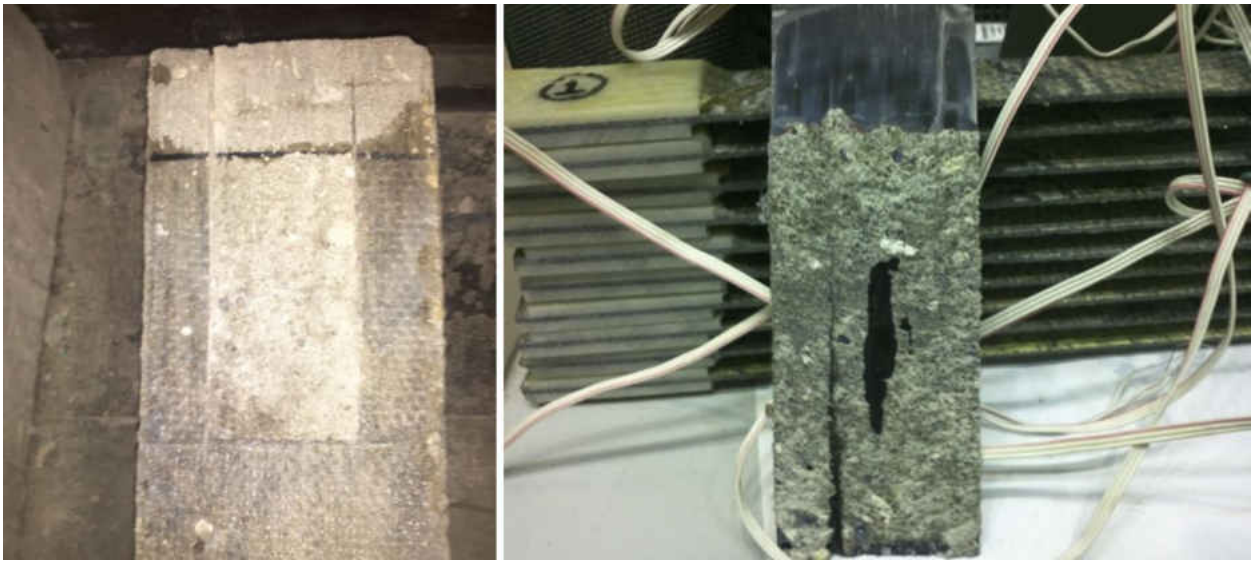

Figure 4.5: Photo of a Typical Epoxy FRP Composite Lap Shear Failure

point loading, the flexural crack opens and continued to widen in all the specimens. However, the epoxy specimens tended to also crack at additional locations near the saw cut, as discussed in more detail below.

Comparison between the plots in figure 4.6 and figure 4.7 illustrates distinctive differences between the epoxy and polyurethane behaviors. The additional stiffness of the epoxy delays the initial crack formation, and results in a higher cracking load (also less noticeable drop in the load at cracking). However, after cracking, the additional strength and stiffness of the epoxy bond does not allow the beam to reach the same ultimate load as the case of polyurethane. This is because of the selected bond length and the ability of the polyurethane to redistribute the stress more evenly over the bonded region, as illustrated in figure 4.3 with the average bond stress at ultimate load.

All tested polyurethane systems, with the exception of the systems employing Ad3, reached significantly higher ultimate loads than the epoxy systems. Debonding, in both PU and epoxy specimens,

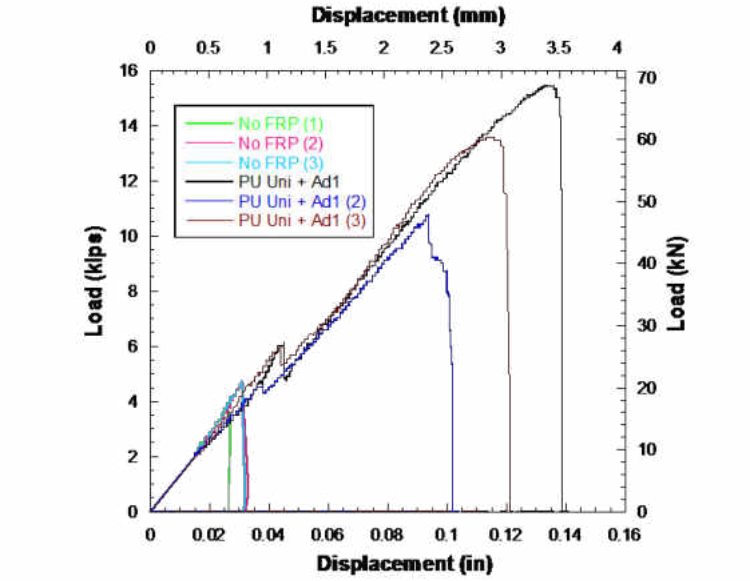


Figure 4.6: Load Versus Displacement for PU Uni + Ad1 Compared with Unreinforced Beams

initiated near the flexural crack in the midspan of the FRP-reinforced beam and propagated outwards towards the end of the FRP plate. The crack forms at a load only slightly higher than the non FRP-reinforced control beams, and none of them were able to delay the cracking load as much as the epoxy systems. The significant drop in load after cracking was a result of immediate transfer of stress to the laminate, and an opening of the flexural crack at the saw cut location. The characteristic failure mode of all the polyurethane specimens is a clean flexural crack in the center after debonding, as shown in figure 4.8.

The epoxy systems fail when the cohesive energy of the top layer of concrete is reached, which happens sooner because of the shorter transfer length. This is apparent from viewing the common failure mode of the epoxy systems (see figure 4.9), whereby the initial flexural crack opens, but also additional flexural cracks approximately 1 in to each side of the saw cut. At the ultimate

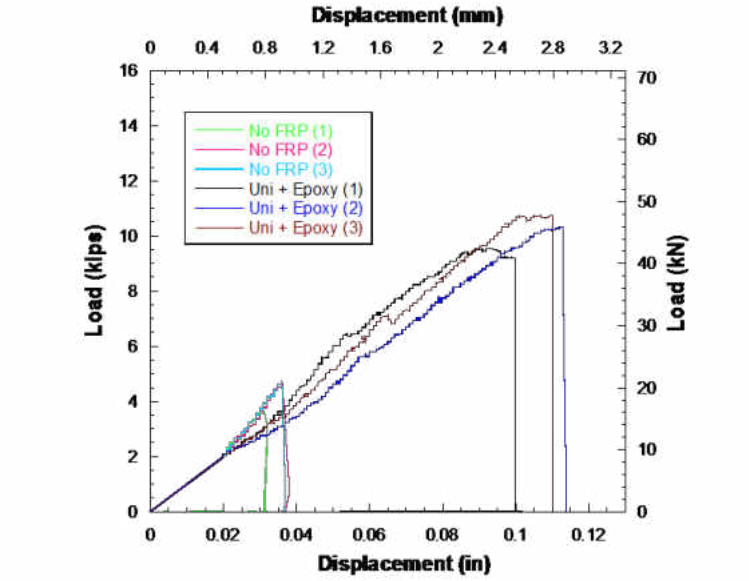


Figure 4.7: Load Versus Displacement for Epoxy Uni Compared with Unreinforced Beams

failure load, the cracks are joined by a diagonal shear crack that results in a triangular wedge of concrete that separates with the laminate, referred to as a mixed-mode failure in this paper.

It is concluded from the flexural tests that the polyurethane systems are a viable retrofitting solution when compared to the epoxy system, when based on the criteria of the ultimate load that is reached after the cracking of the section rather than the normal or shear strength of the matrix alone. As in the lap shear results, the ultimate shear capacity is dependent on the stress distribution along the interface and not only the local bond strength. The flexibility of the polyurethane system allows a better distribution of the stresses along the interface and therefore can outperform stronger epoxy systems under the static loading considered in the study.

Figure 4.8: Polyurethane Uni + Ad1 De-bonding in Adhesive Layer

## 4.3 Large Scale Girders Experimental Results and Findings

### *4.3.1 Damage Phase*

From table 3.3 which shows the girder testing matrix, the first control beam was tested without any FRP retrofitting. The load vs displacement results are shown in figure 4.10. The loading was paused at increments of 5 kips and the cracks were marked. The control beam failed in a progressive manner: Concrete cracking in tension zone, tension steel yielding, and finally concrete crushing. The global yielding of the girder occurred at a load of 12.4 kips at and a displacement

Figure 4.9: Epoxy Uni De-bonding in Substrate Layer plus Mixed mode Failure in Concrete

of 1.2 inches. The concrete crushing in the compression zone occurred at a load of 16.9 kips and a displacement of 2.3 inches. The loading continued until a displacement of 4 inches was reached and one of the tension bars ruptured. Photos from the loading procedure are shown in figure 4.11.

Based on the results obtained from the control, the damage phase loading protocol was generated for the remaining 8 girders. The loading protocol is shown in figure 4.12. The loading protocol is based on the ICC AC 125 sinusoidal loading protocol [1] but altered in order to prevent subjecting the bottom beam (which would be FRP-retrofitted) to compression. The maximum load and displacement levels achieved during the damage phase are shown in figure 4.13.

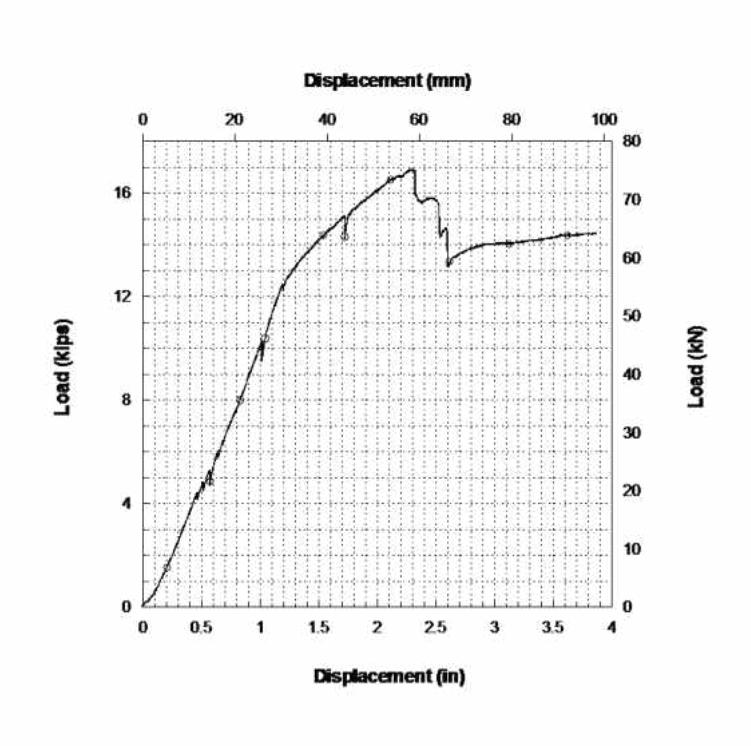


Figure 4.10: Girders Control: Load vs. Displacement

### *4.3.2 Repair Phase*

To understand the bond behavior, the girder FRP repair system was designed with the intension that debonding would occur and not laminate rupture. At the time, the girder testing commenced, the bond characteristics were not clearly defined to obtain the exact number of layers required to restore the flexural capacity of the girders and force a debonding mode of failure. Therefore, two test girders were retrofitted by the application of 2 layers of FRP. One girder was retrofitted with an epoxy system and the other was retrofitted with a PU system. Two layers of FRP were applied. These test girders were not damaged prior to the application of the the FRP laminates. Test results were consistent and revealed that the bond strength was underestimated. Both test girders failed

Figure 4.11: Girders Control: Load vs. Displacement

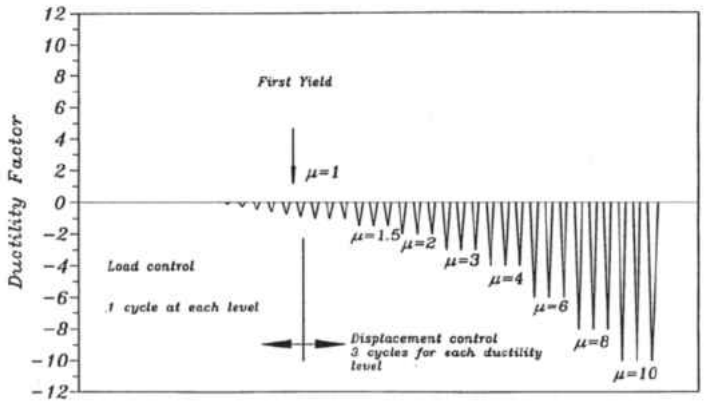


Figure 4.12: Girders Control: Load vs. Displacement

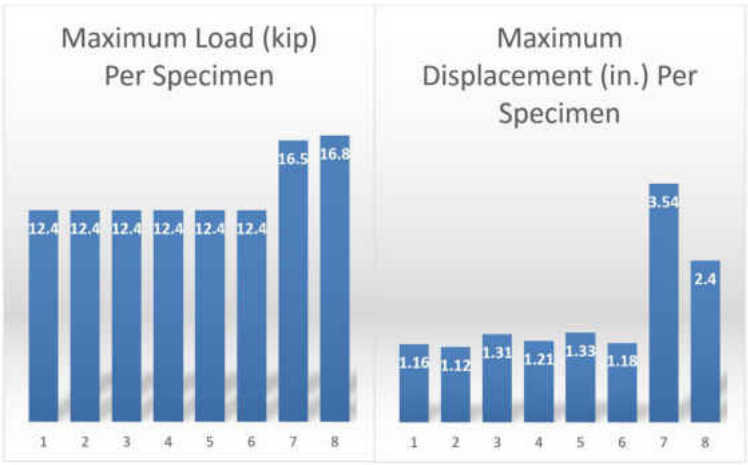


Figure 4.13: Girders Control: Load vs. Displacement

when the FRP laminates ruptured. After the results were analyzed, it was determined that 3 FRP layers would be enough to ensure debonding as a mode of failure.

The beams that were damaged up to ductility level 1 did not need any geometric restoration or compression zone restoration. After beam 8 was damaged to ductility level 2, there was minor (less than 0.5 in) residual deformation after it was unloaded. Therefore it was not reverse-loaded to restore it geometrically. Beam 7 which was damaged up to ductility level 3 had more residual deformation after it was unloaded. It was geometrically restored by reverse-loading the beam. The compression zones for beams 7 and 8 had to be repaired by grouting the areas where concrete spalling occurred. 5000 psi grout was used after chipping the cracked zones in the compression zone only.

The cracks in all 8 beams were epoxy-injected by Vector, a specialty concrete restoration group before FRP was applied. Photos from the epoxy-injection procedure are shown in figure 4.14. After the epoxy injection was performed and prior to applying the CFRP laminate, the tension face of each beam was prepared for FRP installation by grinding the surface to expose the aggregate

Figure 4.14: Epoxy Injection of Cracks in Girders After Damage Phase

per the manufacturer's specifications and then cleaned to ensure the surface was free of grit and other particles. Strain gages were then installed on the concrete surface followed by the installation of the FRP composites for all beams per table 3.3. For all resin systems, the composite laminate was applied to the tension face of the beams using a hand lay-up process. NRI had a patented portable impregnator which was used to impregnate the fibers with resin. The impregnator had its limitations and hand rolling was still required to ensure proper fiber impregnation. The girders were positioned tension face up during the application process. The FRP laminates were applied to the full width of the tension face. Photos from the FRP repair phase are shown in figure 4.15.

### *4.3.3 Post-Repair Testing*

After the repair phase, the girders were set back on the same test setup under which they were damaged. The girders tested under monotonic loading. Displacement control loading was applied at at a rate of 0.2 in per minute. The results of the load versus displacement for the different

Figure 4.15: FRP Repair Photos of Girders After Damage Phase and Epoxy Injection of Cracks

systems are shown in figure 4.16, figure 4.17, and figure 4.18.

The results of the girder tests revealed that the overall behavior of the strengthened girders was different from the control girder. FRP strengthening allowed the moment capacity of all girders to be increased by 1.3 times compared to the control girder. The total deflections at failure and stiffness for all specimens were similar at failure also revealed that the retrofitting was done without compromising the ductility and serviceability of the girders. The stiffness of the girders was increased

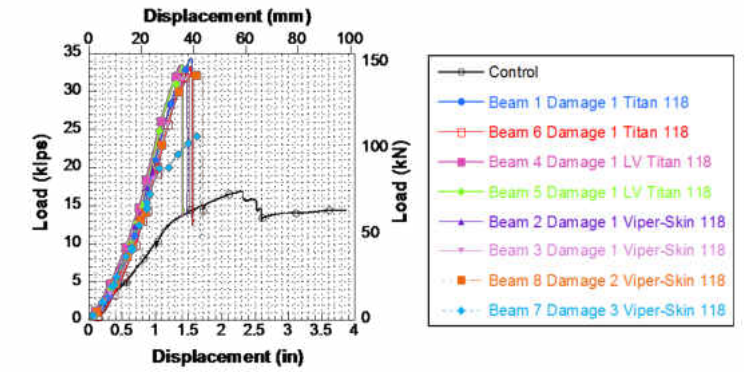


Figure 4.16: Load vs. Displacement Behavior of Repaired Girders Plots Shown alongside the Control Girder

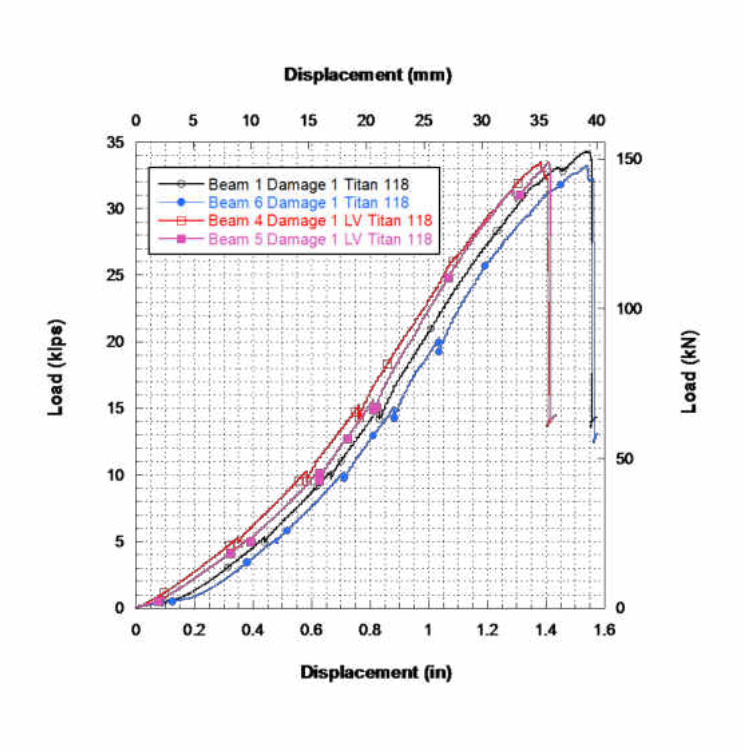


Figure 4.17: Load vs. Displacement for Epoxy-FRP-System Retrofitted Girders

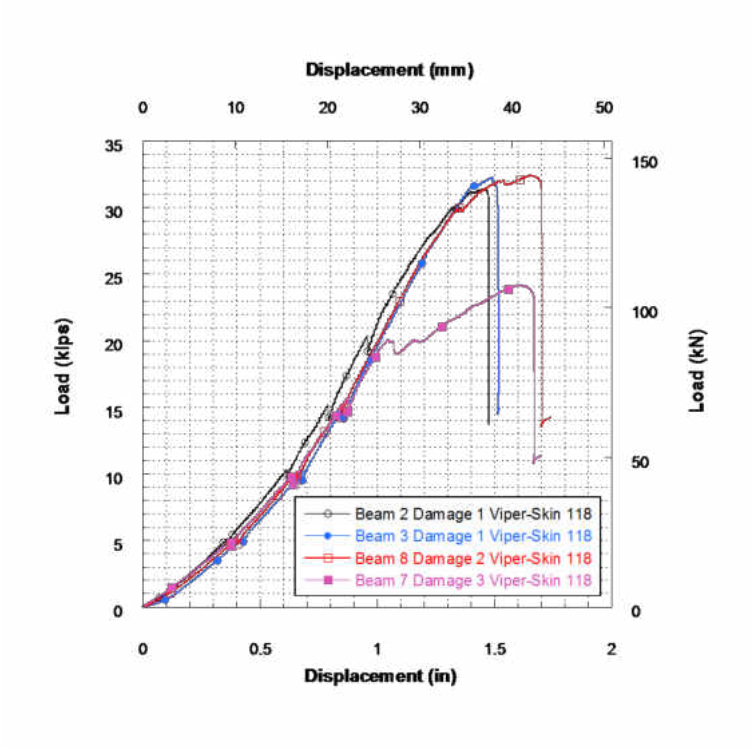


Figure 4.18: Load vs. Displacement for Polyurethane-FRP-System Retrofitted Girders

by approximately 3 times compared to the control girder. This is attributed to the unconventional retrofitting design of the girders. Typically when retrofitting girders with FRP per current design guidelines prescribed by ACI 440 design guidelines [3], the stresses in FRP laminates are limited to prevent the undesirable debonding failures. This leads to two detrimental effects: (1) reduced stiffness in the retrofitted girder, and reduction in bond development due to difference in stiffness and strength between the substrate (concrete) and FRP materials. This was also evident in the results of the small scale experiments performed in the results.

The repeatability of the results is very evident in from the load-displacement plots above. Moreover, all failure criteria were consistent and de-bonding took place in all 8 beams. All polyurethane systems de-bonded in the adhesive (primer) layer, while all epoxy systems de-bonded in concrete-

Figure 4.19: Typical Epoxy Retrofit Failure: Debonding in Concrete-adhesive layer

adhesive layer. Both debonding failures were brittle and sudden failures. Photos from the damage phase are shown in figure 4.19 and figure 4.20. It can be seen from figure 4.19 that parts of the concrete cover broke off when externally bonded FRP plates debonded. In all cases, it appeared that debonding initiated midspan and propagated to the end of the FRP near the support regions.

The similarity in the global behavior of the retrofitted girders was also observed in the strain behavior of the bottom reinforcing (tension) bar. Figure 4.21 shows the strain in the bottom bars at mid-span of the girders vs the total applied load on the 4 point bending testing of girders after repair alongside the strain in the same bar in the control girder. The plot shows that, up to the yield load in the control (12.4 kips), the bar was engaged and loaded equally in all beams, including the control. As the load increases past 12.4 kips, the strain keeps increasing in the bar until a point where the strain starts decreasing slightly indicating that the tension force is being engaged more with the FRP plates.

Even though the global behavior of the two retrofitted systems were ultimately very similar, the

Figure 4.20: Typical Polyurethane Retrofit Failure: Debonding in Adhesive Layer

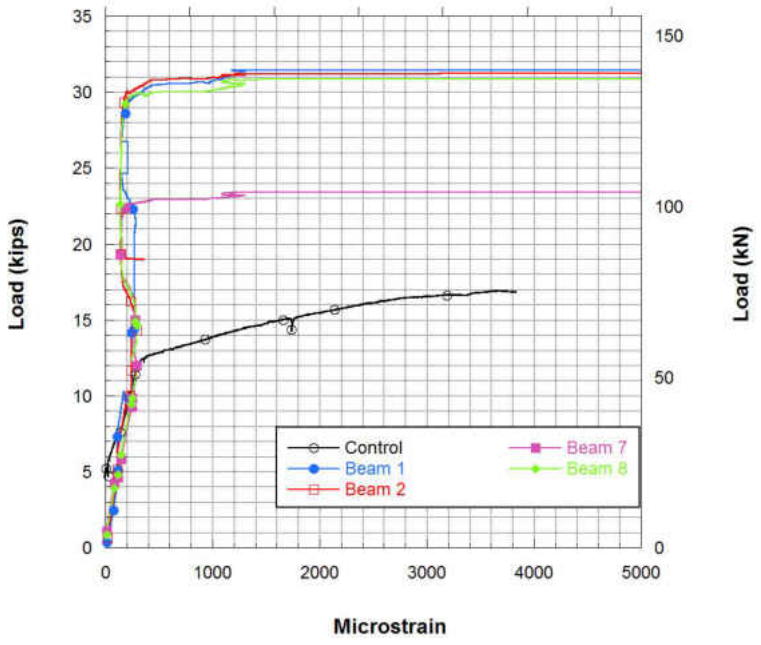


Figure 4.21: Applied Load vs Strain in Bottom Reinforcing Bar in Girders

difference in the mechanics of bond was observed when the strain data from the FRP composite was analyzed. Figure 4.22 and figure 4.23 show the strain distribution along the FRP plates, measured from the centerline of the girders. As the load increased, the strain in the polyurethane FRP plates increased more than those in the epoxy systems. This is attributed to the difference in the stiffness between the two systems. As the load increased and the composite system came closer to debonding, the strain difference between the midspan gages and those closer to the supports is much larger in the epoxy systems as compared to the polyurethane systems. This indicates that increased localized stresses in the bond are more evident in epoxy composites. At low curvature, the flexibility of the polyurethane composite system (bond and FRP plates) allowed a better distribution of the forces along the FRP plate. A better stress distribution along the interface between the FRP and composite allowed a higher performance of the composite system, preventing localized concrete failure at the bond.

The three FRP composite systems were equally effective in repairing the damaged beams. The stiffness for all beams was increased significantly. The ultimate strength of the repaired beams reached more than double that of the undamaged (non-FRP retrofitted) control. Even though the bond mechanisms and debonding failure criteria was different between the two systems, the global behavior of the PU and epoxy systems retrofitted beams was very similar.

## 4.4 Columns Experimental Results and Findings

### *4.4.1 Damage Phase*

Table 3.4 shows the girder testing matrix for the columns, the first control column was tested without any FRP retrofitting. The goal of the damage was to introduce damage to the materials prior to FRP retrofitting. Due to many technical difficulties, the columns were damaged without

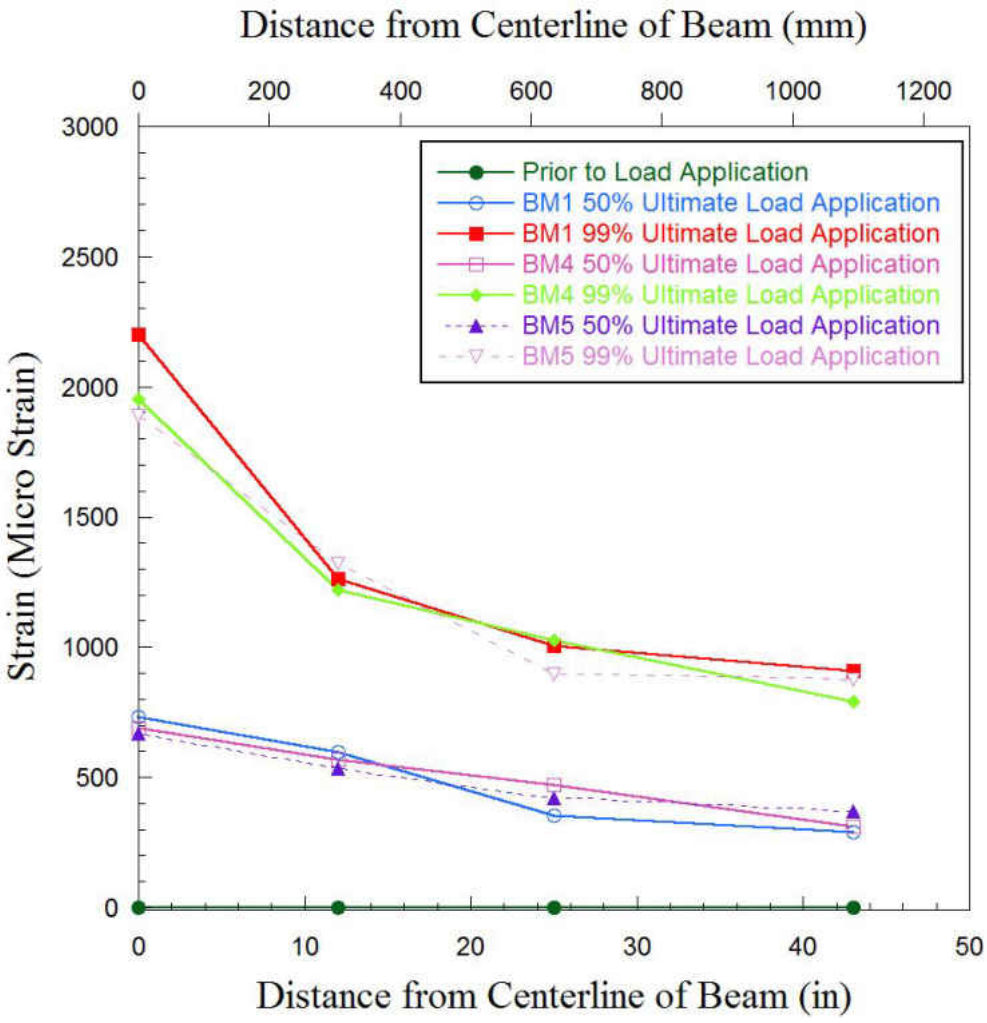


Figure 4.22: Strain Distribution along Beam vs. Applied Load for Epoxy-Retrofitted Girders

the application of the axial load. During the damage phase the technical difficulties were being worked on and resolved. The column was retested with the application of 40 kips of axial load. The load vs displacement results are shown in figure 4.24. The control column failed in a progressive manner: concrete cracking in tension zone, tension steel yielding, and finally concrete crushing in compression zone in the plastic hinge region. The concrete column that was loaded axially experienced more visible cracking and concrete spalling than the column that was loaded laterally

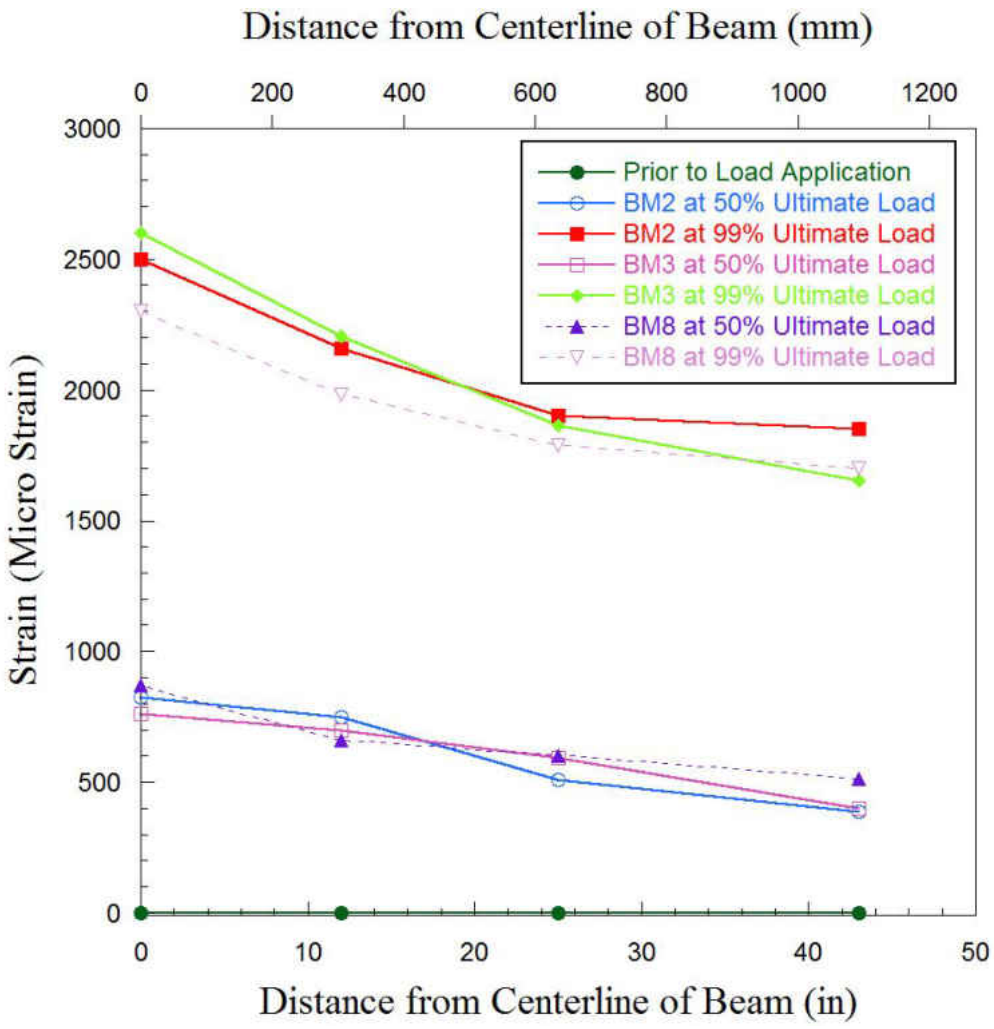


Figure 4.23: Strain Distribution along Beam vs. Applied Load for Polyurethane-Retrofitted Girders

without the axial load.

The control column that was damaged without the axial load damaged to maximum applied displacement of 2.7 in at the tip of the column and a maximum applied moment of of 9.9 kip-ft. The global yielding of the column occurred at a load of 7 kips at and at a displacement of 0.7 in. The column that was loaded axially reached maximum load of 16 kips at a displacement of 0.7 in. The global yielding occurred at 0.1 in and an applied load of 10 kips. A maximum displacement of

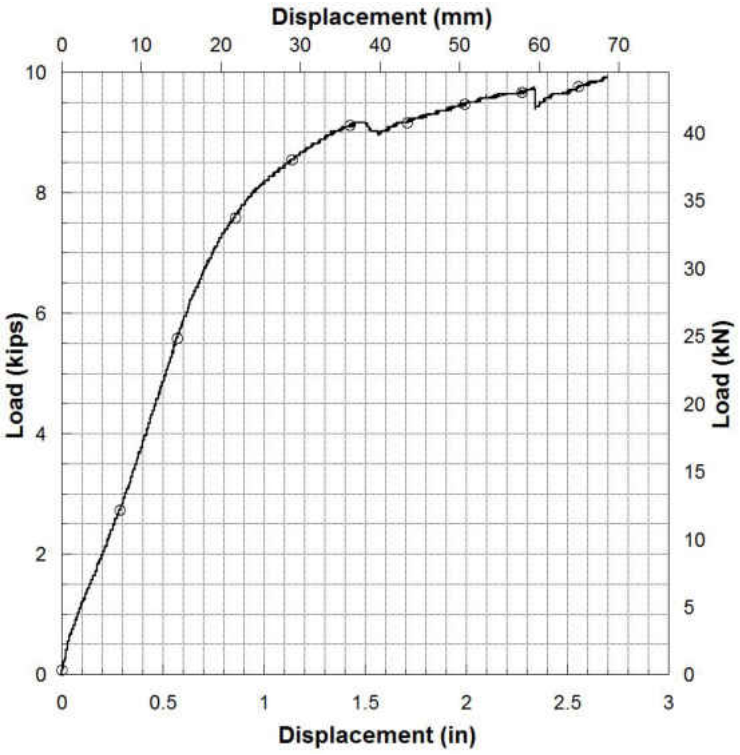


Figure 4.24: Load vs. Displacement for Column Control without Axial Load

5.2 in was applied to the column while it sustained the full axial Load. Photos from the loading procedure and column failures are shown in figure 4.26, figure 4.27, and figure 4.28.

Based on the results obtained from the control column (without axial load application), the damage phase loading protocol was generated for the remaining 4 columns. The loading protocol is shown in figure 4.29 . The loading protocol is based on the ICC AC 125 sinusoidal loading protocol [1]. The typical load-displacement behavior of the columns is shown in figure 4.30 and figure 4.31. The maximum load and displacement levels achieved during the damage phase are shown in figure figure 4.32.

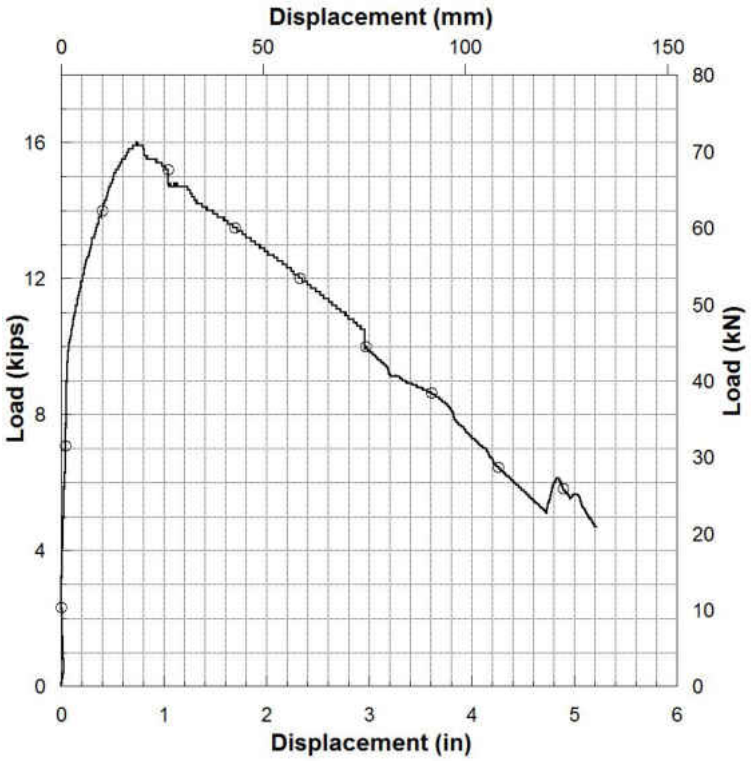


Figure 4.25: Load vs. Displacement for Column Control with 40 kips Axial Load

### *4.4.2 Repair Phase*

The repair design objective was accomplished by utilizing the CFRP sheets in both the transverse and longitudinal directions. During the design process the idea that failure of the FRP laminate system would not occur was kept in mind. The repair of each column was designed to restore the column peak lateral load strength compared to the original test. The strengthening system should also restore the column stiffness and ductility. The regions of the columns at and adjacent to the plastic hinge were repaired by externally bonding FRP composites (epoxy and PU systems) to the columns in the following order: The first layer layer was applied circumferentially to wrap the column, the second layer was applied in the transverse direction to provide transverse reinforce-

Figure 4.26: Column Setup Photo

ment for the unidirectional FRP composite, and the 3rd layer was also used to wrap the column circumferentially.

The first FRP wrap was designed to restore the shear and confinement capacity of the column, the second longitudinal layer to restore the loss from the yielded longitudinal rebar in the column as well as provide confinement to the first circumferential layer of FRP since all the fibers were unidirectional, and the 3rd layer was wrapped on top of the second layer (transverse/ circumfer-

Figure 4.27: Photo of Control Column without Axial Load Application Failure

ential direction)to ensure no FRP laminate failure occurs even though the design did not require that layer. Two regions were defined for retrofitting: the primary region is where the damage was concentrated. This region is the plastic hinge region, which was observed to be about 12 in. The secondary region is the region adjacent to the primary region with the same length which defined the new or expected plastic hinge. Therefore the total length of FRP retrofitted region was 24 inches.

Figure 4.28: Photo of Control Column with Axial Load Application Failure

The control columns that were damaged to high ductility levels and needed geometric restoration. They were geometrically restored by reverse-loading the columns under the same setup. Control columns experienced concrete spalling failures in the plastic hinge region. 10000 psi high strength grout was applied after chipping the heavily cracked zones. The cracks in all 6 columns were epoxy-injected by a specialty concrete restoration group, C & R Epoxy Systems, before FRP was applied. After the epoxy injection was performed and prior to applying the CFRP laminate, the columns were prepared for FRP installation by grinding the surface to expose the aggregate per

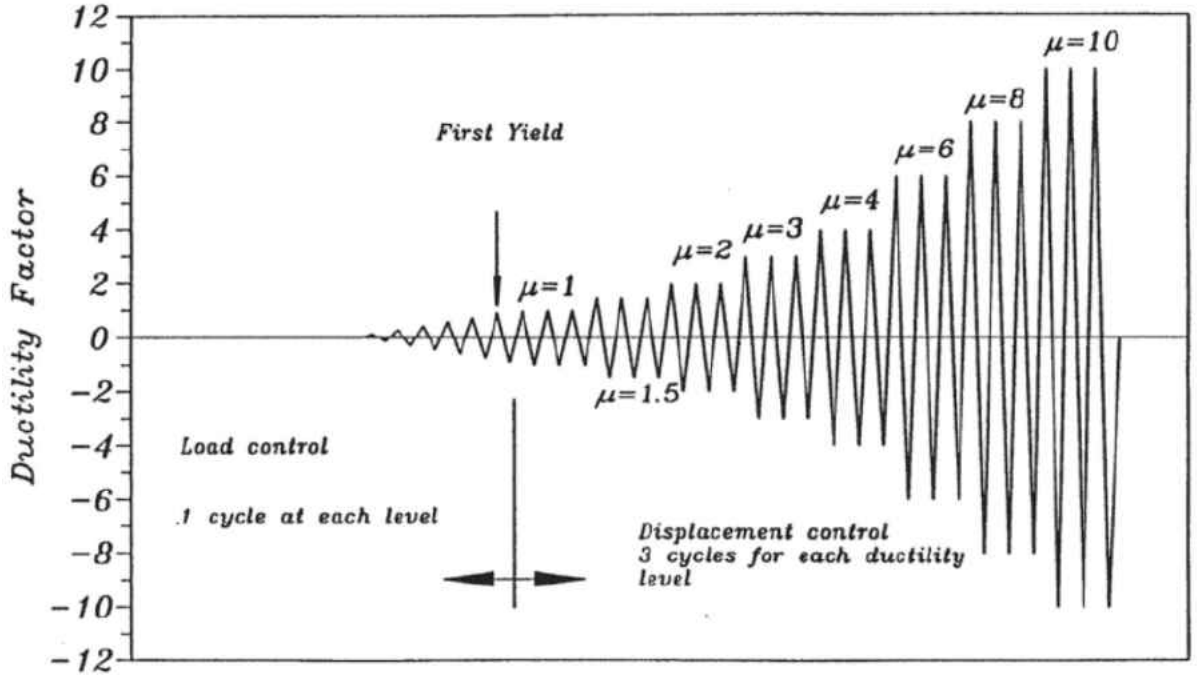


Figure 4.29: Load Protocol Used in Damage Phase [1]

the manufacturers specifications and then cleaned to ensure the surface was free of grit and other particles. After the epoxy injection and surface preparation, the FRP composites for all columns were installed per table 3.4 and as prescribed above.

### *4.4.3 Post-Repair Phase*

After the repair phase, the columns were set back on the same test setup under which they were damaged. The girders tested under cyclic loading using the same load protocol shown in figure 4.29. The load displacement results for control column 1, which was damaged at high ductility levels until complete failure with the application of axial load, revealed that the FRP wrap did not restore the lateral capacity of the column even though the cracks and concrete spalling from the

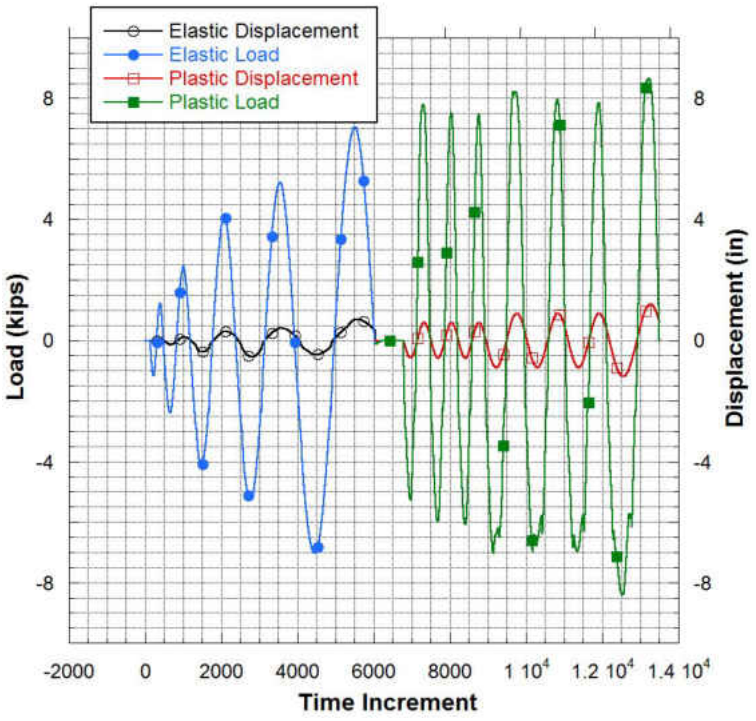


Figure 4.30: Typical Load and Displacements of Columns During Damage Phase Versus Time Increment

damage phase appeared to have formed only on the face of the column in the 8 in plastic hinge region and not in the foundation. The load-displacement results for the control column 1 are show in figure 4.33. It can be seen from these plots that the lateral stiffness of the column had decreased 93 % for column 1 in the first cycle.

The load-displacement plots for column 2, which was damaged at a ductility level of 4, is shown in figure 4.35. It can be seen that the PU composite restored the capacity of the column. However the behavior of the column appeared to have differed from the columns which were damaged at a lower ductility. This is attributed to the severe damage of the longitudinal bars during the damage phase. Photos from the damage phase of column one revealed buckled longitudinal bars. Photos

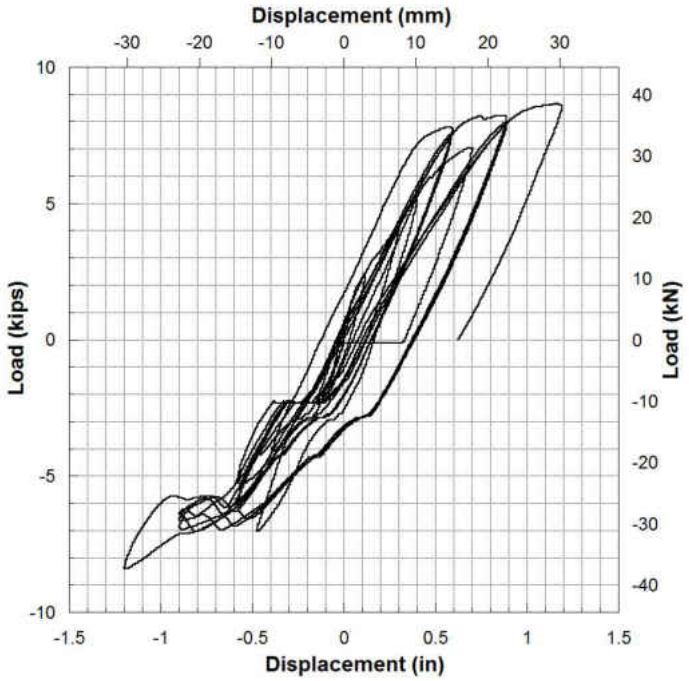


Figure 4.31: Typical Load Versus Displacement for Columns in Damage Phase without Axial Load

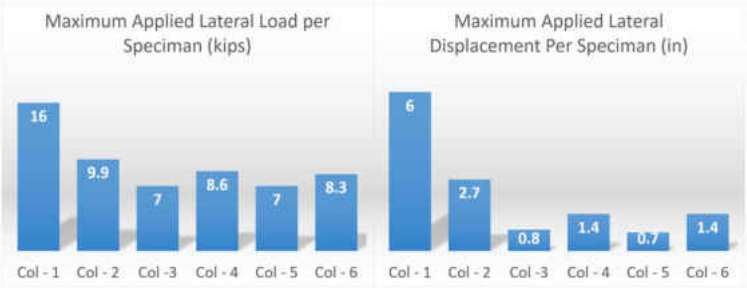


Figure 4.32: Maximum Applied Lateral Loads and Displacements on the Columns During Damage Phase

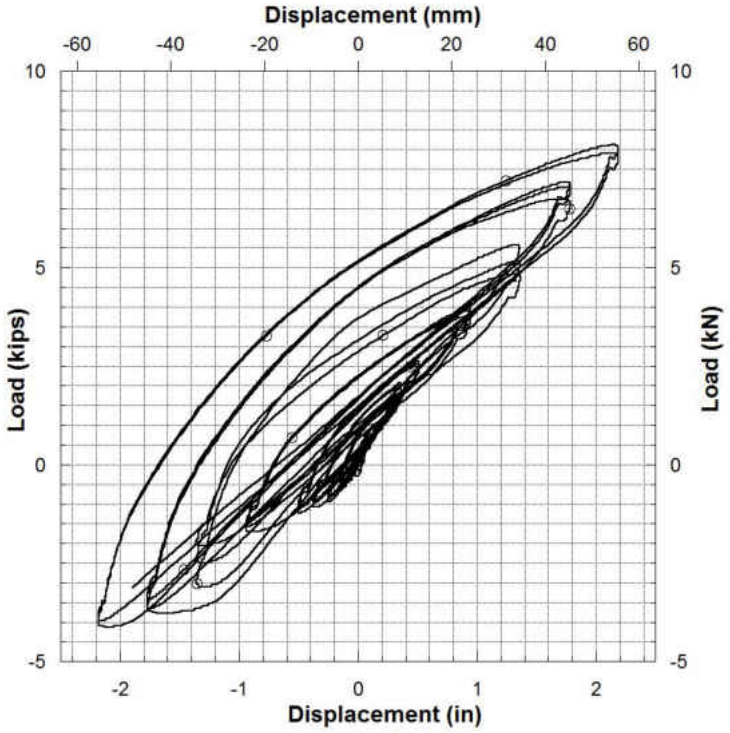


Figure 4.33: Post-Repair Load-Displacement Plot for Column 1

of the damage of the longitudinal bar during the damage phase are seen in figure 4.34. The load displacement results for columns 4 and 6 are shown in figure 4.36 and figure 4.37 respectively.

As shown in the figures above, the column behaved asymmetrically in the positive cycle and the negative cycle. This can be attributed to the unsymmetrical damage in the columns from the previous testing phase. The results confirmed that the strength of the column can be restored using both systems, epoxy and polyurethane. Not only was the capacity restored, but the strength and ductility of the column proved to have even been enhanced for the columns that were damaged at low ductility levels without the severe damage to longitudinal bars. A reduction in stiffness of the columns was also observed due to stiffness degradation of the reinforcing steel and concrete cracking of the column. The displacement capacity of the repaired columns, which were damaged

Figure 4.34: Photo Showing Longitudinal Reinforcing Bar Buckling from the Damage Phase

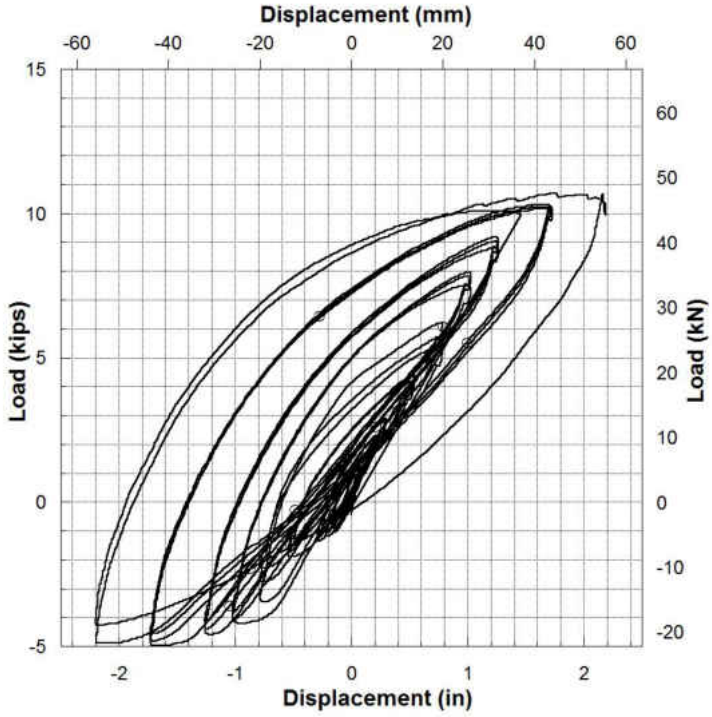


Figure 4.35: Post-Repair Load-Displacement Plot for Column 2

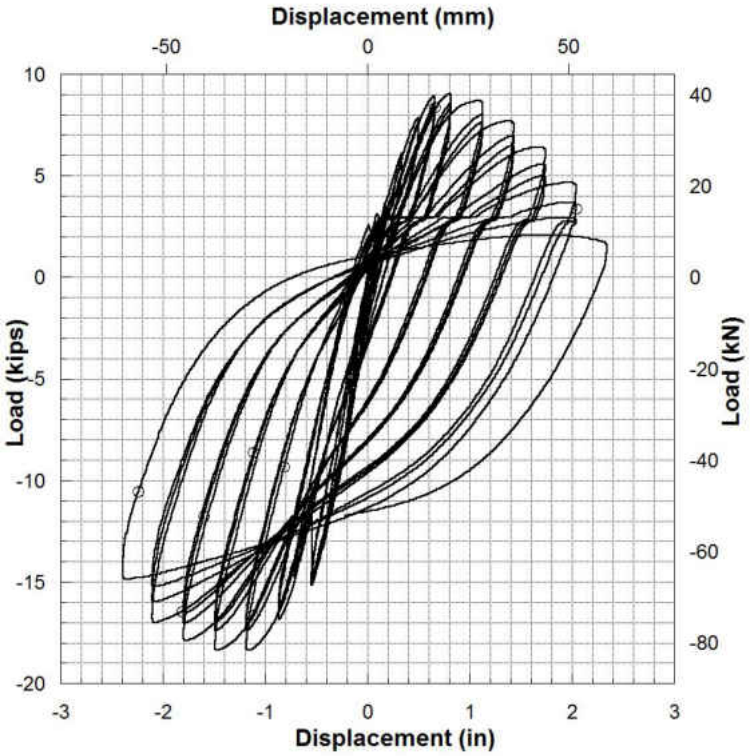


Figure 4.36: Post-Repair Load-Displacement Plot for Column 4

at low ductility levels without severe damage to the longitudinal bars, was restored nearly to that of the original condition. The retrofitted columns failed by forming a plastic hinge in the foundation, just below the FRP composite location (figure 4.38).

Another important observation can be concluded from comparing the column behavior during the damage phase and post-repair phase, is that the energy dissipation during the cyclic loading of the post-repaired columns is much larger than that which was observed during the damage phase. However, it should be noted that that the columns which were damaged under cyclic loads did not have any superimposed axial load as in the post-repair phase. The behavior of the columns during the damage phase can be different if a superimposed axial load was applied.

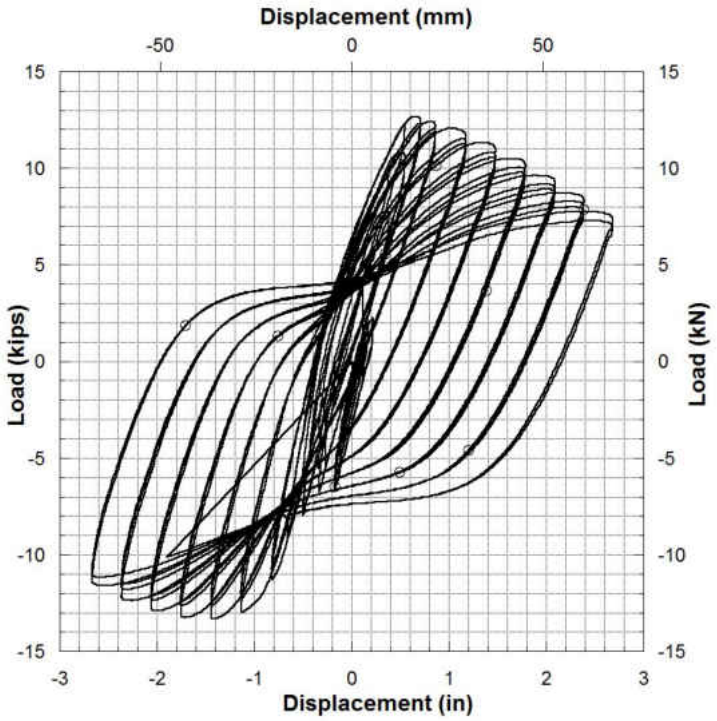


Figure 4.37: Post-Repair Load-Displacement Plot for Column 6

Figure 4.39 shows the load vs. displacement superimposed for column 4 and column 6 which were repaired with epoxy and PU respectively. It can be observed from the figure that both FRP composite systems provided very similar confinement retrofitting for the damaged columns. The load capacity of the columns was restored for both columns. The difference in the stiffness between the PU and epoxy retrofitting systems was not observed in the behavior of the repaired columns. This could lead to believe that the effect of the bond was negligible compared to the effect of the confinement provided by the circumferential FRP laminate, given the high strength and stiffness of the multiple layers of FRP that were used in both systems.

Figure 4.38: Post-Repair Typical Column Failure

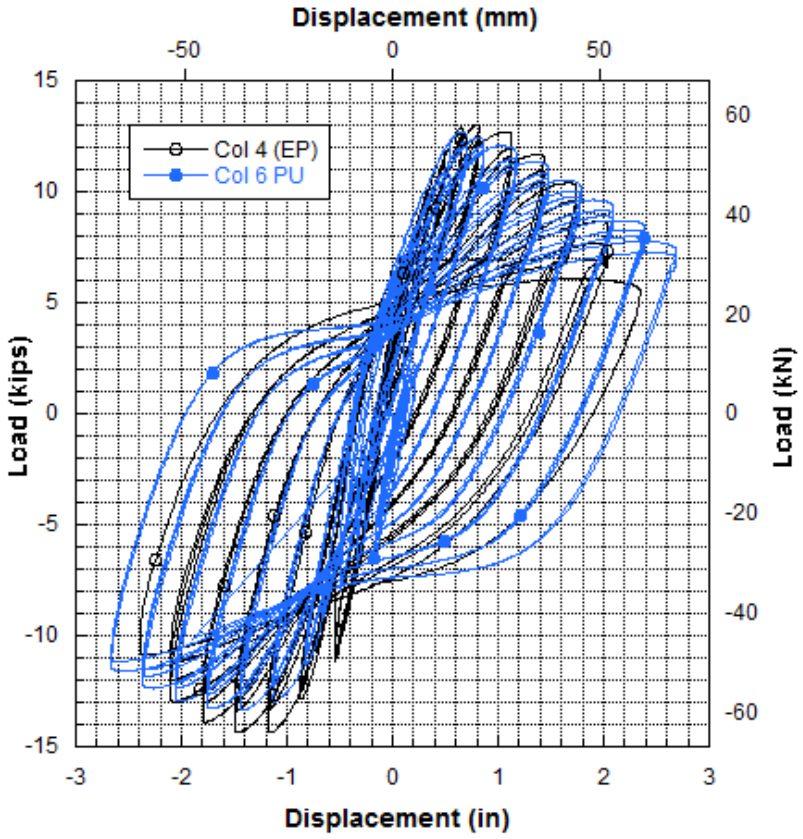


Figure 4.39: Post-Repair Load-Displacement for Columns 4 and 6

# CHAPTER 5: FINITE ELEMENT MODELING

The goal of the analytical modeling was not to reproduce the experimental curves through parameter calibration. Rather, it was desirable to see if the material and lap shear test data were sufficient to reproduce the different mechanisms observed in the epoxy versus polyurethane specimens during flexural tests. MARC was used in the nonlinear finite element modeling of the beams. Eight-node brick elements were used in the modeling of concrete and laminate elements. Additional interface elements were used to model the delamination and interfacial response, typical of composites where each ply is modeled with solid elements. A cohesive model defines the material behavior of these elements. The bond-slip relationships obtained from the lap shear experiments were used to calibrate the interface elements. The relationships assumed for the analytical models are shown together with the experimental curves in figure 5.1 and figure 5.2 and described in more detail in the following section. Since there was not have enough information about the interfacial shear between the FRP layers to develop interface elements for the cohesive zone model in MARC, the 3 layers were modeled as a single element. This eliminates the effects of the interfacial shear between the FRP layers. This modeling assumption leads to a stiffer FRP layer.

The non-linear concrete cracking formulation used in the analysis is built-in by MARC and is based on "Buyukozturk" model. Figure 5.3 shows the strain softening relationships of concrete vs the modeled forms in MARC. The area under the tension softening region represents fracture energy $G_f$. When tension-softening, $E_s$, is not included, material loses all load-carrying capacity; Therefore, stress goes to zero upon cracking. The properties of concrete were obtained from 28-day cylinder tests and the 3-point bending tests. The average of 6 concrete cylinder tests per ASTM C39/C39M was 5809 psi for the small scale beams and 6325 psi for the girders. The fracture energy average $G_f$ was 0.55 lb/in for the small scale beams and 0.61 lb/in for the girders. A modulus of rupture of 0.64 ksi, and shear retention factor of 0.0089, and ultimate compression strain of 0.003

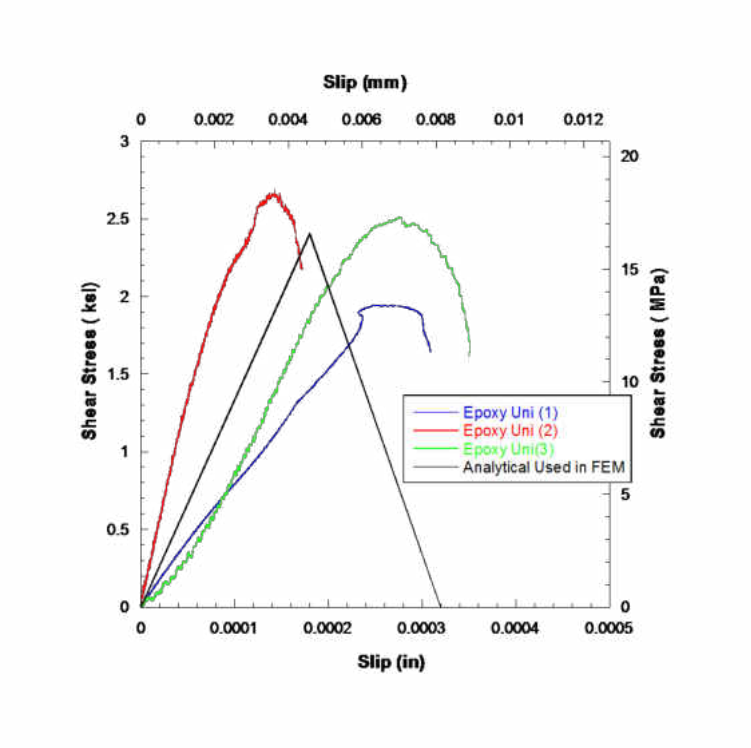


Figure 5.1: Epoxy Uni to Concrete Bond-Slip Model

were used in the concrete model.

The steel reinforcement for both longitudinal rebars and stirrups, were modeled using truss elements with discrete modeling of rebar with the concrete, which means rebar and concrete elements shared common nodes; that is, no concrete-steel interface elements were developed. The steel material was modeled as a bilinear elastic-plastic (nearly perfectly plastic) with a modulus of elasticity of 29000 ksi, Poisson's ratio of 0.3, and steel yield stress of $F_y$ = 60 ksi. The FRP materials were modeled as linear elastic materials with stress and strain properties obtained from experimental results provided by the manufacturer. A modulus of elasticity of 15.1 Msi and an ultimate stress of 127.5 ksi were used for the polyurethane composite, and a modulus of elasticity of 20.6 Msi and an ultimate stress of 181.4 ksi for the epoxy composite.

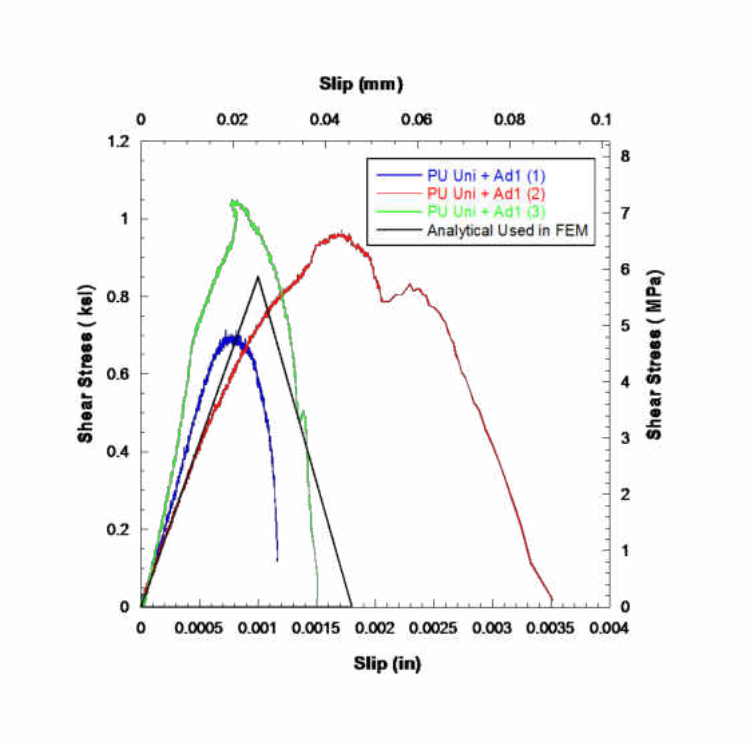


Figure 5.2: Polyurethane Uni to Concrete Bond-Slip Model

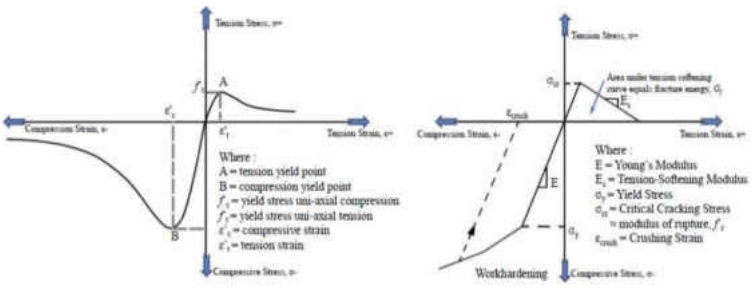


Figure 5.3: Typical Concrete Stress Strain Diagram vs. Uniaxial Stress-Strain Diagram

## 5.1 Bond Modeling and FEM Results for Small Scale Flexural Beams and Larger Scale Girders

The material properties for the bond were defined as interface elements in MARC. This element type is used to simulate the onset or progress of delamination. These interface elements are used to associate the material properties of the bond or cohesive material to a cohesive zone model in MARC. The cohesive material is defined using the cohesive energy (also called critical energy release rate), which equals the area below the equivalent traction versus equivalent relative displacement curve. The shape of this curve can be bilinear, exponential, or combined linear-exponential. In this model presented in this report, the bilinear form was used.

MARC uses cohesive zone modeling to simulate progress of delaminating. The constitutive behavior of these interface elements is expressed in terms of tractions versus relative displacements between the top and bottom surface of the elements. The effective traction, $t$, is introduced as a function of the effective opening displacement or slip, $v$. The critical effective opening, $v_c$ is obtained from figure 5.1 and figure 5.2 which show the bond slip models obtained from the single lap shear experiments. An average value of 0.0021 is used for the polyurethane polyurethane FRP model and 0.000128 for the epoxy FRP model. The cohesive energy, $G_c$, which defines the energy release rate, was also extracted from the bond slip models. The numerical values used in the model were $G_c$ of 0.00114 and 0.00045 for polyurethane Uni + Ad1 and epoxy Uni, respectively.

The load vs displacement plots comparing the FEM results with the experimental curves are shown for the epoxy FRP-reinforced small-scale beams and polyurethane FRP-reinforced small-scale beams in figure 5.4 and figure 5.5, respectively. The load vs. displacement data in figure 5.5 show the same damage progression observed in the flexural tests (cracking, drop in load, followed by post-cracking transfer to the laminate). The FEM results have consistently lower initial stiffness and cracking load due to the parameters associated with the concrete low-tension damage model. However, no attempt was made at calibrating to match the experimental results, data was drawn

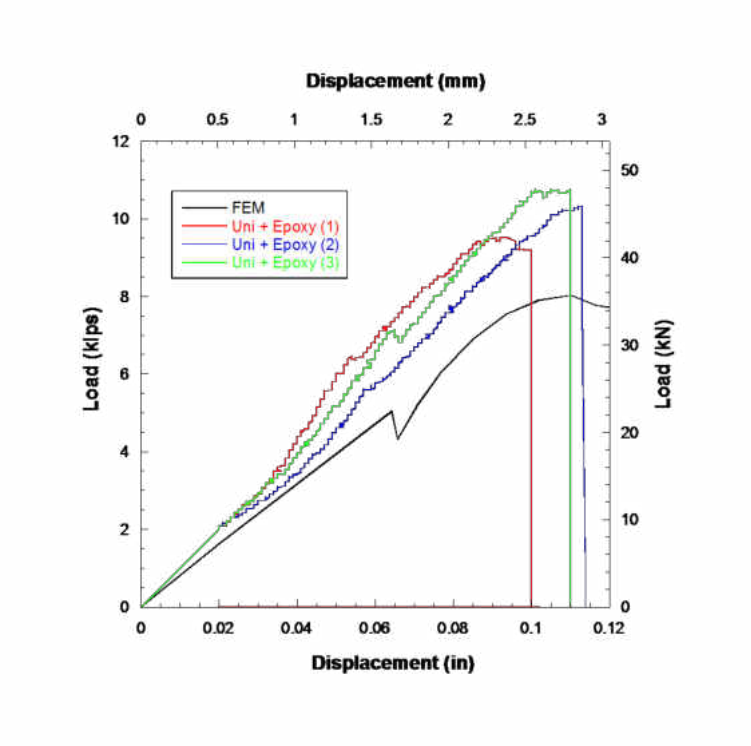


Figure 5.4: Experimental and FEM Load-Displacement Results for Epoxy Retrofitted Small-Scale Beams

directly from each of the material characterization tests directly.

Using the modeling criteria described above the reinforced concrete girders were also modeled. Without any calibration to match the results and using the basic constitutive models described above the load-displacement plot of the RC girder vs the experimental results were produced. These results are shown in figure 5.6. It can be observed from the results that the pre-cracking and post-cracking stiffness of the girder was captured in the FEM model within close proximity given the assumptions that were made.

The ultimate load before concrete crushing from the analytical model was 18 kips with a midspan displacement of 4 in while the experimental ultimate load and displacement were 16.9 kips and 2.1

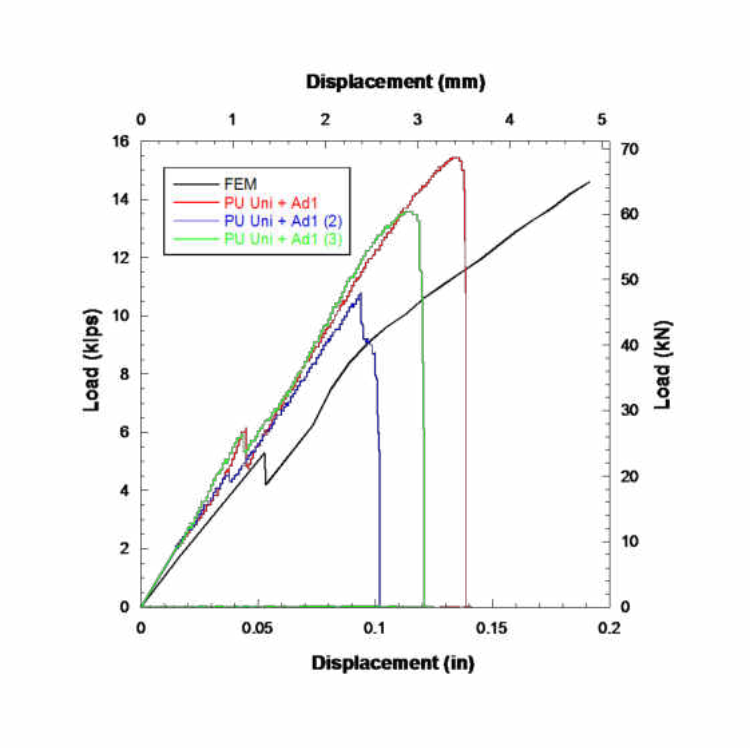


Figure 5.5: Experimental and FEM Load-Displacement Results for Polyurethane Retrofitted Small-Scale Beams

in. The cracking load was observed to be at 6.8 kips for the FEM compared to 4 kips in the tested control beam.

When modeling the retrofitted girders, no damage was induced to the girders. This decision was made based on three criteria: 1- the cracks were repaired with epoxy injection 2- the complexity of inducing damage to the finite element of the girders is very high especially when it comes to including the epoxy injection materials in specified crack locations, 3- the concrete model is not calibrated to match the exact behavior of the experimental results. Therefore, the same control girder model was used and the two composite systems were applied in the same way they were applied in small-scale beams, where interface elements were used to model the adhesive layer and

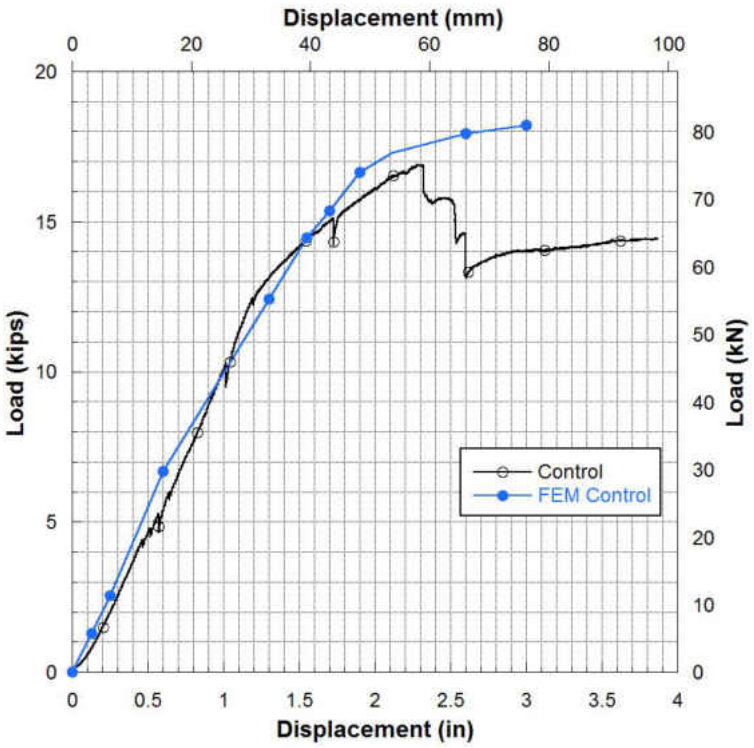


Figure 5.6: Experimental and FEM Load-Displacement Results for Control Girder

using linear elastic FRP materials. The results of the finite element models for the retrofitted girders are shown in figure 5.7. The analytical model revealed interesting behavior where both systems had similar post-crack stiffness which was close to the post-cracking stiffness of the test girders. The ultimate loads that were obtained from the analytical models were 36 kips and 32 kips while the displacements were 2.5 in and 2.6 in for the epoxy FRP retrofitted girders and polyurethane FRP retrofitted girders respectively.

The cracking load and displacement in the FE model were closer to the experimental results in the case of the polyurethane system than the epoxy system. This can be largely attributed to the consistent failure within the adhesive layer, and the lack of stress concentrations in the concrete because of the flexibility of the cohesive material (interface). To compare the failure modes observed

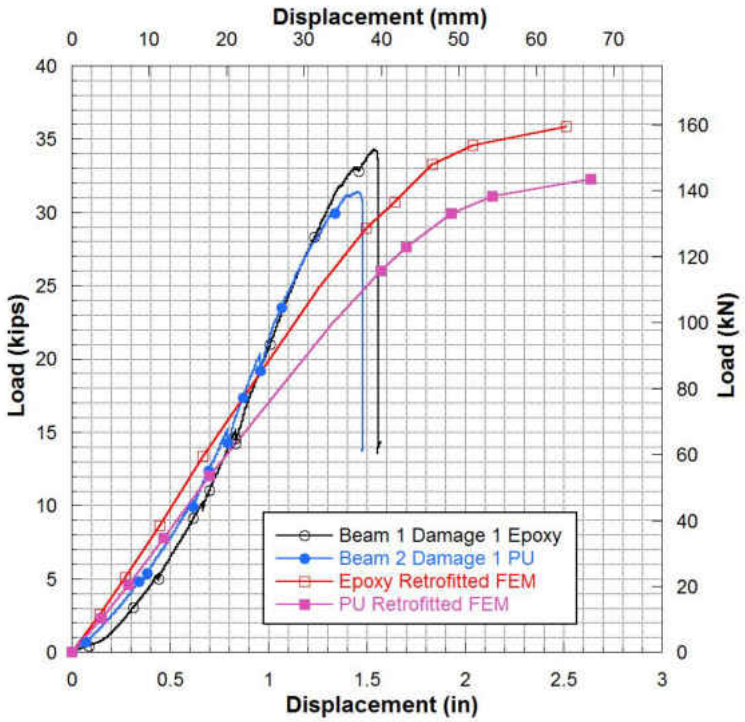


Figure 5.7: Experimental and FEM Load-Displacement Results for Retrofitted Girders

in the PU FRP-reinforced flexural tests (figure 4.8), the principal cracking strains were generated in the FEM at a load corresponding to the post-cracking region of the response. The contours of the principal cracking strain for the polyurethane FRP model are shown in figure 5.8. The flexural crack at the saw cut location continues to widen until debonding occurs (cohesive failure in the interface). The different bond properties in the model also caused the PU model to fail at a higher load than the epoxy model. This observation is consistent with the results of the lap shear average bond stress (figure 4.3) and a consequence of the stress distribution along the bonded area.

On the other hand, the load and displacement response from the model of the epoxy-reinforced beam showed lesser agreement with the experimental data. As mentioned in the discussion of the lap shear failure modes, the calibrated bond-slip curve used in the FEM represents failure in the top

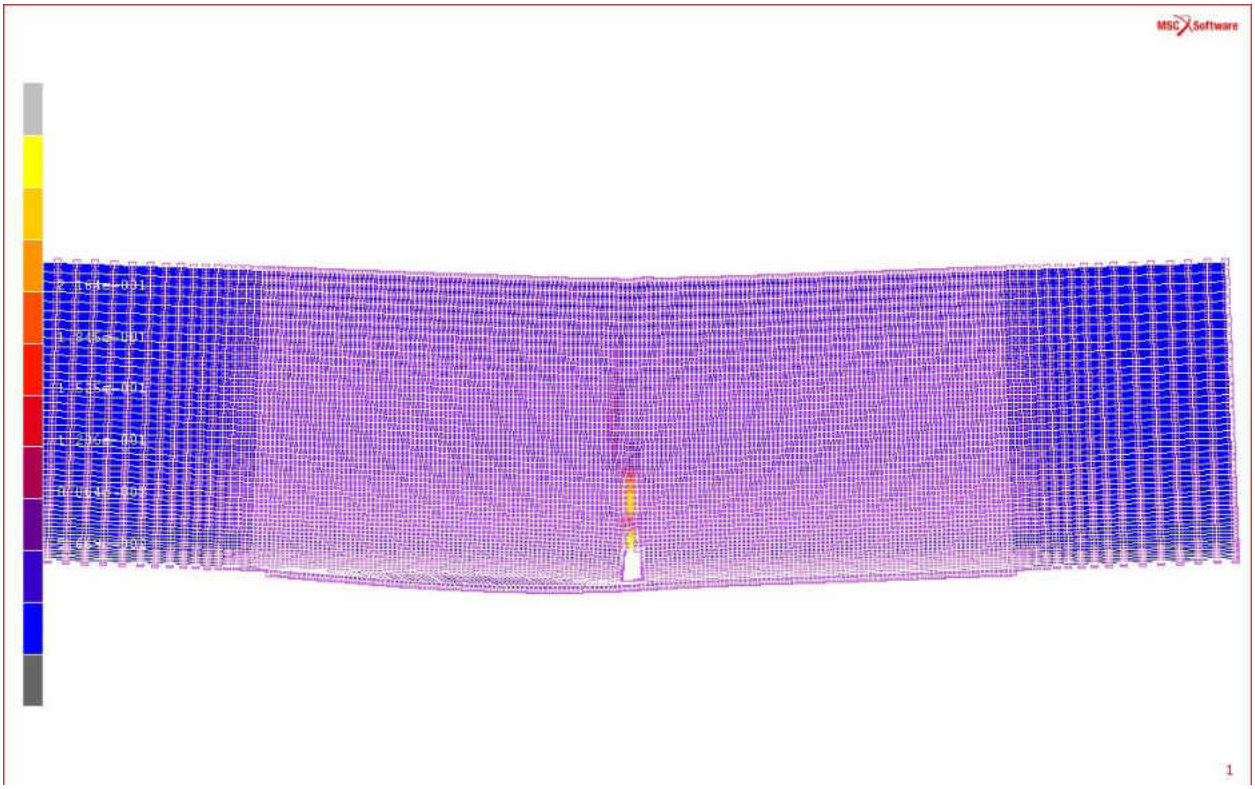

Figure 5.8: Cracking Stains for Polyurethane FRP Retrofitted Beams

layer of substrate, implying that the true local bond strength of the epoxy adhesive layer may be significantly higher than that measured. The FEM results show lower stiffness, cracking load, and ultimate load. The concrete material model can degrade in shear (because of diagonal tension); therefore, the epoxy local bond strength should be increased to better match the experimental results. Similarly, the ultimate load is lower than the experiment because it receives a contribution from the concrete material in the model as well as the interface. The principal cracking contours for the epoxy FEM are shown in figure 5.9 to compare with the failure modes observed during the flexural tests. The epoxy specimens de-bonded in the concrete layer with a mixed mode behavior (figure 4.9); however, the model indicates only that the epoxy interface model is sufficiently stiff to

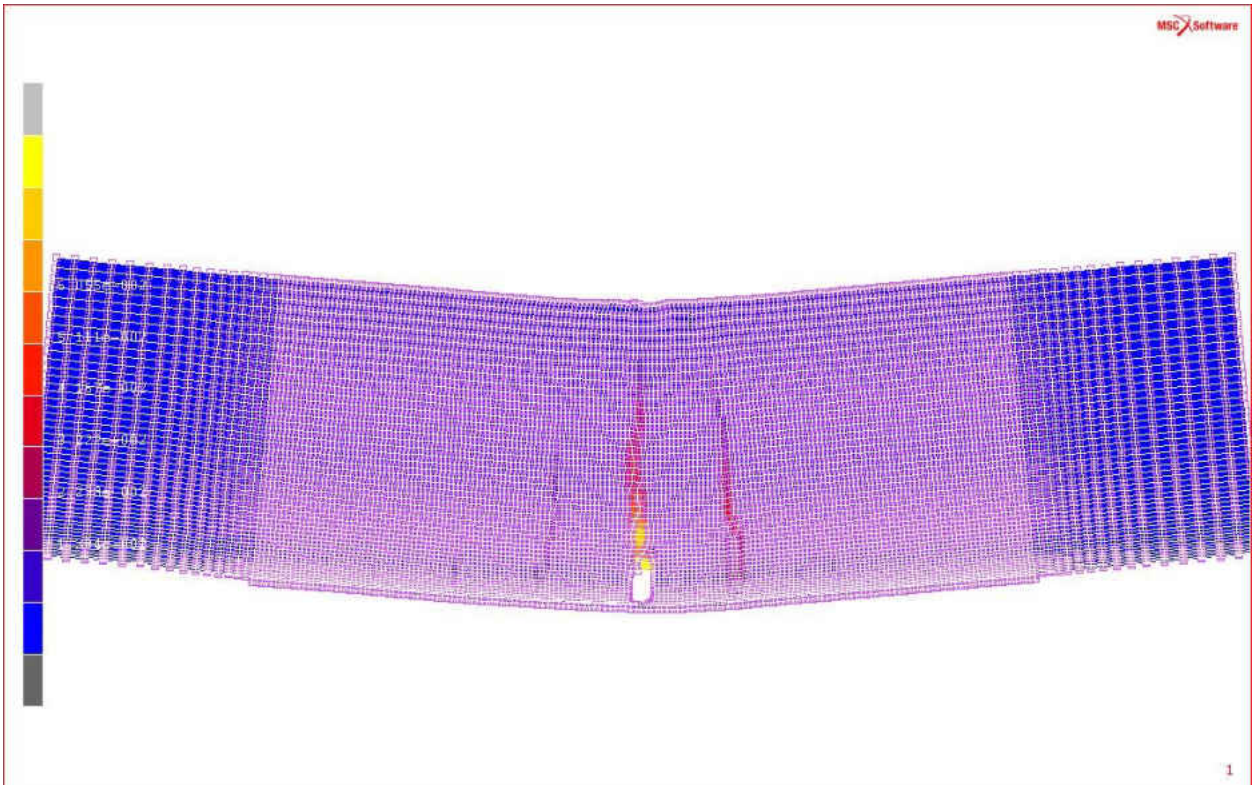


Figure 5.9: Cracking Stains for Epoxy FRP Retrofitted Beams

generate several distributed flexural cracks. The wedge due to the inclined crack does not develop in the model to the same extent as would be observed if the bond strength of the interface was increased.

# CHAPTER 6: DISCUSSIONS AND CONCLUSIONS

The extensive experimental program presented in this dissertation was developed to compare the behavior of epoxy FRP composites versus polyurethane FRP composites in external strengthening of concrete beams in flexure and columns. In the small scale experiments, 3 different fabrics were paired with each of four different matrices (3 polyurethane with differing adhesives, and 1 epoxy). Single lap shear experiments were performed to determine the bond properties of each system to concrete, and to compute bond-slip relationships for use in finite element models. Small-scale three-point flexural tests were performed on the same matrix of systems. Results indicated that the epoxy FRP-reinforced beams demonstrated a higher cracking load; however, the PU FRP-reinforced beams reached a higher ultimate load. Similarly in the lap shear experiments, the ultimate load at debonding in most PU systems was higher than the epoxy systems. In both types of experimental tests, the polyurethane systems all debonded consistently in the adhesive layer, whereas the epoxy specimens failed in the substrate (top layer of concrete bonded to the laminate).

FRP strengthening allowed the moment capacity of all girders to be increased by 1.3 times compared to the undamaged control girder without FRP strengthening. The total deflections at failure and stiffness for all specimens, those retrofitted with the PU composite system and those retrofitted with the epoxy composite system, were similar at failure. The results also revealed that the retrofitting was done without compromising the ductility and serviceability of the girders. The stiffness of the girders was increased by approximately 3 times compared to the control girder. The repeatability of the results is evident in from the load-displacement plots. Moreover, all failure criteria were consistent and de-bonding took place in all 8 beams. All polyurethane systems de-bonded in the adhesive (primer) layer, while all epoxy systems de-bonded in concrete-adhesive layer. Both debonding failures were brittle and sudden failures.

The column results revealed that not only was the capacity restored, but the strength and ductility of the column proved to have even been enhanced for the columns that were damaged at low ductility levels. The displacement capacity of the repaired columns, which were damaged at low ductility levels, was restored nearly to that of the original condition. The retrofitted columns failed by forming a plastic hinge in the foundation, just below the FRP composite location. Moreover, the energy dissipation during the cyclic loading of the post-repaired columns was shown to be significantly larger than that which was observed during the damage phase. The repair of the columns which were damaged to higher ductility levels was not successful. This is due to severe damage and buckling of the longitudinal bars. It was concluded that a proper way to retrofit such severely damaged columns using externally bonded FRP composite systems is by providing longitudinal FRP reinforcing anchored to the foundation to replace the lost capacity of the damaged bars.

Bond-slip relationships were derived from the strain data recorded during the single lap shear tests. The polyurethane FRP composite systems showed lower interfacial bonding stiffness and local bond strength. However, the flexibility allows local stress redistribution and a larger interfacial slip while avoiding local de-bonding. Chen et. al. (2001) [23] did not study different bond strengths but pointed out that the ultimate bond capacity is governed not only by the bond strength but also by the stress distribution along the bonded area. This observation was also confirmed during the flexural tests, and from the finite element models that were used to compare the responses, where higher ultimate loads were achieved. The finite element models were not calibrated to match the experimental responses, but rather used only data from the lap shear and material tests, yet they yielded the same flexural behaviors and failure modes as observed in the experiments.

The only minimum strength criteria that is prescribed in ACI 440.2R [3], which is the current guide for the design of externally bonded FRP systems for strengthening of concrete structures in the US, specifies that for bond critical applications (flexural and shear retrofitting for example), the

tension adhesion strength shall exceed 200 psi and the failure shall be exhibited within the concrete substrate. The normal pull off tests of polyurethane adhesives reveal values that are significantly less than the above minimum prescribed value. Therefore, per this guide polyurethane systems do not qualify as a retrofitting application per the current design code. This research proved that normal strength of the adhesive (or tension strength) does not represent the bond strength in shear nor mechanics in most bond critical applications, specifically flexural retrofitting and shear.

ACI 440 also stipulates that an unacceptable failure mode is within the adhesive layer. Additionally, a cohesive failure of substrate material is considered an acceptable but not preferable mode of debonding failure although it is explicitly mentioned ACI440.2R. These guidelines lead to stress limitations preventing high strength FRP to be fully utilized in externally-bonded FRP systems in flexural retrofitting applications. This puts limits on the capacity of the retrofitting systems. The repeatability of the experimental results, specifically in the flexural experiments, proved the debonding is not unpredictable as ACI states. The results of this research from the flexural retrofitting experiments (small scale beams as well as large scale girders) and lap shear experiments proved that retrofitting capacities can be achieved even though the mechanics of the interfacial shear are different between epoxy systems and polyurethane systems. The repeatability of the tests and preliminary finite element analysis also prove that bond failure can be predicted and is not an undesirable mode of failure as the guidelines state. Knowing the shear bond capacity in the adhesive layer with a good level of confidence allows (due to the repeatability of the tests), it was shown in this research that the designer can design for a debonding failure mode in the adhesive layer. Given the achievable high flexibility of polyurethane composites [15], polyurethane adhesives potentially may be developed for non brittle, which makes debonding a more desirable mode of failure than other brittle mode of failure which are currently acceptable in ACI 440.

# APPENDIX A: FLEXURAL TEST RESULTS FOR DIFFERENT POLYURETHANE SYSTEMS

This appendix presents the results obtained for the different polyurethane adhesive combinations and epoxy with the different fibers which were described in the body of the dissertation. Alongside the load-displacement plots obtained from the experiment, photos showing the failure criteria for each specimen are shown next to the plots.

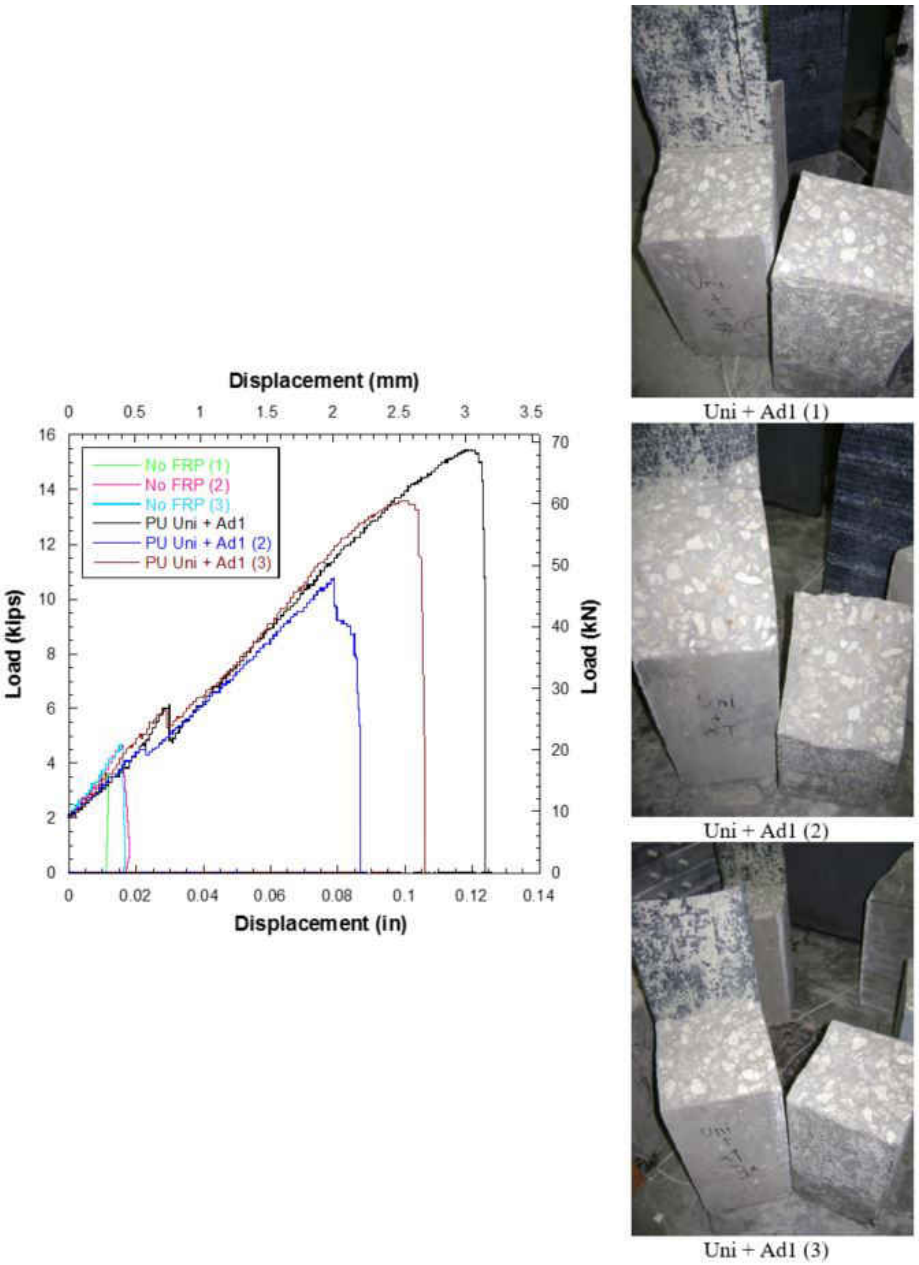


Figure A.1: Small Scale Flexural Beam: Uni Fibers + Ad1 (PU)

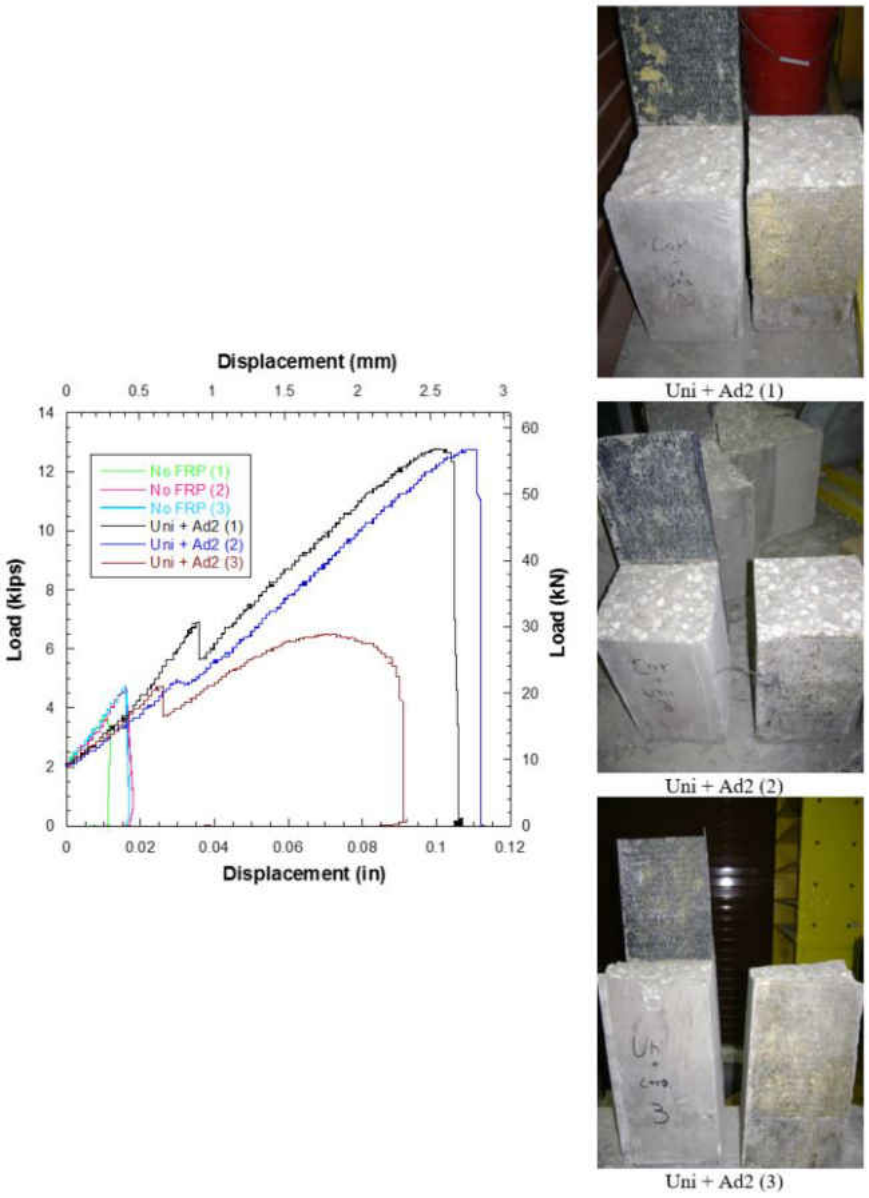


Figure A.2: Small Scale Flexural Beam: Uni Fibers + Ad2 (PU)

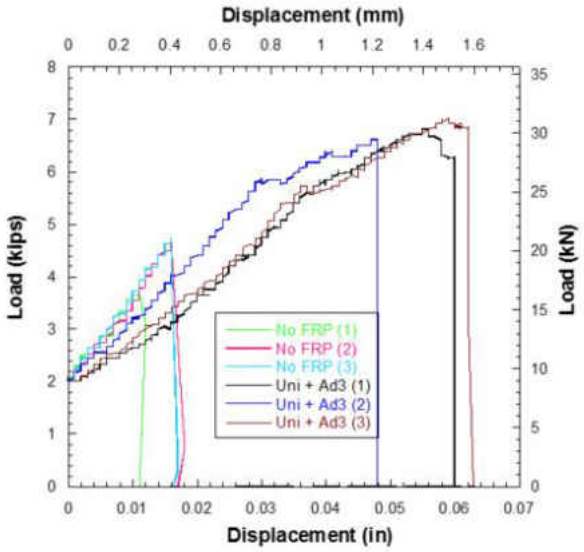


Uni + Ad3 (1)

Uni + Ad3 (2)

Uni + Ad3 (3)

Figure A.3: Small Scale Flexural Beam: Uni Fibers + Ad3 (PU)

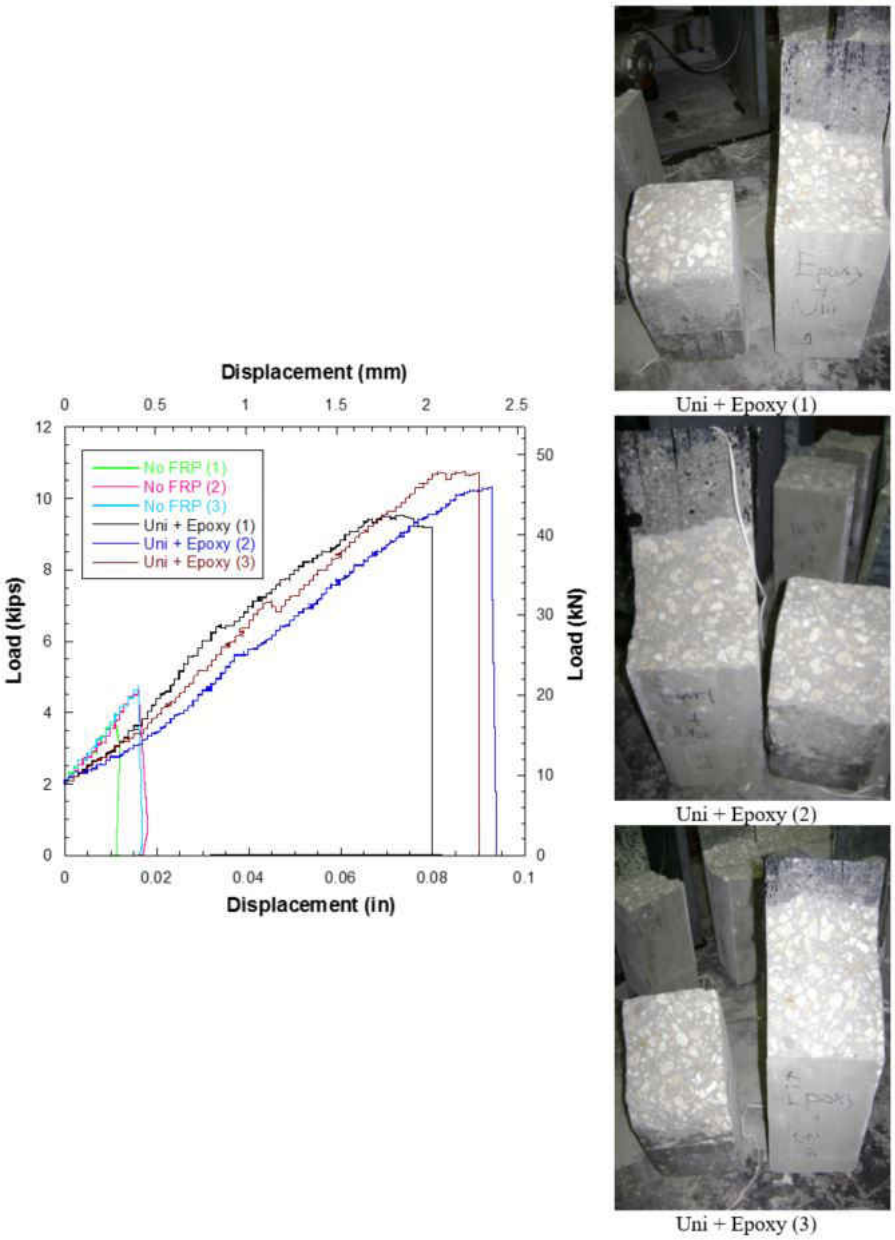


Figure A.4: Small Scale Flexural Beam: Uni Fibers + Epoxy

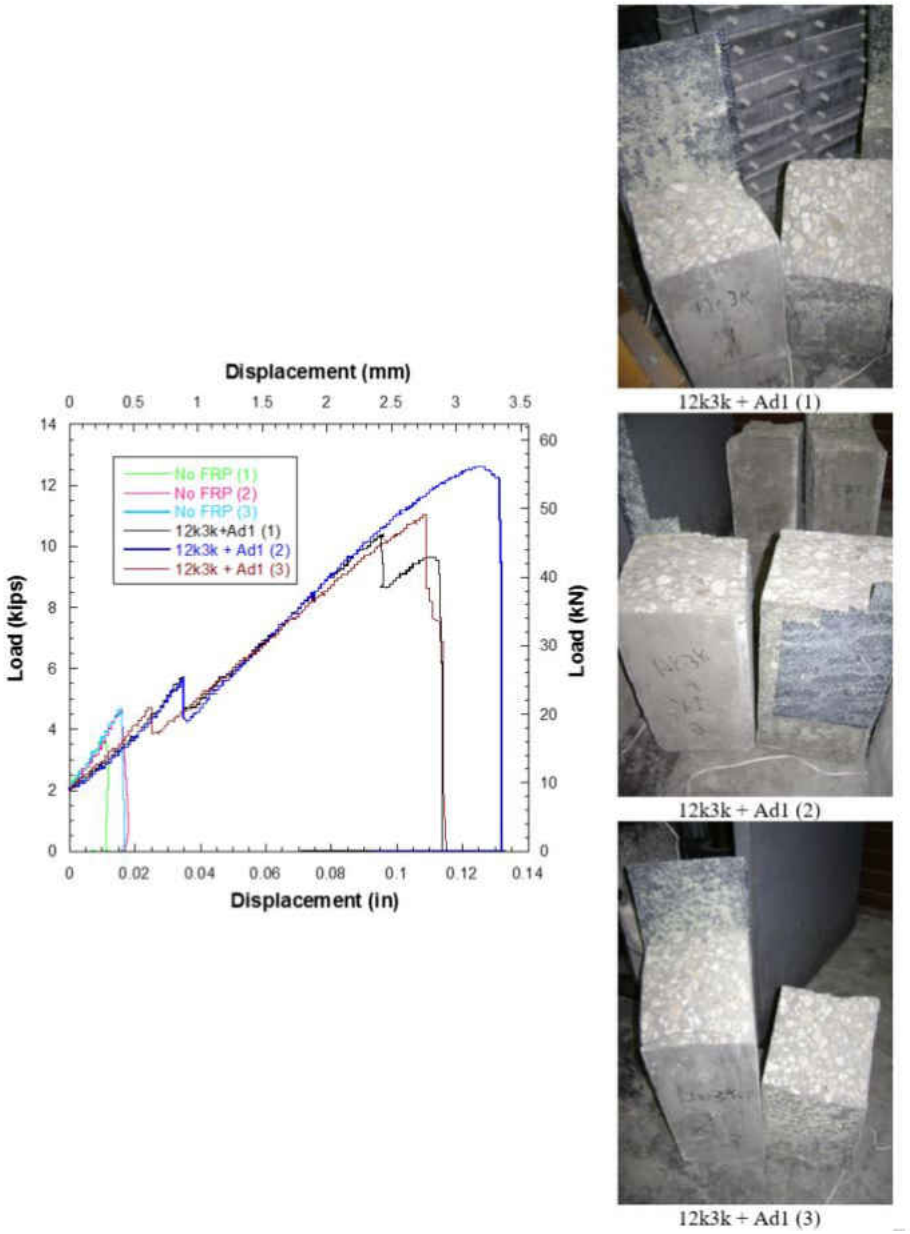


Figure A.5: Small Scale Flexural Beam: 12k3k Fibers + Ad1 (PU)

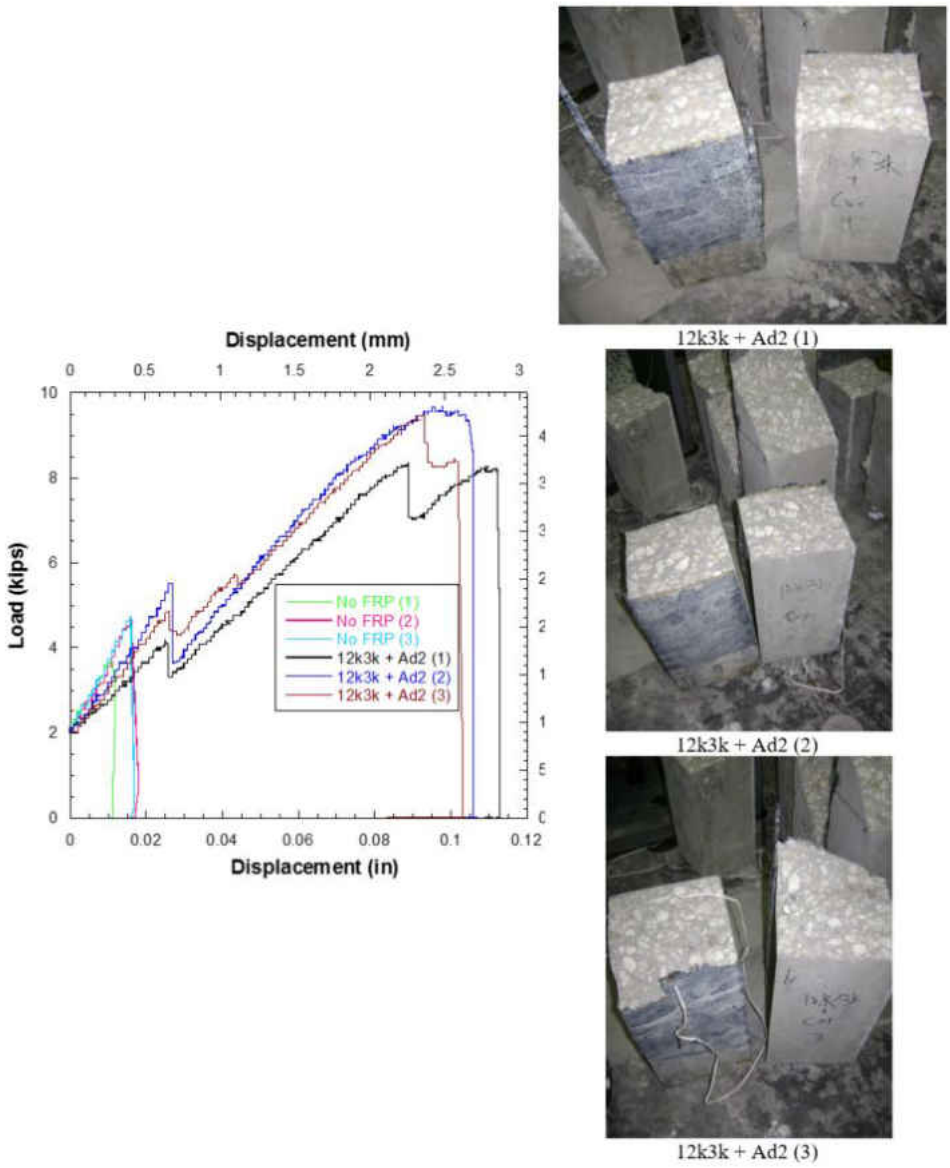


Figure A.6: Small Scale Flexural Beam: 12k3k Fibers + Ad2 (PU)

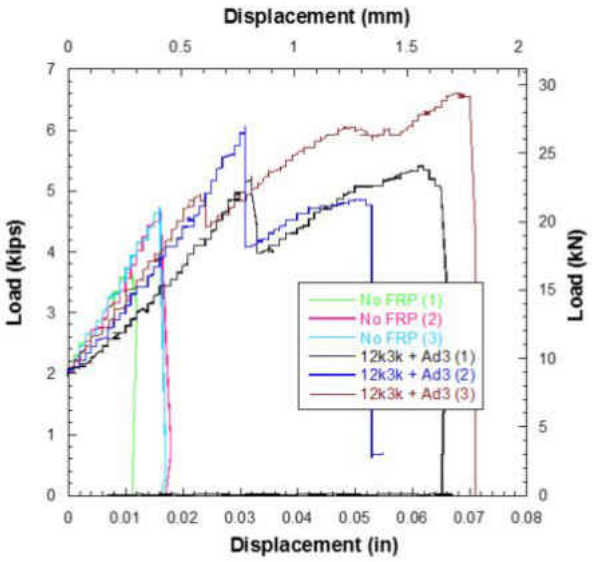


12k3k + Ad3 (1)

12k3k + Ad3 (2)

12k3k + Ad3 (3)

Figure A.7: Small Scale Flexural Beam: 12k3k Fibers + Ad3 (PU)

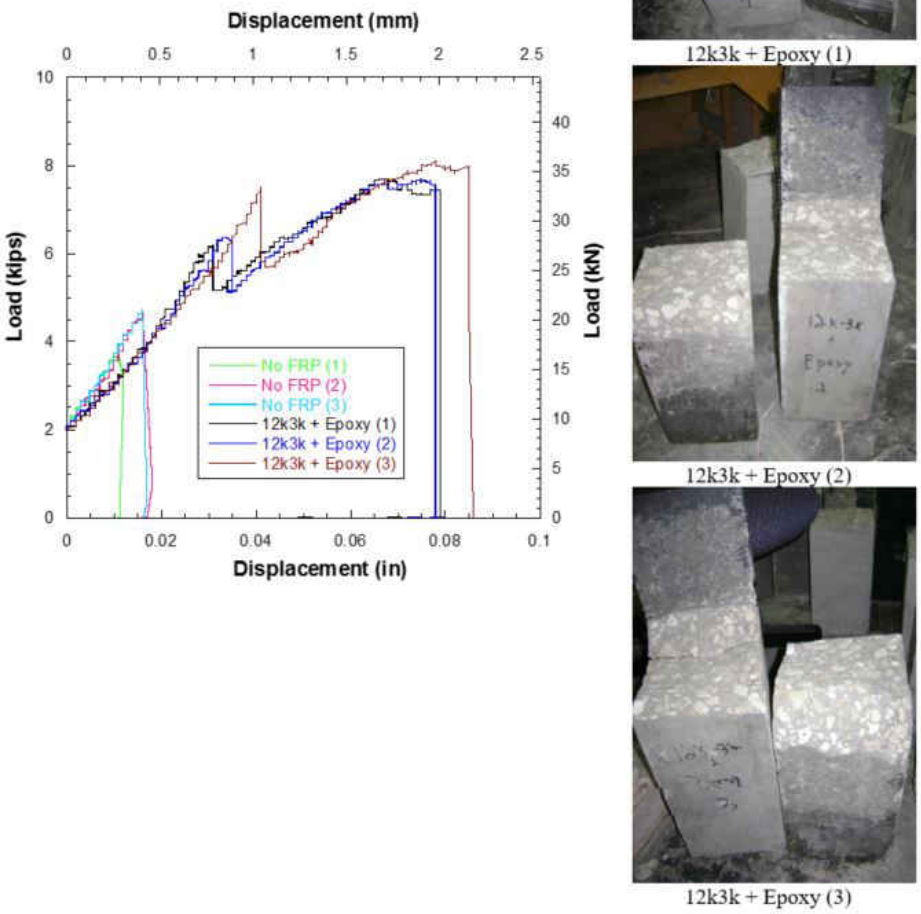


Figure A.8: Small Scale Flexural Beam: 12k3k Fibers + Epoxy

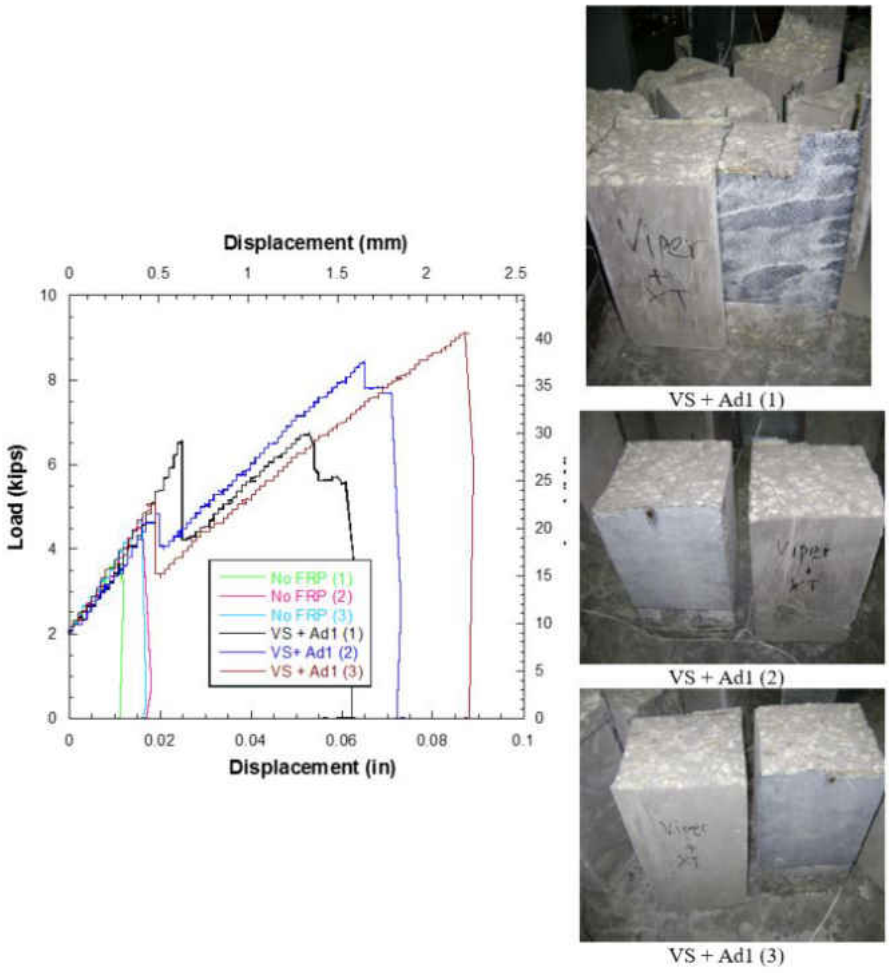


Figure A.9: Small Scale Flexural Beam: ViperSkin Fibers + Ad1 (PU)

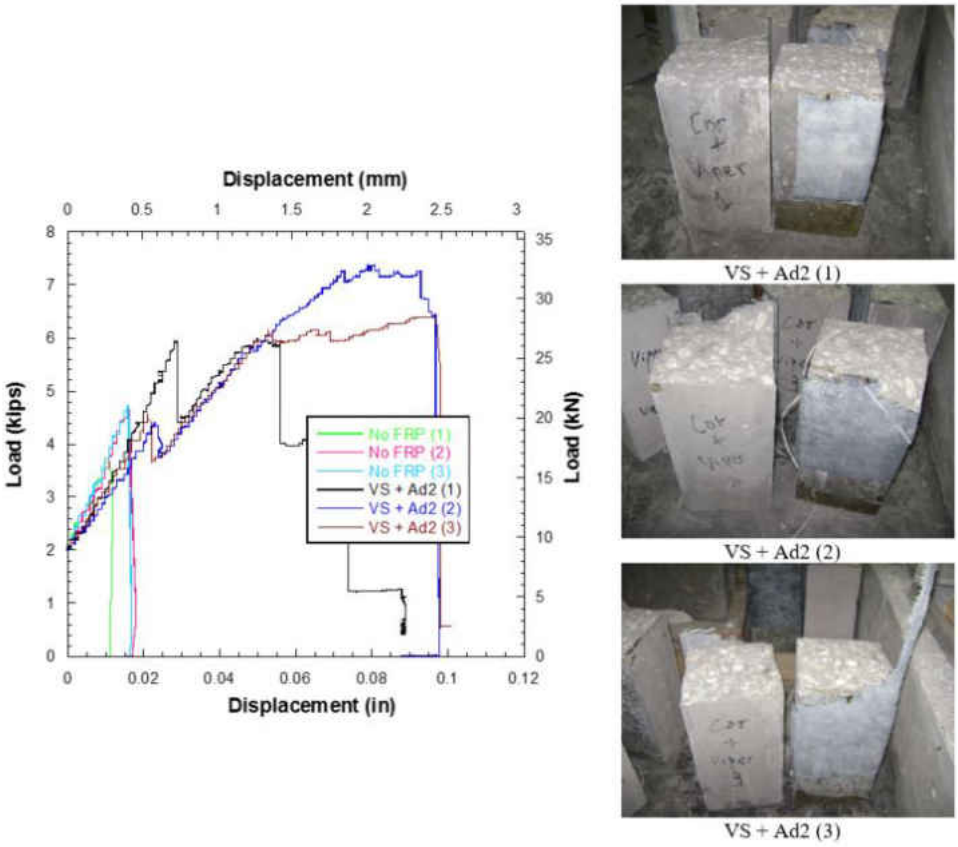


Figure A.10: Small Scale Flexural Beam: ViperSkin Fibers + Ad2 (PU)

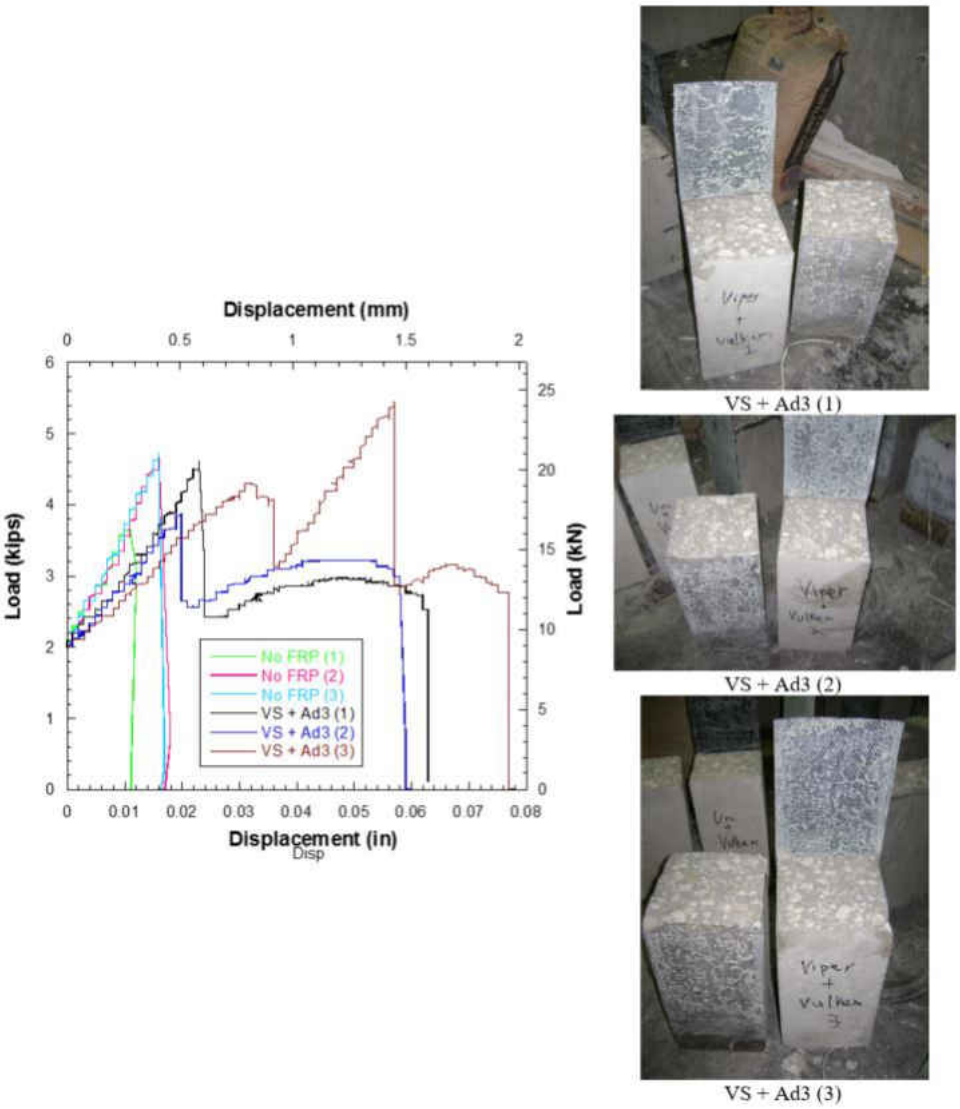


Figure A.11: Small Scale Flexural Beam: ViperSkin Fibers + Ad3 (PU)

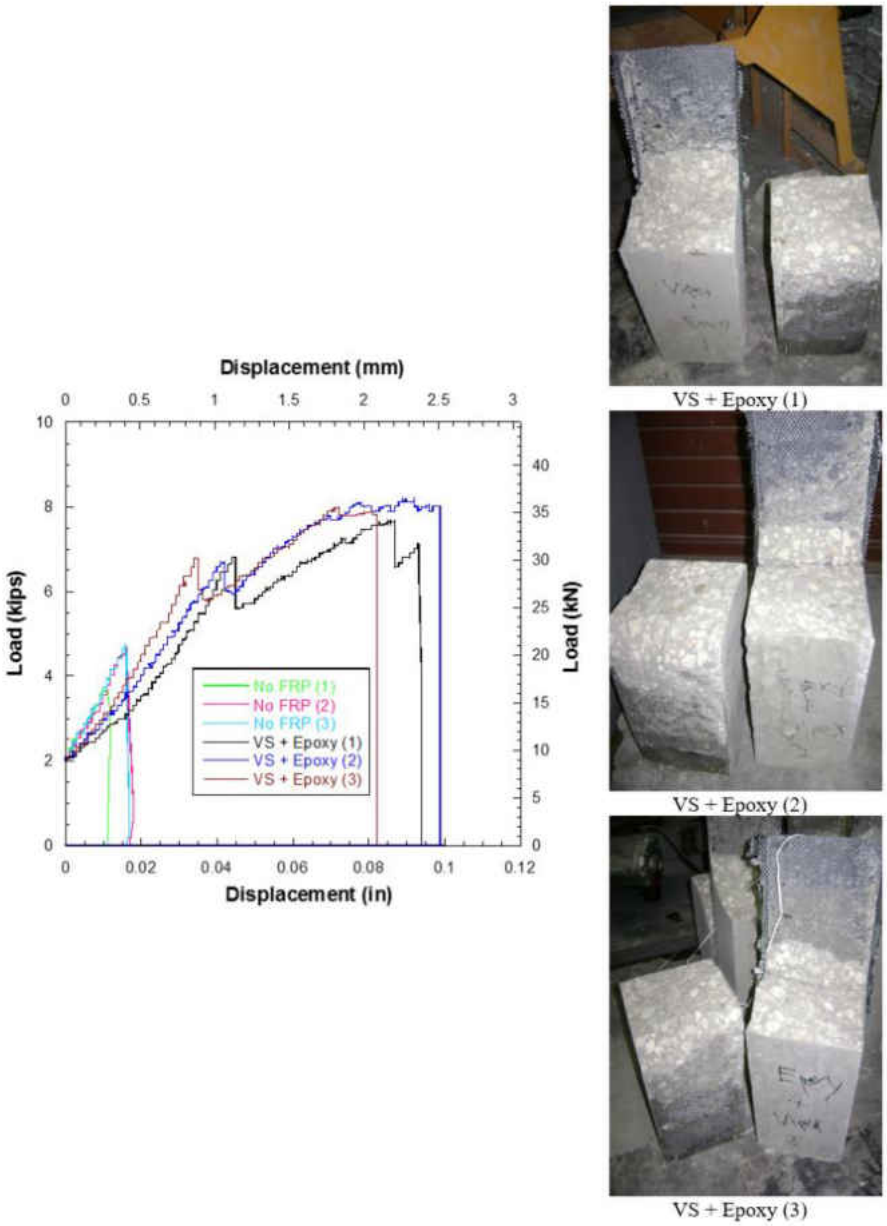


Figure A.12: Small Scale Flexural Beam: ViperSkin Fibers + Epoxy

# APPENDIX B: CONCRETE MIX DESIGN USED IN PROJECT

Table B.1: Beams and Lap Shear Specimens Concrete Mix Content

| **Material** | **Source** | **Description** | **Specific Gravity** | **Weight** ($lb/yd^3$) |
|---|---|---|---|---|
| Cement | CEMEX | Type I Cement per ASTM C-150 [40] | 3.15 | 570 |
| Fine AGG. | CEMEX | Natural Sand per ASTM C-33 [41] | 2.63 | 1260 |
| Coarse AGG. | CEMEX | #57 LimeStone per ASTM C-33 [41] | 2.45 | 1755 |
| Water | | ASTM C-94 [42] | 1 | 275 |
| Addmixture 2 | W.R. Grace | WRDA 60 per ASTM C-494 [43] | | |
| | | | **Totals** | **3860** |

## B.1 Concrete Mix Design for Small Scale Beams, Lap Shear Specimens, and Girders

Supplier : CEMEX WINTER PARK

Mix Code Number: 1396193

Description : 5000 psi in 28 days - Regular

Control Number : 1131JR085

Designed Slump: 4 in $+/-$ 1 in

Designed Air: 2.0 % Entrapped

Designed Unit Weight: 142.9 $lb/ft^3$

Designed Water Cement Ratio: 0.48

Table B.2: Column Concrete Mix Content

| **Material** | **Source** | **Description** | **Specific Gravity** | **Weight** ($lb/yd^3$) |
|---|---|---|---|---|
| Cement | CEMEX | Type I Cement per ASTM C-150 [40] | 3.15 | 594 |
| Fine AGG. | CEMEX | Natural Sand per ASTM C-33 [41] | 2.63 | 1327 |
| Coarse AGG. | CEMEX | #57 LimeStone per ASTM C-33 [41] | 2.45 | 1381 |
| Pozzolan | CEMEX | Class F Fly Ash per ASTM C-618 [44] | 2.45 | 148 |
| Water | | ASTM C-94 [42] | 1 | 275 |
| Addmixture 2 | W.R. Grace | WRDA 60 per ASTM C-494 [43] | | |
| | | | **Totals** | **3767** |

## B.2 Concrete Mix Design for Columns

Supplier : CEMEX WINTER PARK

Mix Code Number: 1401315

Description : 5000 psi in 28 days - Pea Rock Pump

Control Number. : Not Provided

Designed Slump: 5 in $+/-$ 1 in

Designed Air: 3.0 % Entrapped

Designed Unit Weight: 139.5 $lb/ft^3$

Designed Water Cement Ratio: 0.43

# APPENDIX C: COLUMN PHOTOS AND REACTION BLOCK DESIGN DRAWINGS AND PHOTOS

Figure C.1: Column Photo Prior to Pour

Figure C.2: Column Photo Prior to Pour

Figure C.3: Column Photo Prior to Pour

Figure C.4: Column Photo Prior to Pour

Figure C.5: Transporting Columns to Pour Site

Figure C.6: Columns at Pour site Pour

Figure C.7: Columns during Pouring of Concrete

Figure C.8: Slump Test from Column Pour

Figure C.9: Poured Columns

The reaction blocks that were used in the column testing were designed to sustain a maximum of 150 kips in any direction. The blocks were designed to be used for future testing by providing connections at locations in the block. They were designed to attach to the UCF strong floor, using 2" to 3.5" rods. After approaching many construction companies and precasters with our design, Gate Precast Company was the only company who agreed to donate the blocks to UCF, and to them we are very thankful. Photos of the reaction blocks along with photos from different phases of column construction are shown in this appendix.

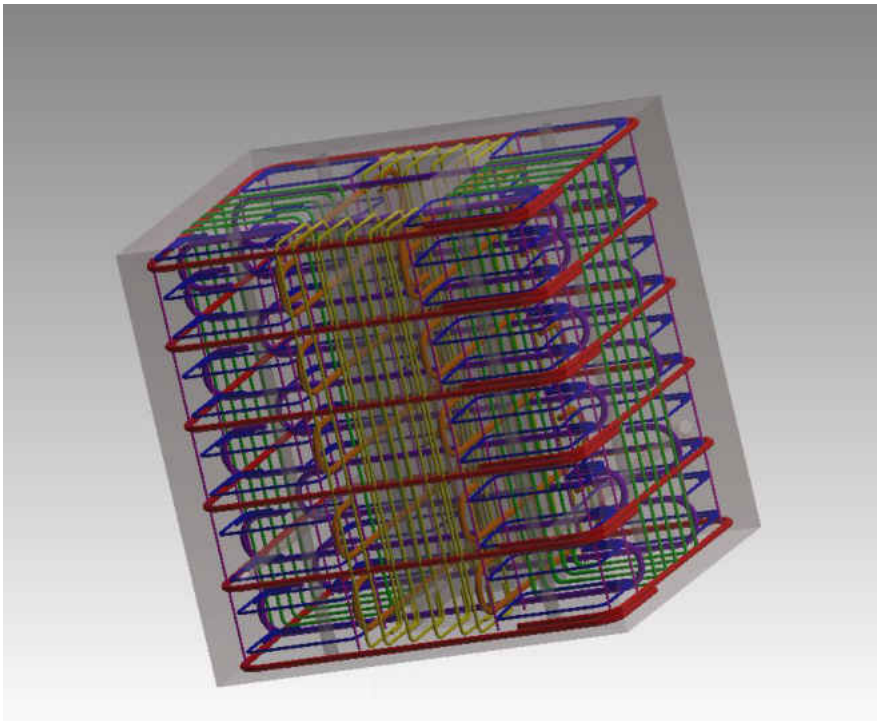

Figure C.10: 3D Schematic of the Reaction Blocks

Figure C.11: Reaction Block at Gate Precast Company Prior to Pour

Figure C.12: Reaction Block at Gate Precast Company Prior to Pour

# APPENDIX D: COLUMN LOAD-STRAIN GRAPHS

This appendix shows load vs. strain graphs for the different tested columns. Each different color in the graph below represents the strain from a different strain gage along the longitudinal bar.

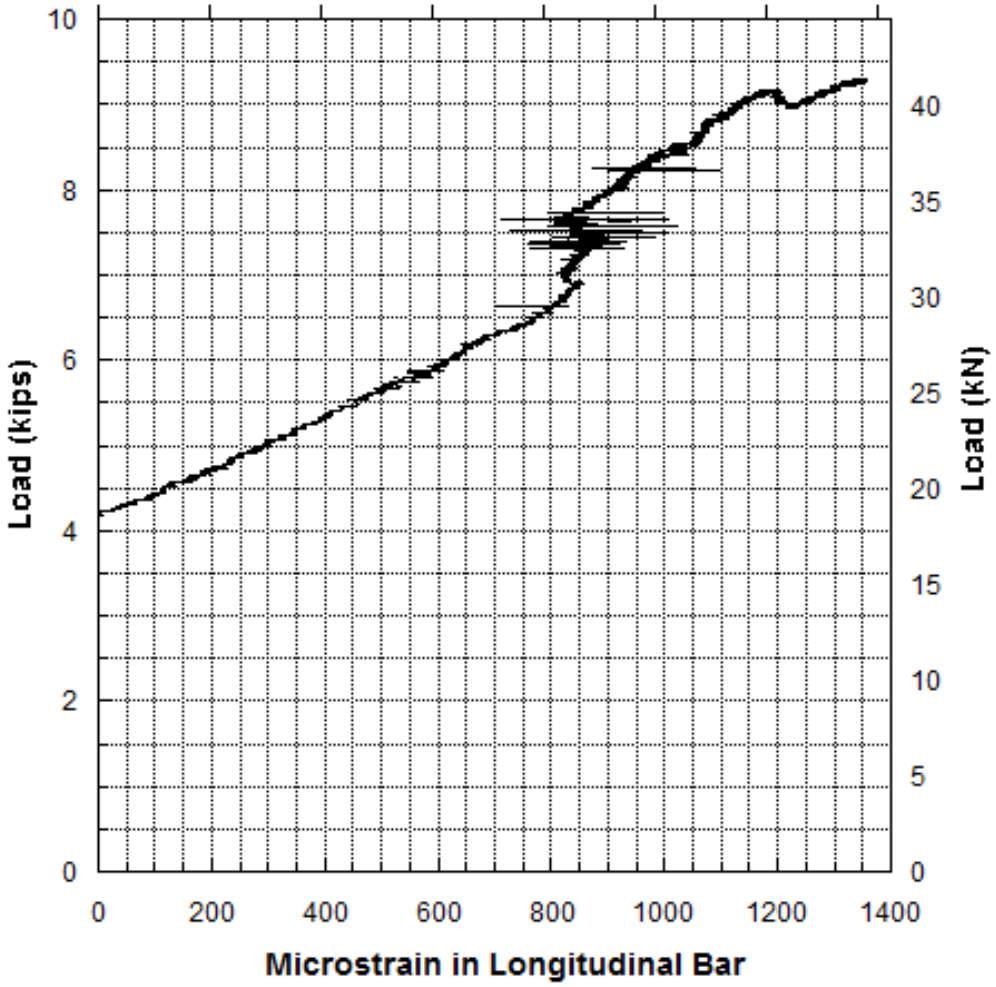


Figure D.1: Control Without Axial Load Application: Load vs Strain in Longitudinal Bar During the Damage Phase

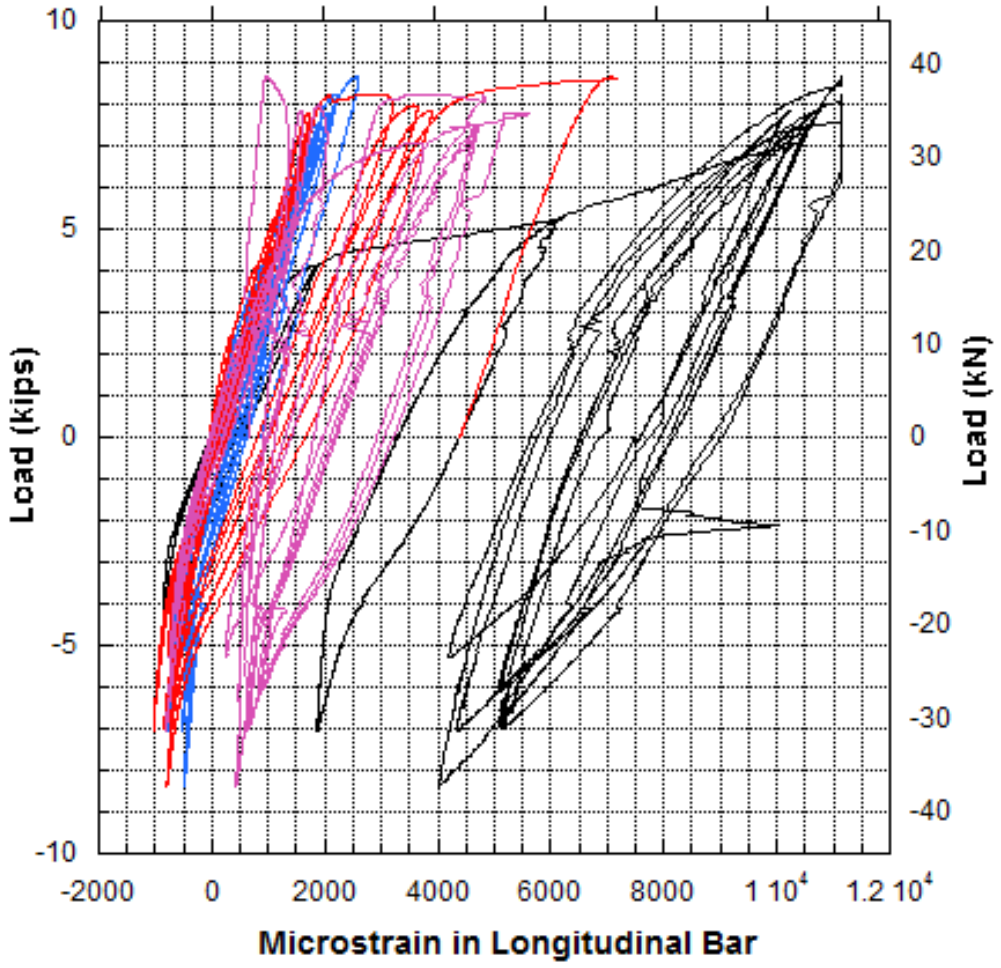


Figure D.2: Column 6 Load vs Strain in Longitudinal Bar During the Damage Phase

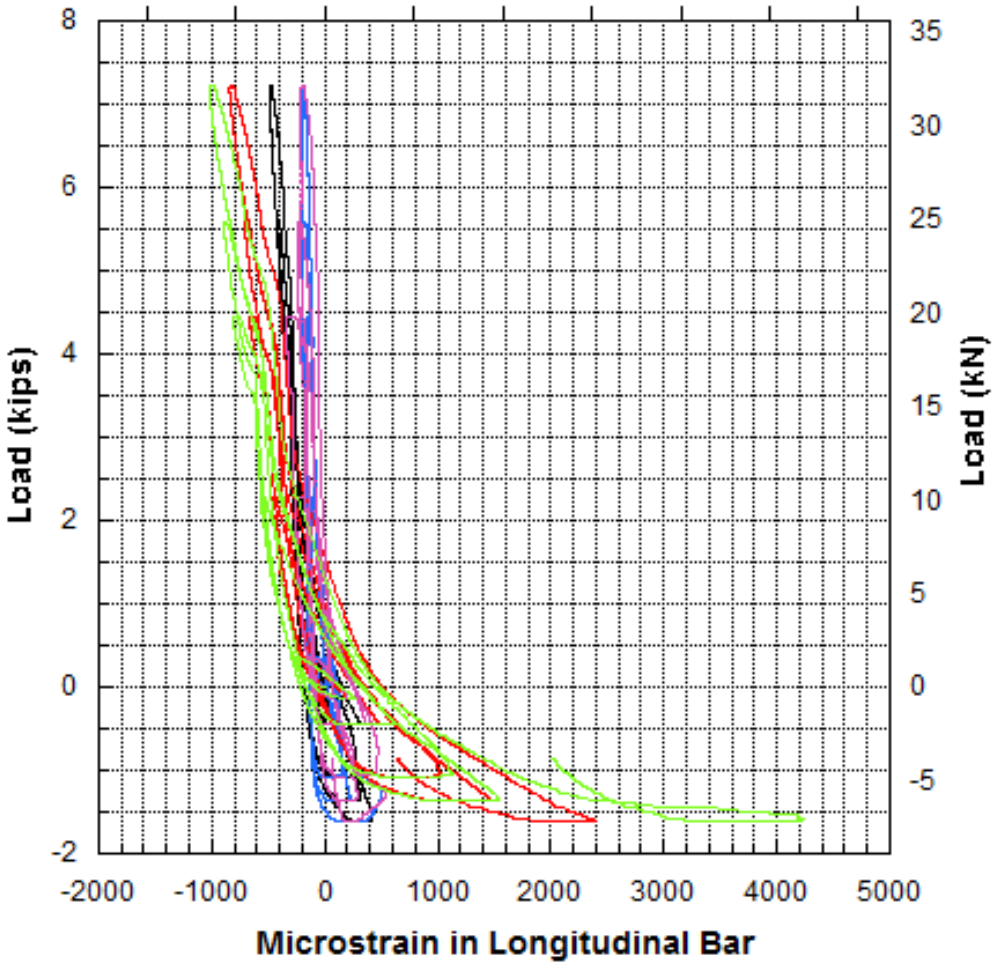


Figure D.3: Column 3 Load vs Strain in Longitudinal Bar During the Damage Phase

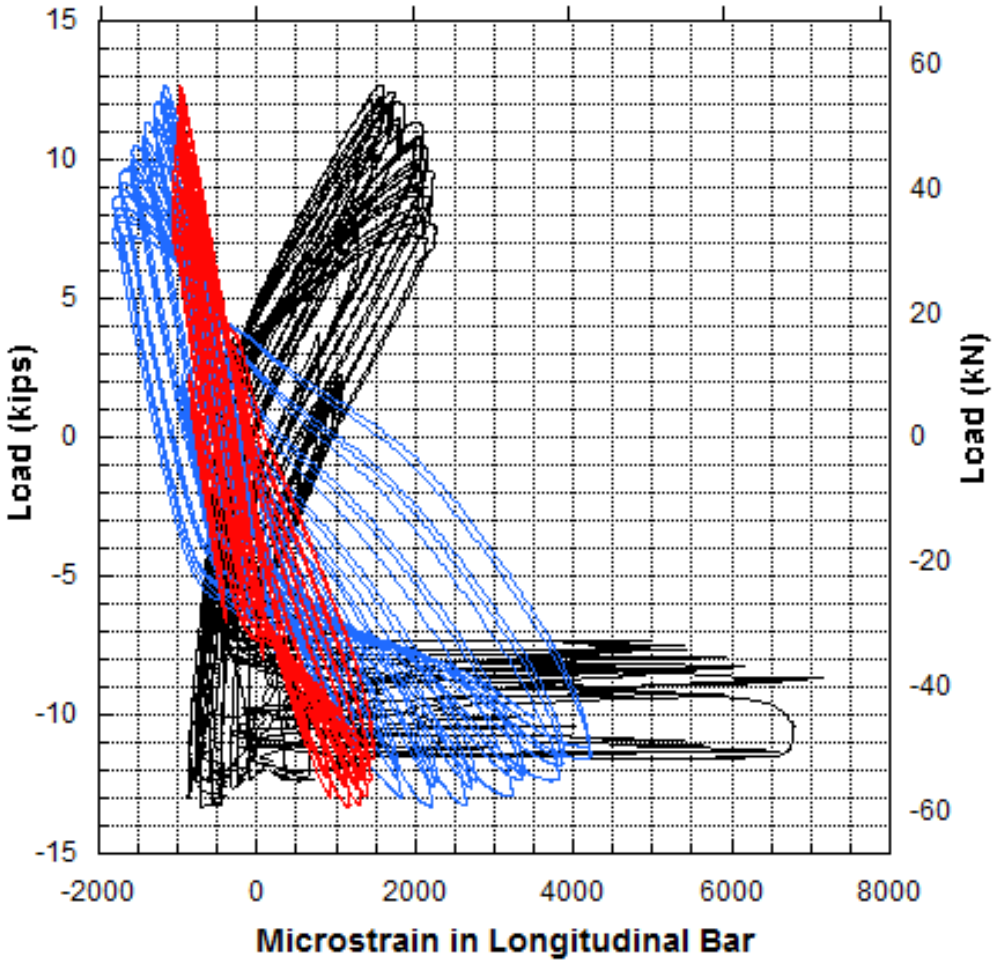


Figure D.4: Column 6 Load vs Strain in Longitudinal Bar During the Post-Repair Phase

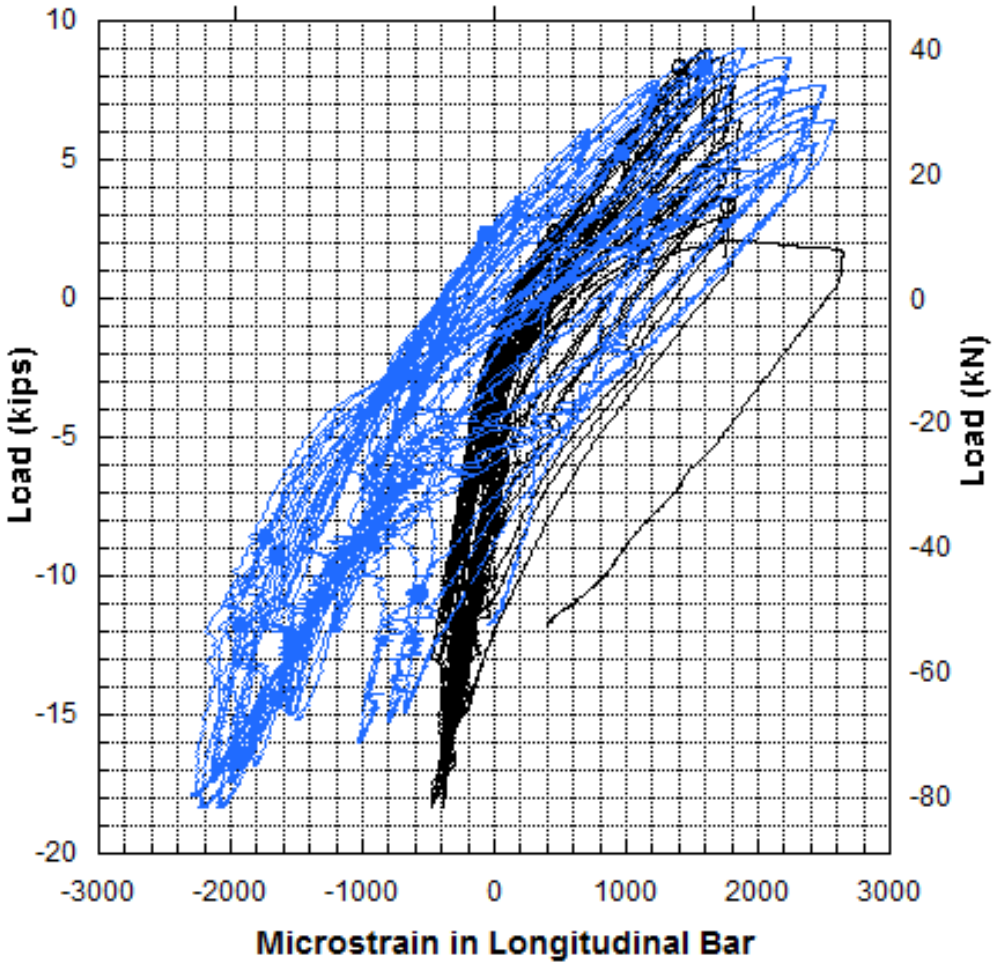


Figure D.5: Column 4 Load vs Strain in Longitudinal Bar During the Post-Repair Phase

# LIST OF REFERENCES


[1] ICC Evaluation Services, Whittier, CA, *Acceptance Criteria for Concrete and Reinforced Masonry Strengthening Using Externally Bonded Fiber-Reinforced Polymer (FRP) Composite Systems*, 2010.

[2] L. C. Bank, A. Barakatt, and T. R. Gentry, "Accelerated test methods to determine long term behavior of frp composite structures: Environmental effects," *Journal of Reinforced Plastics and Composites*, vol. 15, pp. 283–294, 1995.

[3] American Concrete Institute (ACI), Farmington Hills, MI, *Guide for the Design and Constructuon of Externally Bonded FRP Systems for Strengthening of Concrete Structures*, aci 440.3r-12 ed., 2008.

[4] American Concrete Institute (ACI) Committee 440, Farmington Hills, MI, *Guide for the Design and Construction of Externally Bonded Fiber-Reinforced Polymer Systems For Strengthening Unreinforced Masonry Structures*, 2010.

[5] The International Federation for Structural Concrete (FIB), Lausanne, Switzerland, *Externally Bonded FRP Reinforcement for RC Structures*, 2001.

[6] The Concrete Society, Camberley, Surrey, England, *Design Guidence for Strengthening Concrete Structures Using Fibre Composite Materials*, technical report 55 ed., 2004.

[7] Canadian Standards Association, Toronto, Ontario, *Design and Construction of Building Components with Fibre-Reinforced PPolymer*, 2002.

[8] A. A. Torres-Acosta, "Galvanic corrosion of steel in contact with carbon-reinforced polymer composites," *Journal of Composites for Construction*, vol. 6, no. 2, pp. 116–122, 2002.

[9] G. Cooks, *Mechanics of Composite Materials*, ch. 2, pp. 23–40. CRC Press Taylor and Francis Group, 2006.

[10] P. K. Mallick, *Fiber-Reinforced Composite*. CRC Press Taylor and Francis Group, 2008.

[11] Y. Setiadi, P. Har, T. Kuboki, and J. Cheng, "Comparison of damage development in random fiber reinforced ppolymer under cyclic loading," *Journal of Composite Materials*, vol. 40, pp. 71–91, 2005.

[12] N. Saenz and C. Pantelides, "Short and medium term durability evaluation on frp confined circular concrete," *Journal of Composites for Construction*, pp. 244–253, 2006.

[13] Z. B. Haber, "On the use of polyurethane matrix carbon fiber ccomposite for strengthening of concrete structures," Master's thesis, University of Central Florida, Orlando, FL, 2010.

[14] U. Meier-Westhues, *Polyurethanes: Coatings, Adhesives and Sealants*. Vincentz Network GmbH & Co KG, 2007.

[15] B. Burchardt, *Advances in Structural Adhesive Bonding*. Woodhead Publishing Limited, 2010.

[16] American Concrete Institute (ACI) Committee 318, Farmington Hills, MI, *Building Code Requirements for Structural Concrete (ACI318-08) and Commentary*, 2008.

[17] M. J. Chajes, T. A. T. Jr., T. F. Januszka, and W. W. F. Jr., "Flexural strengthening of concrete beams using externally bonded composite materials," *Construction and Building Materials*, vol. 8, pp. 191–201, 1994.

[18] S. F. Brena, R. M. Bambletta, S. L. Wood, and M. E. Kreger, "Increasing flexural capacity of reinforced concrete beams using carbon fiber-reinforced polymer composites," *American Concrete Institute Structural Journal*, vol. 100, pp. 36–46, 2003.

[19] N. F. Grace and S. B. Singh, "Durability evaluation of carbon fiber-reinforced polymer strengthened concrete beams: Experimental study and design," *American Concrete Institute Structural Journal*, vol. 102, no. 1, pp. 40–53, 2005.

[20] H. Toutanji, L. Zhao, Y. Deng, Y. Zhang, and P. Balaguru, "Cyclic behavior of rc beams strengthened with carbon fiber sheets bonded by inorganic matrix," *Journal of Materials in Civil Engineering*, vol. 18, no. 1, pp. 28–35, 2006.

[21] J. F. Bonacci and M. Maalaj, "Behavioral trends of rc beams strengthened with externally bonded frp," *Journal of Composites for Construction*, vol. 5, no. 2, 2001.

[22] O. Buyukozturk and T. Yu, "Understaunder and assesment of debonding failures in frp-concrete systems," in *Seventh International Congress on Advances in Civil Engineering*, (Istanbul, Turkey), 2006.

[23] J. F. Chen and J. G. Teng, "Anchorage strength models for frp and steel plates bonded to concrete," *American Society of Civil Engineers Journal of Structural Engineering*, vol. 127, no. 7, pp. 784–791, 2001.

[24] X. Z. Lu, J. G. Teng, L. P. Ye, and J. J. Jiang, "Bond slip models for frp sheets/plates externally bonded to concrete," *Engineering Structures*, vol. 27, pp. 920–937, 2005.

[25] X. Z. Lu, L. P. Ye, J. G. Teng, and J. J. Jiang, "Meso-scale finite element model for frp sheets/plates," *Engineering Structures*, vol. 27, pp. 564–575, 2005.

[26] X. Z. Lu, J. G. Teng, L. P. Ye, and J. J. Jiang, "Bond slip models for frp sheet/plate to-concrete interfaces," in *Proceedings of the 2nd International Conference of Advanced Polymer Composites for Structural Applications in Construction (ACIC)*, (Cambridge, England), Woodhead Publishing Limited, 2004.

[27] C. Mazzotti, M. Savonia, and B. Ferracuti, "Frp-concrete delamination results adopting defference experimental pure shear setups," tech. rep., University of Bologna, Bologna, Italy, 2009.

[28] M. A. Harnoun and H. M. Elsanadedy, "Fiber-reinforced plastic jackets for ductility enhancement of reinforced concrete bridge columns with poor lapsplice detailing," *American Society of Civil Engineers Journal of Bridge Engineering*, vol. 1, no. 6, pp. 749–757, 2005.

[29] R. D. Iacobucci, S. A. Shekh, and O. Bayrak, "Retrofit of square concrete columns with carbon fiber-reinforced polymer for seismic resistance," *American Concrete Institute Structural Journal*, vol. 100, pp. 785–794, 2003.

[30] F. Pitcher, P. Rochette, and P. Labossiere, "Confinement of concrete cylinders with cfrp," in *Proceedings of ICCCI's 1996 Conference*, (Tuscon, AZ), pp. 829–841, 1996.

[31] J. B. Mander, M. N. Priestley, and R. Park, "Theoretical stress-strain model for confined concrete," *American Society of Civil Engineers Journal of Structural Engineering*, vol. 114, no. 8, pp. 1804–1826, 1988.

[32] Kestner, Harris, Pessiki, Sause, and Riches, "Rehabilitation of reinforced concrete columns using fiber reinforced polymer composite jackets," Tech. Rep. 97-07, Advanced Technology for Large Structural Systems, 1997.

[33] R. S. Harichandran and I. M. Baiyasi, "Repair of corrosion-damaged columns using frp wraps," Tech. Rep. RC-1386, Michigan Department of Transportation, Lansing MI, 2000.

[34] F. E. Richard, A. Brandzaeg, and R. L. Brown, "A case study of failure of concrete under combined compressive stresses," tech. rep., University of Illinois, Urbana-Champaign, IL, 1928.

[35] A. Nilson and G. Winter, *Design of Concrete Structures*. New York, NY: Mcgraw-Hill, 1991.

[36] J. Restrepol and B. Devino, "Enhancement of the axial load carrying capacity of reinforced concrete columns by means of fiberfiber epoxy jackets," in *Proceedings of Advanced Composite Materials in Bridges and Structures II*, (Montreal, Canada), pp. 547–553, 1996.

[37] S. T. Rutledge, M. J. Kowalsky, R. Seracino, and J. M. Nau, "Repair of reinforced concrete bridge columns containing buckeled and fractured reinforcement by plastic hinge relocation," *Journal of Bridge Engineering, American Society of Civil Engineers (ASCE)*, vol. A4013001, pp. 1–10, 2013.

[38] Department of Transportation Standard Specifications State of California Business, Transportation and Housing Agency, Sacramento, CA, *Seismic Design Criteria*, May 2006.

[39] P. Laplace, D. H. Sanders, M. Saidi, and B. Douglas, "Shake table testing of flexure dominated reinforced concrete bridge columns." Civil Engineering Department, University of Nevada, Reno, Report No. CCEER-99-13, December 1999.

[40] ASTM Standard C1530/C150M, Frederick, Maryland, *Standard Specifications for Portland Cement*, 2012.

[41] ASTM C33/33M -13, Frederick, MD, *Standard Specification for Concrete Aggregates*, 2013.

[42] ASTM C94/C94M, Frederick, MD, *Standard Specification for Ready-Mixed Concrete*, 2013.

[43] ASTM C494 / C494M - 13, Frederick, MD, *Standard Specification for Chemical Admixtures for Concrete*, 2013.

[44] ASTM C618-12a, Frederick, MD, *Standard Specification for Coal Fly Ash and Raw or Calcined Natural Pozzolan for Use in Concrete*, 2012.